Studies of fluctuations in systems of self-propelled particles

A Thesis submitted for the degree of

Doctor of Philosophy (Science)

in

Physics (Theoretical)

by

Subhadip Chakraborti

Department of Physics

University of Calcutta

2018

Dedicated to all the taxpayers who actually 'funded' my research fellowship.

Published works to be included in the thesis

1. *Additivity, density fluctuations and nonequilibrium thermodynamics for active Brownian particles*, Subhadip Chakraborti, Shradha Mishra, and Punyabrata Pradhan, Phys. Rev. E **93** 052606 (2016).

2. *Additivity and fluctuations in nonequilibrium steady states*, Subhadip Chakraborti, Sayani Chatterjee, Arghya Das, and Punyabrata Pradhan, Proceedings of the workshop "Recent Advances in Research of Statistical Physics: A School for Undergraduate Students - 2017", page 16 (July, 2017).

Other works to be included in the thesis

1. *Additivity and particle-number fluctuations in Vicsek-like models*, Subhadip Chakraborti, Shradha Mishra, and Punyabrata Pradhan (to be submitted).

2. *Hydrodynamics of lattice models with persistent and long-range hopping*, Subhadip Chakraborti, Arghya Das, and Punyabrata Pradhan (work in progress).

Acknowledgements

I wondered for a while before writing this section, as where to start from .....Those who have truly helped me during this long tenure are not waiting for my acknowledgement. Yet, since I have to write, its better to start writing.

At first I would like to mention that person whose contribution is unparalleled my supervisor Dr. Punyabrata Pradhan. Before joining his group, I had asked Sayanidi primarily about two things - how Sir was as a person and as a teacher. I got positive reply for both. The next five years proved it to be true. I never asked how he is as a researcher because I didnt have any idea about what research was until I joined Ph.D. I chose research only due to my love for the field of statistical mechanics. Sir literally taught me each and every step of research, starting from checking the email and arxiv daily, which sections to focus while reading a paper, in one word everything, with immense patience. He gave me enough freedom to make room for independent thinking, he taught me how to think about various problems on my own and solve them, at least how to reach nearer to the solutions. Without his help, my Ph.D. would have never been possible (a trivial statement though!).

I would like to thank all my teachers while mentioning at least some of them. One is my higher secondary teacher Shri Rathin Lahiri who taught me to love physics. Another is my University teacher Dr. Soumen Kumar Roy who introduced the beauty of Statistical Physics to me. This fatherly figure taught me to have fun in programming also. The list would be incomplete if I do not mention Dr. Dhruba Banerjee.

We used to have Stat-physics journal club every week. I used to enjoy every session of it because there we had the opportunity to discuss difficult topics in a very informal and friendly manner. The presence of Punyabrata Sir, Sakuntala Madam, Shraddha Madam and Manna Sir made the discussions worthwhile. Also, we used to get tasty food at the end of each such discussion sessions.

I feel fortunate to have got Sayanidi and Arghyada as senior group members. The first one would voluntarily shoulder all the group pressure, and second one only understood pressure meant thermodynamic pressure. Such honest and helpful souls are rarely found these days. Recently, two uncivilized junior, Dhiraj and Anirban joined the group. When there is a need, they are so innocent but otherwise they drive me nuts.

Now I would mention those people without whom I cannot imagine these five years of my SNB life. Among them on one hand I have such idealistic people as Arghyada, Sayanidi, Biplabda, Subhasishda, Rakesh, Rajkumar, Sagarda, Nirnay, on the other hand I have Poulami, Subrata, Souvanik, Aslam, Kartik, Sarowarda, Debashis, Ananda, Sudipta, Arindamda(Das), Sumanto, Somnath, Arpita, Karan, Krishnendu for these people only one line suffice - With such friends, one wouldn't need enemies. Other than them, I am also thankful to every co-member of SNB Students, specially its social wing, SNB Mess, SNB Khaja Band (which honored my yelling by calling it singing) and SAC, each one has helped in making my SNB life complete. I would like to thank whole of SNB family for bearing with me these five years. My Jadavpurian friends, Sabana, Mandira, Arindam, Ashis, Manada, Chottuda, Arnab, Chankida, Biplabda, Laljuda, Bachhada, Rajarshida should apologize to the SNB people for making me such an poisonous person.

I acknowledge SNBNCBS for providing me funding, a good research atmosphere and such a beautiful and green campus.

Lastly, without the unconditional love and support of these people I couldn't have come so far, my Ma, Baba, Didi (with Chhana), Ranada (my medical advisor), Chotomama, Dada, Tito (my financial and legal advisor) and Tanusri (my friend, philosopher, guide and frustration absorber) my thankfulness would fall short for them. Still now, my mother asks me whether I do my study and homework regularly, and it amazes her every time when she learns that I gave a presentation in English.

Contents

Acknowledgements **iii**

List of Figures **vii**

1 Introduction **1**
1.1 Equilibrium and nonequilibrium statistical mechanics 1
1.2 Additivity in previous works 4
1.3 Active matters 5
1.3.1 Vicsek model 6
1.3.2 Active nematics 9
1.3.3 Run-and-tumble particles 11
1.3.4 Active Brownian particles 12
1.4 Macroscopic fluctuation theory 17
1.5 Outline of thesis 21

2 Additivity, and density fluctuations in active Brownian particles **24**
2.1 Introduction 24
2.2 Framework of additivity 26
2.3 Model and fluctuating hydrodynamics 30
2.4 Calculation of particle-number fluctuations 32
2.4.1 Linearized hydrodynamics 32
2.4.2 Noise-strengths and fluctuations 34
2.5 Additivity and nonequilibrium thermodynamics 39
2.5.1 Chemical potential and free energy function 39
2.5.2 Subsystem particle-number distributions 40
2.5.3 Phase transition 43
2.6 Summary and concluding perspective 45

3 Additivity and density fluctuations in Vicsek-like models **48**
3.1 Introduction 48
3.2 Framework of additivity 49
3.3 Number fluctuations in Vicsek Model 54
3.4 Number fluctuations in variant - I of Vicsek Model 59

3.5 Number fluctuations in variant - II of Vicsek model 63
3.6 Summary 65

4 Hydrodynamics of active lattice gases: Persistent and long-range hopping 68
4.1 Introduction 68
4.2 Lattice models with persistent hopping 75
4.2.1 Particle-number fluctuations 78
4.2.2 Hydrodynamics 80
4.2.3 Simulations 84
4.2.4 Characterization of density relaxations 86
4.3 Lattice models with long-range hopping 88
4.3.1 Hydrodynamics 92
4.3.2 Comparison with simulations 100
4.3.3 Fluctuation, response and Einstein relation 101
4.3.4 Characterization of density relaxations 103
4.4 Comparison between persistent-hop and long-hop models 105
4.5 Summary 109

5 Summary of the thesis 112

List of Figures

2.1 Simulations in the active Brownian particles. Scaled variance σ^2, for $Pe = 0$ (magenta triangles), 5 (blue squares), 10 (sky-blue diamonds), 20 (green inverted triangles), 50 (red circles) and 100 (black left-triangles), as a function of scaled density ρ/ρ_m, with $\rho_m \approx 1.15$, is compared with Eq. 2.30 with $P \approx 0$ (magenta dashed line), 0.5 (blue dashed double-dotted line), 2.0 (sky-blue dotted line), 4.3 (green double-dashed dotted line), 8.0 (red solid line) and 10 (black dashed dotted line), respectively. Points - simulations, lines - theory. 38

2.2 Panel (a): The scaled activity parameter P (as defined in Eq. 2.30) is plotted as a function of Peclet number Pe for densities $\rho \approx 0.26$ (green circles) and 0.34 (red squares). Panel (b): Pair correlation $g(r)$ (blue solid line) is plotted as a function of distance r for density $\rho \approx 0.5$ and $Pe = 50$; the magenta dashed line (fitting function) shows an exponential decay of the pair correlation function at large distance, with correlation length $\xi \sim 1$ (distance is in unit of diameter a of the particles). Points - simulations, lines - theory with fitting parameter. 39

2.3 Subsystem particle-number distributions for activity parameter $Pe = 50$, obtained from simulations (points), are compared with theory Eq. 2.12 (lines) with corresponding scaled activity parameter $P = 8$, for densities $\rho \approx 0.11$ (black circles, black dashed line), 0.19 (red triangles, red dashed double-dotted line), 0.26 (magenta diamonds, magenta dotted line), 0.34 (green inverted triangles, green doubled-dashed dotted line), 0.41 (blue squares, blue solid line) and 0.56 (violet asterisks, violet dashed dotted line). 42

2.4 At moderately large density $\rho \approx 0.41$ and large activity $Pe = 50$, subsystem particle-number distribution $P_{\mathcal{V}}(\mathcal{N})$ (blue squares), which deviates from Poisson (black dashed double-dotted line) as well as Gaussian (red dashed line) distributions, is quite well captured by theory Eq. 2.12 (blue solid line). 42

2.5 Scaled variance $\sigma^2(\rho)$ (Eq. 2.30) and corresponding chemical potential $\mu(\rho) = \int^{\rho} 1/\sigma^2 d\rho$ (Eq. 2.32) are plotted in panels (a) and (b), respectively as a function of the scaled density ρ/ρ_m for various values of the scaled activity parameter $P = 0$, 1, 2, 4, 8, 12 and 15. Chemical potential becomes a nonmonotonic function of density beyond a critical value of the scaled activity parameter, $P > P_c = 8$. 44

3.1 Order parameter v_a as a function of noise strength η for different densities ρ and fixed self propelled speed $v_0 = 0.5$. 50
3.2 Top: Subsystem particle number fluctuation $\sigma^2_{\mathcal{V}}(\rho)/\mathcal{V}$ as a function of density ρ for different noise strength η and fixed self propelled speed $v_0 = 0.5$. 51
3.3 (Vicsek model) We plot subsystem particle number distribution $P_{\mathcal{V}}(\mathcal{N})$ with $\mathcal{N}$. Red lines- additivity results, red points- simulation results and blue lines- corresponding Gaussian plots. Top panel: $\eta = \frac{\pi}{2}$ and $\rho_0 = 0.1$; middle panel: $\eta = \frac{2\pi}{3}$ and $\rho_0 = 0.1$; bottom panel: $\eta = \frac{2\pi}{3}$ and $\rho_0 = 0.2$. 53
3.4 (Vicsek model) We plot the scaled distribution function $\frac{1}{\mathcal{V}} \log[\mathcal{Z} P_{\mathcal{V}}(\mathcal{N})]$ [Eq. (3.5)] calculated from simulation, as a function of density $\rho = \mathcal{N}/\mathcal{V}$ for different subsystem sizes. Red lines- additivity results, points- simulation results and blue lines- corresponding Gaussian plots. Top panel: $\eta = \frac{\pi}{2}$ and $\rho_0 = 0.1$; middle panel: $\eta = \frac{2\pi}{3}$ and $\rho_0 = 0.1$; bottom panel: $\eta = \frac{2\pi}{3}$ and $\rho_0 = 0.2$. 55
3.5 Order parameter v_a as a function of noise strength η for different densities ρ and fixed self propelled speed $v_0 = 0.5$. 57
3.6 Top: Subsystem particle number fluctuation $\sigma^2_{\mathcal{V}}(\rho)/\mathcal{V}$ as a function of density ρ for different noise strength η and fixed self propelled speed $v_0 = 0.5$. 58
3.7 (Variant - I of Vicsek model) We plot subsystem particle number distribution $P_{\mathcal{V}}(\mathcal{N})$ with $\mathcal{N}$. Red lines- additivity results, red points- simulation results and blue lines- corresponding Gaussian plots. Top panel: $\eta = 0.5$ and $\rho_0 = 0.1$; middle panel: $\eta = 0.6$ and $\rho_0 = 0.1$; bottom panel: $\eta = 0.6$ and $\rho_0 = 0.2$. 60
3.8 (Variant - I of Vicsek model) We plot the scaled distribution function $\frac{1}{\mathcal{V}} \log[\mathcal{Z} P_{\mathcal{V}}(\mathcal{N})]$ [Eq. (3.5)] calculated from simulation, as a function of density $\rho = \mathcal{N}/\mathcal{V}$ for different subsystem sizes. Red lines- additivity results, points- simulation results and blue lines- corresponding Gaussian plots. Top panel: $\eta = 0.5$ and $\rho_0 = 0.1$; middle panel: $\eta = 0.6$ and $\rho_0 = 0.1$; bottom panel: $\eta = 0.6$ and $\rho_0 = 0.2$. 62
3.9 (Variant - II of Vicsek model) We plot the scaled distribution function $\frac{1}{\mathcal{V}} \log[\mathcal{Z} P_{\mathcal{V}}(\mathcal{N})]$ [Eq. (3.5)] calculated from simulation, as a function of density $\rho = \mathcal{N}/\mathcal{V}$ for different subsystem sizes. Red lines- additivity results, points- simulation results and blue lines- corresponding Gaussian plots. Top panel: $\eta = 0.5$ and $\rho_0 = 0.05$; middle panel: $\eta = 0.6$ and $\rho_0 = 0.05$; bottom panel: $\eta = 0.6$ and $\rho_0 = 0.1$. 64

4.1 Exact mapping between one dimensional lattice model of persitent hardcore particles and the corresponding unbounded mass model. . 76
4.2 Scaled variance $\sigma^2(\rho)$ is plotted as a function of density ρ for different tumbling rates $D_r = 0.05$ (blue), 0.3 (green), and 1.0 (magenta) along with the mean-field result [given by Eq. (4.16)] (yellow line). . 80

4.3 Comparison between density evolution of mean-field hydrodynamic Eq. (4.29) [lines] and that obtained from simulations [points], at different times $\tau = 0$ (magenta), 500 (green), 1000 (yellow), 2500 (blue) and 5000 (red), for different values of tumbling rate $D_r = 0.01$, 0.02, 0.05, 0.3, 1.0 and $D_r \to \infty$. It shows that mean-field theory can not capture the simulation result at lower value of D_r. . 85
4.4 Upper panel: Width of density $\Delta^2(\tau)$ [as defined in Eq. (4.31)] is plotted with time τ for tumbling rate $D_r = 0.01$ (red), 0.02 (yellow), 0.05 (blue), 0.3 (green) and 1.0 (magenta). Lower panel: diffusion coefficient D is plotted with inverse of effective hop length $l_{hop} = 1/D_r$. 87
4.5 Exact mapping between one dimensional hardcore lattice gas model with long-range hopping and the corresponding unbounded mass model. 90
4.6 Breakdown of Kolmogorob criterion in one dimensional lattice model with long-range hopping and in corresponding unbounded mass model. 91
4.7 Two transport coefficients, diffusion coefficient $D(\rho)$ and conductivity $\chi(\rho)$, which are numerically calculated using Eq. (4.54), are plotted as a function of density ρ for velocities $v = 1$ and 10. 95
4.8 Mass-mass correlation $C(r) = \langle m_i m_{i+r} \rangle - \rho^2$ is plotted as a function of inter particle distance r for global density $\rho = 0.3$ and velocities $v = 1$, 10 and $v \to \infty$. 99
4.9 Comparison between hydrodynamic theory and simulation at different times $\tau = 0$ (magenta), 1000 (green), 2000 (yellow), 5000 (blue) and 10000 (red) starting from initial condition Eq. (4.66), for $v = 10$ and $v \to \infty$. In the left panel, lines are the numerically calculated hydrodynamic evolution of density for $v = 10$, whereas, in the right panel, the lines are the mean-field hydrodynamic evolution plots for $v \to \infty$. 100
4.10 Scaled subsystem particle number fluctuation $\sigma^2(\rho)$ calculated from simulation, is plotted as a function of density ρ for velocities $v = 1$ (green filled circles) and 10 (yellow filled square). We compare $\sigma^2(\rho)$ with the ratio of two transport coefficients $\chi(\rho)$ and $D(\rho)$, respectively, calculated numerically using Eq. (4.54), for velocities $v = 1$ (green empty circles) and 10 (yellow empty square). It shows existence of an ER in this non-equilibrium model. 102
4.11 Density evolution at different times $\tau = 0$ (magenta), 1000 (green), 2000 (yellow), 5000 (blue) and 10000 (red), starting from initial condition Eq. (4.66) for different velocities $v = 2$, 4, 10 and $v \to \infty$ [points] and compare them with that for $v = 1$ (simple exclusion process) [lines] in each panel. 103
4.12 Upper panel: Width of density $\Delta^2(\tau)$ [as defined in Eq. (4.67)] is plotted with time τ for velocities $v = 1$ (magenta), 2 (green), 4 (blue), 10 (yellow) and $v \to \infty$ (red). Lower panel: diffusion coefficient D is plotted with inverse of effective hop length $l_{hop} = v$. 104

4.13 Upper panel: Comparison between scaled subsystem mass fluctuation $\sigma^2(\rho)$ of persistent model and model with long-range hopping. We plot $\sigma^2(\rho)$ as a function of density ρ of persistent model for effective hop length $l_{hop} = 1/D_r = 3$ (blue filled circle) and 10 (blue empty circle), and of model with long-range hopping for $l_{hop} = v = 3$ (yellow filled square) and 10 (yellow empty square). Lower panel: Comparison between behavior of diffusion coefficient D with inverse of effective hop length l_{hop} of persistent model (red circle) and model with long-range hopping (green square). 106

4.14 Single-site mass distribution $P(m)$ (equivalently, cluster size distribution of vacancies, or holes, in the lattice gas version with exclusion constraint) is plotted as a function of mass m at a particular site for different values of $l_{hop}^{-1} = 1.0$ (magenta), 0.5 (green), 0.25 (blue), 0.1 (yellow) and 0.01 (red). Upper panel: Persistent-hop model. Lower panel: Long-hop model. Appearance of the second peak (or mode) in the mass distribution in long-hop model for $v = l_{hop} \to \infty$ indicates the condensate formed in the system. Note that there is no such peak in the distribution in persistent-hop model, indicating there is no phase separation as such. We have taken global mass density $\rho = 1$ in all simulations. 107

4.15 We calculate the large-mass cut-off m^* in the single-site mass distribution $P(m) \sim \exp(-m/m^*)$ and plot inverse of the cut-off m^* as a function of the inverse of the effective hop length l_{hop} for persistent-hop model (red circles) and long-hop model (green squares). We have taken global mass density $\rho = 1$ in all simulations. 108

Chapter 1

Introduction

1.1 Equilibrium and nonequilibrium statistical mechanics

Statistical mechanics is a branch of physics, which deals with the fundamental problem of connecting macroscopic (thermodynamic) and microscopic properties of matter, and started in the end of eighteenth century with the great works of Maxwell, Boltzmann, Gibbs and Einstein. Though there has been great progress made throughout the past decades in understanding equilibrium phenomena such as phase transitions in various materials, understanding vast range of nonequilibrium phenomena, and bringing them under a universal thermodynamic framework, still remain elusive. Let us first start by describing equilibrium thermodynamics, which would help us to understand the difficulty in finding a thermodynamic description for nonequilibrium systems. Thermodynamics is a macroscopic description of matter and is essentially a phenomenological theory, derived from experiments. It deals with measurable macroscopic quantities (observables), called *thermodynamic variables*, such as extensive variables energy, volume, particle-number and corresponding intensive variables temperature, pressure, chemical potential, respectively. A thermodynamic state of a system is specified by a set of thermodynamic variables. A system is said to be in a steady state, or time-stationary

state, when the thermodynamic variables of the system does not change with time. A steady state can be equilibrium or non-equilibrium, depending on the energy current, charge current or particle current, which may be flowing in the system. If all possible currents are on average zero, the steady state is said to be an equilibrium state; otherwise, the state is a non-equilibrium state one, where currents are nonzero. To simply illustrate this point, let us consider a metal rod, whose one end is kept in contact with boiling water and the other end with ice. Eventually, the system reaches a steady state where temperature of each point of the rod will not change with time. However, the temperature measured at each point of the rod would not be the same, resulting in a heat flow through the rod in the steady state. Here the rod is said to be in a nonequilibrium steady state. Now, if the boiling water and the ice are removed and the rod is kept in contact with environment, each point of the rod eventually will reach the temperature of the environment, and the system would be in equilibrium.

It is expected that the macroscopic or the large-scale properties of a system emerge from the underlying interactions among microscopic constituents of the system. Statistical mechanics constitutes a bridge between the macroscopic and microscopic worlds. In order to make the description more precise, we need to formalize the above discussions, leading to theory of thermodynamic ensembles. Throughout the thesis, we consider only stochastic dynamics. Suppose a microscopic configuration of a system is denoted by $\mathcal{C}$, in the *configuration space* (specified by positions of particles, say) or *phase space* (specified by both positions and momenta of particles). If probability of finding a system in a configuration $\mathcal{C}$ at time t is denoted by $P(\mathcal{C}, t)$, the time evolution of $P(\mathcal{C}, t)$ is governed by master equation,

$$\frac{\partial P(\mathcal{C}, t)}{\partial t} = \sum_{\mathcal{C}' \neq \mathcal{C}} \left[W(\mathcal{C}' \to \mathcal{C}) P(\mathcal{C}', t) - W(\mathcal{C} \to \mathcal{C}') P(\mathcal{C}, t) \right], \tag{1.1}$$

where $W(\mathcal{C} \to \mathcal{C}')$ is the transition rate from one configuration $\mathcal{C}$ to another configuration $\mathcal{C}'$. At steady state, the probability of a configuration will no longer depend on time *i.e.*, $P(\mathcal{C}, t)$ will simply be $P(\mathcal{C})$. And also the left hand side of Eq. (1.1) will vanish at steady state. Moreover, at equilibrium, the probability

that the system goes from one particular configuration $\mathcal{C}$ to another configuration $\mathcal{C}'$ is same as the probability of going from $\mathcal{C}'$ to $\mathcal{C}$), alternatively known as *detailed balance*, is given by,

$$W(\mathcal{C}' \to \mathcal{C})P(\mathcal{C}') = W(\mathcal{C} \to \mathcal{C}')P(\mathcal{C}). \tag{1.2}$$

This definition of equilibrium is equivalent to the physical description of a thermodynamic equilibrium given previously in this chapter, where it was stressed that this is a state with no macroscopic currents of physical quantities (such as energy, charge, and particles) present in the system. These physical macroscopic currents are necessarily developed at the microscopic level by probability currents between configurations. Further, from Eq. (1.3) we have,

$$\frac{P(\mathcal{C})}{P(\mathcal{C}')} = \frac{W(\mathcal{C}' \to \mathcal{C})}{W(\mathcal{C} \to \mathcal{C}')} = \exp[-\beta\{E(\mathcal{C}) - E(\mathcal{C}')\}], \tag{1.3}$$

where, $\exp[-\beta E(\mathcal{C})]$ is the Boltzmann-Gibbs factor for probability distribution of a equilibrium configuration $\mathcal{C}$ and $E(\mathcal{C})$ is the energy function of the same configuration. However, there in no such a-priori known prescription for the probability distribution of a nonequilibrium configuration; in other words, one has to solve Eq. 1.1 to find the steady state, which is a formidable task for a system driven out of equilibrium. So, the nonequilibrium systems are beyond the scope of the familiar Boltzmann-Gibbs framework of statistical mechanics. Moreover, nonequilibrium systems contain non-vanishing current, macroscopic energy/particle current and/or probability current in the configuration-space, due to the presence of an external force. The presence of nonzero currents in the configuration space violates detailed balance and much of the intuitions developed from equilibrium statistical mechanics do not work in out-of-equilibrium systems. That is why the problem of characterization of driven many-particle systems has drawn much attention in the past decades [1, 4]. The problem is however quite hard to tackle, mainly due to the reasons mentioned above. In this thesis, we consider only systems having a nonequilibrium steady state, arguably the closest counterpart to equilibrium state.

1.2 Additivity in previous works

A simple characterization of the steady-state systems in general would certainly be desirable and, to this end, several attempts have been made in the past [6–8]. Recently, a formulation based on equilibrium-like additivity property provides a framework [9–11], which helps one to describe a broad class of nonequilibrium systems, through characterizing fluctuations of a conserved quantity, e.g., mass or particle-number [12–16]. Here we describe briefly the main features of additivity in equilibrium systems.

A cornerstone of equilibrium statistical mechanics is an additivity property which holds irrespective of the microscopic details of the system, provided that the interactions are short ranged in nature. An additivity property states that, if we break a system in large number of smaller subsystems such that the subsystem sizes are much larger than the correlation length present in the system, then the free energy (or, entropy of an isolated system) of the total system can be written as a sum of the free energies of individual subsystems. For instance, consider a system of total number of particles N is kept in contact with a bath of temperature T. Now, we divide the system in two parts of size V_1 and V_2, having N_1 and N_2 number of particles, respectively, with the total number of particles $N = N_1 + N_2$ is constant. N_1 and N_2 are two fluctuating quantities as the subsystems can exchange particles among them. According to additivity theory, if V_1 and V_2 are much larger than the correlation length present in the system, the free energy of the original system could be written as $F(N) = F_1(N_1) + F_2(N_2)$ with the total particle number N is conserved, where F_1 and F_2 are the free energies of the two subsystems. In other words, as the subsystems are considered to be statistically independent of each other, the joint particle number distribution of the subsystems can be written approximately in product form given by,

$$\mathcal{P}(N_1, N_2) \simeq \frac{1}{Z} e^{-\beta F_1(N_1)} e^{-\beta F_2(N_2)} \delta(N_1 + N_2 - N), \tag{1.4}$$

where $Z = \exp(-\beta F)$ is the partition sum. The most probable state in the long-time limit could be found by minimization of total free energy F with respect to N_1 or N_2, which leads to the equalization of two intensive quantities,

$$\mu_1 = \frac{\partial F}{\partial N_1} = \frac{\partial F}{\partial N_2} = \mu_2, \tag{1.5}$$

where μ_1 and μ_2 are the chemical potentials of the two subsystems. A direct consequence of additivity is a fluctuation-response relation (FR) which relates the average number of particles in the subsystem $\langle n \rangle$ to response function due to change in chemical potential μ, as,

$$\frac{d\rho}{d\mu} = \sigma^2_{eq}, \tag{1.6}$$

where, scaled variance of number of particles $\sigma^2_{eq} = \lim_{\mathcal{V}\to\infty}[\langle n^2 \rangle - \langle n \rangle^2]/\mathcal{V}$ in a subsystem of size $\mathcal{V}$, and density $\rho = \langle n \rangle / \mathcal{V}$. A free energy density $f(\rho)$ can also be obtained satisfying $\mu(\rho) = df/d\rho$ such that Eq.(1.6) can be written as,

$$\frac{1}{f''(\rho)} = \sigma^2_{eq}(\rho). \tag{1.7}$$

Here, we address the question, in the context of systems of self-propelled particles, whether an equilibrium-like additivity property can be used to obtain large deviation probability for particle-number in a subsystem, or alternatively coarse-grained density fluctuations - the central object in statistical mechanics theory. The self-propelled particles, which are driven by an internal chemical energy through some propulsion mechanism, are inherently far from equilibrium system.

1.3 Active matters

Self-propelled particles (SPPs), also called active matters, are prevalent in nature - in living systems, e.g., bacterial colony [22], fish school [23], flocks of birds [24], insect swarm [25] as well as in nonliving systems, e.g., photoactivated or chemically

powered colloids, thermophoretic Janus particles [26], etc. They have been realized in experiments [27] and intensively studied through simulations and theories [28–35, 37]; for reviews, see [38–40]. These particles propel themselves by converting chemical energy to mechanical one, which is continually dissipated to the medium. The steady flow of energy keeps the system out of equilibrium and a novel non-equilibrium steady state (NESS) emerges. Such a non-equilibrium steady state manifests itself by exhibiting rich collective phenomena, e.g., self-assemblies and pattern formations, otherwise impossible in equilibrium. In the following, we try to categorize the model systems of active matters studied in the literature in four classes: Vicsek model, active nematics, run-and-tumble particles (RTPs), and active Brownian particles (ABPs) and discuss the work done on these models, which would provide some physical insights into their interesting properties.

1.3.1 Vicsek model

The first, and arguably the simplest, model of self-propelled particles was introduced by Vicsek [71] *et al.* several decades ago. They proposed a system of N polar point particles in a periodic square box. The model is defined as follows: At any discrete time t, the system is specified by position $\mathbf{r}_i(t)$ and self-propulsion direction $\theta_i(t)$ of ith particle with $i = 1, \ldots, N$. The particles follow their neighbours by averaging the directions of motion of all neighbouring particles within a circle of radius R. They also make some errors in direction when attempt to follow their neighbour of amount $\Delta\theta_i(t)$. $\Delta\theta_i(t)$ is uniform and white noise with $\langle \Delta\theta_i(t) \rangle = 0$ and $\langle \Delta\theta_i(t)\Delta\theta_j(t') \rangle = \eta\ \delta_{ij}\delta_{tt'}$. The equations of motion for $\mathbf{r}_i(t)$ and $\theta_i(t)$ are given below.

$$\theta_i^R(t) = \arctan\left[\frac{\langle \sin\theta_j(t)\rangle_i^R}{\langle \cos\theta_j(t)\rangle_i^R}\right] \tag{1.8}$$

$$\theta_i(t+1) = \theta_i^R(t) + \Delta\theta_i(t) \tag{1.9}$$

$$\mathbf{r}_i(t+1) = \mathbf{r}_i(t) + v_0[\cos\theta_i(t+1), \sin\theta_i(t+1)]\Delta t \tag{1.10}$$

where the average in Eq (1.8) is over all particles j satisfying $|\mathbf{r}_j(t)-\mathbf{r}_i(t)| < R = 1$, v_0 is the self propulsion speed and we set discrete time step $\Delta t = 1$. At large density ρ and/or small η, the particles tend to move in the same spontaneously selected direction indicating a phase transition. This phase transition is characterized by determining the absolute value of the average normalized velocity of all particles

$$v_a = \frac{1}{Nv_0}|\sum_{i=1}^{N}\mathbf{v}_i|.$$

v_a is the orientation order parameter for the ordered to disordered phase transition. Clearly v_a will take value 1 when all the particles in the system are moving in the same direction and it is zero when all the particles are oriented in completely random direction.

Tonar and Tu [72, 73] proposed a set of hydrodynamic equations for Vicsek model. Hydrodynamic model usually deals with large-scale properties of slow variables, in other words, the slow spatio-temporal modes with large wave lengths and small frequency, where the relaxation times of the modes are usually large *i.e.*, the modes for which characteristic frequency $\omega \to 0$ as wave vector $q \to 0$. For simple fluids, the slow variables, or hydrodynamic modes, are the density field ρ of the conserved particle number, and the velocity field $\mathbf{v}$ (related momentum density). Toner and Tu considered in their analysis a set of phenomenological coarse-grained equations, which include terms on grounds of symmetry and can be written as follows [61, 72, 73],

$$\partial_t\mathbf{v} + \lambda(\mathbf{v}.\nabla)\mathbf{v} = (\alpha - \beta\mathbf{v}.\mathbf{v})\mathbf{v} + D\nabla(\nabla.\mathbf{v}) - \nabla P(\rho) + \mathbf{f}, \quad (1.11)$$

$$\partial_t\rho + \nabla.(\mathbf{v}\rho) = 0, \quad (1.12)$$

with $\alpha < 0$ in the disordered homogeneous state and $\alpha > 0$ in the ordered state. If we ignore all gradient terms in Eq. (1.11), a phase transition will occur by tuning α from the disordered phase $\mathbf{v} = 0$ to an ordered phase with $|\langle\mathbf{v}\rangle| = \sqrt{\alpha/\beta}$. This nonequilibrium phase transition spontaneously breaks the rotational symmetry in $d = 2$, in contrast to equilibrium systems, which cannot spontaneously

break a continuous symmetry in $d = 2$, according the Mermin-Wagner theorem. The Nambu-Goldstone mode associated with this spontaneously broken rotational symmetry can be shown to be related to the fluctuations of velocity $\delta\mathbf{v}_\perp$ transverse to the mean ordering direction and is very slow to decay at small wave vector $\mathbf{q}$. Here D is the diffusion constant which controls the elastic restoring forces to distortions in the ordered phase. The random errors originally introduced in the Vicsek model are accounted by the Gaussian white noise $\mathbf{f}$ with correlations $\langle f_i(\mathbf{r},t)f_j(\mathbf{r}',t')\rangle = \Delta\delta_{ij}\delta^d(\mathbf{r}-\mathbf{r}')\delta(t-t')$ where Δ is a constant. The Navier-Stokes-like advective term (with a factor λ) on the left hand side of Eq. (1.11) essentially says that the distortions in $\mathbf{v}$ are advected by $\mathbf{v}$ because $\mathbf{v}$ is not only an order parameter but also a velocity. $P(\rho)$ is the pressure, which maintains the local number density $\rho(\mathbf{r})$ at its mean value ρ_0. Eq. (1.12) is a continuity equation corresponding to conservation of total number of particles. The nonequilibrium character of the Toner-Tu model enters only through the advective λ term in Eq. (1.11) and the current in Eq. (1.12). Here all the phenomenological coefficients $\alpha,\ \beta,\ \lambda,\ D,\ \Delta$ are functions of ρ and $|\mathbf{v}|^2$.

To this end, one can linearize Eqs. (1.11) and (1.12) about a uniform ordered state with $|\langle\mathbf{v}\rangle| = v_o,\ \rho = \rho_0$, and see how small disturbances $\delta\rho,\ \delta\mathbf{v} \equiv (\delta\mathbf{v}_\perp, \delta v_\parallel)$ behave, where directions along and transverse to $\langle\mathbf{v}\rangle$ are denoted by $\perp$ and $\parallel$. $\delta\mathbf{v}_\perp$ is the Nambu-Goldstone mode associated with the spontaneous symmetry breaking. Hence, when noise is included, the steady-state variance $\langle|\delta v_{\perp\mathbf{q}}|^2\rangle$ of the q^{th} Fourier component should diverge at small wavenumber q as $\langle|\delta v_{\perp\mathbf{q}}|^2\rangle \sim 1/q^2$. However, nonlinearities in Eqs. (1.11) and (1.12) are strongly relevant in $d = 2$ and lead to $\langle|\delta v_{\perp\mathbf{q}}|^2\rangle$ diverging more slowly than $1/q^2$ thus preserving long-range order [72, 73]. Now the linearized theory says that the perturbation in density and velocity field are related by $\delta\rho \sim \sqrt{\rho_0/P'(\rho_0)}\delta v_\perp$. Therefore, the variance $\langle|\delta\rho|^2\rangle$ of density deviation $\delta\rho$ should also diverge at small q. In real space, this implies that the variance in the particle-number ΔN grows faster than N, which indicates a giant particle-number fluctuations (GNFs), studied extensively in the literature in the past decades.

1.3.2 Active nematics

Another set of striking nonequilibrium properties have been explored by Ramaswamy *et al.* [58–61] in *active nematics*. They considered a collection of head-tail symmetric, or apolar particles (confined on a solid surface) unlike the polar boids in Vicsek model [71–73]. Here, individual particles can move by a self-propulsion force, but due to their apolar nature, they can move in forward or backward direction equally likely, resulting in a zero macroscopic velocity. These systems form a state with spontaneous, uni-axial orientational order with a macroscopic axis $\hat{\mathbf{n}}$ with $\hat{\mathbf{n}} \to -\hat{\mathbf{n}}$ symmetry, called nematic or apolar order, in contrast to the vectorial or polar order found in Vicsek model where $\hat{\mathbf{n}}$ and $-\hat{\mathbf{n}}$ are not equivalent.

The drive or activity distinguishes such *active nematics* from the usual (equilibrium) case [62]. In particular, here, as in polar flocks, giant number fluctuations (GNFs) has been predicted [58] in the ordered phase, based on the analysis of phenomenological hydrodynamic equations, derived from symmetry arguments, even though the order parameter here is not a velocity. The prediction says that the number fluctuations in regions containing N particles on average have a standard deviation $\Delta N \propto N^{1/2+1/d}$ with d the dimension of the space. They [58] also found a long-time tail $\sim t^{-d/2}$ in the auto-correlation of the particle velocities in spite of absence of a hydrodynamic velocity field.

First confirmation of the existence of the GNFs in active nematics, as predicted by Ramaswamy *et al.* in a hydrodynamic theory, was done by Chate *et al.* [63] in computer simulations of a microscopic model of active nematics. The model they proposed was an apolar version of the two-dimensional Vicsek model (polar) described in Sec. 1.3.1. Chate *et al.* consider N point particles, each having an axis, rather than a unit vector, in a two-dimensional box of size $L \times L$. The particles move by a fixed distance $v_0 \Delta t$ in a discrete time step Δt. If θ_j is the orientation of the axis of the j^{th} particle, it can move along θ_j or $\theta_j + \pi$ with equal probabilities. Each particle j aligns itself parallel to the mean of its neighbor's

axes by updating its orientation at every time step following the rule,

$$\theta_j^{t+\Delta t} = \Theta(\mathbf{Q}_j^t) + \eta\xi_j^t, \tag{1.13}$$

where, $\Theta(\mathbf{Q}_j^t)$ is the direction of the first eigenvector of the local tensorial traceless order parameter

$$\mathbf{Q}_j = \begin{pmatrix} \langle\cos^2\theta_k\rangle - \frac{1}{2} & \langle\cos\theta_k \sin\theta_k\rangle \\ \langle\cos\theta_k \sin\theta_k\rangle & \langle\sin^2\theta_k\rangle - \frac{1}{2} \end{pmatrix}. \tag{1.14}$$

The averages in Eq. 1.14 are taken over all particles k within the interaction range $R = 1 > v_0\Delta t$, including the particle j. The second term in the RHS of Eq. (1.13) is the additional noise term in the angle which is responsible to make the system disorder where ξ_j^t is a white noise $\in [-\pi/2, \pi/2]$, η the noise strength. The scalar order parameter *i. e.* twice the positive eigen value of $\mathbf{Q}$ is given by,

$$S = \sqrt{(\langle\cos^2\theta\rangle - 1/2)^2 + \langle\cos\theta\sin\theta\rangle^2}. \tag{1.15}$$

Clearly, $S = 1$ for perfect nematic order ($\eta \to 0$), and $S = 0$ for complete disorder ($\eta \to 1$). Beside presence of a quasi-long-range orientational order in the ordered state, Chate *et al.* found a disorder-to-order phase transition, similar to the Kosterlitz-Thouless type [64] phase transition. Moreover, the standard deviation ΔN of the average number of particles N in a given subsystem, is proportional to N and not $\sqrt{N}$ as expected in equilibrium, in agreement with the prediction in Ref. [58]. If we make $v_0 = 0$, the nematic phase survives but with normal number fluctuations ($\sqrt{N}$), because detailed balance now holds. Another numerical study of a simple microscopic model of active nematics [60] identifies the connection between the GNFs in active nematics and the phenomenon of fluctuation-dominated phase ordering [65].

Experiments.– Living melanocytes, the cells which distribute pigment in skin, have been found to show [66] apolar, nematic order as concentration is increased. This type of cells are head-tail symmetric and propel themselves in both way by

rhythmic movement of the cell body as well as two long projections called dendrites. This movement of dendrites and the cell body is also responsible for the inter-cell interaction. Although this experiment can capture the nematic order at higher density regime, but it does not look at the behavior of density fluctuations. Narayan *et al.* [67, 68] performed a systematic study of density fluctuations in a vertically agitated monolayer of head-tail symmetric copper-wire segments. They confirmed the presence of GNFs in the nematic ordered state as predicted in Ref. [58].

1.3.3 Run-and-tumble particles

A broad class of bacteria propel themselves by performing a series of straight-line "runs" and random reorientation in their direction, called "tumbles". Modelling them as run and tumble particles (RTPs) is a big step in understanding active matters. In Ref. [42], Tailleur and Cates introduced both interaction and noise in RTPs to study the many body behavior in one dimension. The model is defined as following. Suppose, the *tumbles* occur stochastically with rate α and the *runs* take place at constant speed v. The master equations for a single RTP in one dimension are given by,

$$\dot{R} = -\partial_x(v_R R) - \alpha R + \alpha L, \tag{1.16}$$

$$\dot{L} = -\partial_x(v_L L) + \alpha R - \alpha L, \tag{1.17}$$

where $R(x,t)$ and $L(x,t)$ the probability of finding a single particle in right moving state and left moving state, respectively, at position x and time t, v_R and v_L the velocity rightward and leftward, respectively. When mean run speed v and tumble rate α depend on the local density ρ, more specifically, v is a decreasing function or mean tumble time $\tau \sim 1/\alpha$ is an increasing function of ρ, they exhibit self trapping, also known as the motility induced phase separation (MIPS), which happens in the *absence* of any attractive microscopic interaction, unlike a passive phase separation which happens in the presence of an attractive interaction between particles.

In two dimension, the similar master equation *i.e.*, the evolution equation of $\mathcal{P}(r,\theta,t)$, the probability of finding a particle at position $\mathbf{r}$ and direction θ at time t will be [40, 43, 53],

$$\partial_t \mathcal{P}(r,\theta,t) = -\nabla.[v\mathbf{u}(\theta)\mathcal{P}(r,\theta,t)] - \alpha\mathcal{P}(r,\theta,t) + \frac{\alpha}{2\pi}\int d\theta' \mathcal{P}(r,\theta',t) \tag{1.18}$$

with self-propulsion direction $\mathbf{u}(\theta) = \{\cos\theta, \sin\theta\}$.

Eq. (1.18) could be coarse grained by using a moment expansion to obtain a Langevin equation for the density field $\rho(\mathbf{r})$ of N interacting RTPs. The interaction is incorporated in the coarsed grained Langevin equation by considering the bulk parameters as function of density field $\rho(\mathbf{r})$. The density $\rho(\mathbf{r})$ then obey the many-body Langevin equation

$$\dot{\rho} = -\nabla.(\mathbf{V}[\rho]\rho - D[\rho]\Delta\rho + (2D\rho)^{1/2}\mathbf{\Lambda}) \tag{1.19}$$

where bulk velocity $\mathbf{V}[\rho] = -v\Delta v/2\alpha$, bulk diffusivity $D[\rho] = v^2/2\alpha$, Λ is white noise with $\langle\Lambda(\mathbf{r},t)\rangle = 0$ and $\langle\Lambda_i(\mathbf{r},t)\Lambda_j(\mathbf{r}',t')\rangle = \delta_{ij}\delta(\mathbf{r}-\mathbf{r}')\delta(t-t')$.

1.3.4 Active Brownian particles

This model was first introduced by Fily and Marchetti in Ref. [31] where they considered two dimensional disks of diameter a as active particles. Each particle is self-propelled by a constant force. The particles are immersed in a medium and confined in a two dimensional periodic square box. The only interaction between active particles is soft repulsive interaction. There is no alignment interaction between particles like in Vicsek model and transmission of torque between particles is also excluded in the model. The particles are polar, *i.e.*, the i^{th} particle propels itself in a direction defined by an axis $\mathbf{u}_i = \{\cos\phi_i, \sin\phi_i\}$. The system evolves in time through the following over-damped Langevin equations [31, 34], for the

positions $\{\mathbf{R}_i(t)\}$

$$\dot{\mathbf{R}}_i = -\beta D_0 \sum_{j \neq i} \nabla U(|\mathbf{R}_i - \mathbf{R}_j|) + v_0 \mathbf{u}_i + \sqrt{2D_0}\vec{\eta}_i^T \tag{1.20}$$

and for the orientations $\{\phi_i(t)\}$ of the velocity vectors

$$\dot{\phi}_i = \sqrt{2D_r}\eta_i^R, \tag{1.21}$$

where $\beta = 1/k_BT$ inverse temperature, $U(|\mathbf{R}_i - \mathbf{R}_j|)$ the soft repulsive interaction potential between i^{th} and j^{th} particle, v_0 self-propulsion speed, D_0 and D_r translational and rotational diffusion constant, respectively. The translational noise $\vec{\eta}^T$ comes from the interaction of the active particles with the medium particles and the rotational noise η^R comes from the random selection of direction by the particle itself. Both the η's are Gaussian white noises with $\langle \eta_i \rangle = 0$ and $\langle \eta_i(t)\eta_j(t') \rangle = \delta_{ij}\delta(t - t')$. Fily and Marchetti in Ref. [31] chose the interaction force $\mathbf{F}_{i,j} = \nabla U(r_{i,j}) \propto (r_{i,j} - 2a)\hat{\mathbf{r}}_{i,j}$ if $r_{i,j} < 2a$ and $\mathbf{F}_{i,j} = 0$ otherwise, with $r_{i,j} = |\mathbf{R}_i - \mathbf{R}_j|$. Choice of the interaction potential $U(r_{i,j})$ varies from model to model like $U(r_{i,j}) \propto \exp(-r_{i,j}^2)$ (Gaussian), $U(r_{i,j}) \propto (r_{i,j} - 1)^2$ (harmonic) and $U(r_{i,j}) \propto \exp(-r_{i,j})/r_{i,j}$ (Yukawa) [33, 35]. The mostly used interaction potential in this model is WCA potential $U(r_{i,j}) = 4\epsilon[(a/r_{i,j})^{12} - (a/r_{i,j})^6] + \epsilon$ if $r_{i,j} < 2^{1/6}a$ and zero otherwise, $\epsilon = \beta^{-1}$, a diameter of the particles [36].

Several groups [31–35, 40, 43, 44, 48, 52, 53] have studied active Brownian particles (ABPs) numerically and analytically in the last few years. All of them have found a phase separation beyond a critical density and velocity with two phases, a homogeneous fluid phase and a clustered phase, independent of the employed pair potential. This system does not exhibit an orientational ordered state as observed in active nematic or Vicsek model. As a signature of active system, *giant number fluctuation* [$\Delta N \sim N^\alpha, \alpha > 0.5$] is also reported [31] in the clustered state of ABPs. But the most interesting result in ABPs is the dynamical instability *i.e.*, the formation of cluster in high velocity and high density limit, in spite of repulsive interaction of particles. The origin of this phenomena is following: particles collide

and block each other when the density is high and form a small cluster. A particle sitting at the boundary of the small cluster need to wait a time $\sim 1/D_r$ to come out of the cluster by turning its axis outward. Now if propulsion speed is high enough so that the collision time is much smaller than that waiting time, then the particle at the periphery will be surrounded by many other particles before leaving the cluster. Thus there would be a flux towards the denser region of the system, resulting in a *motility induced phase separation* (MIPS).

To study ABPs analytically, Fily and Marchetti in Ref. [31] proposed a sets of continuum phenomenological hydrodynamic equation for a density field $\rho(\mathbf{r},t)$ and a polarization density field $\mathbf{p}(\mathbf{r},t)$,

$$\partial_t\rho = -\nabla.\left[v(\rho)\mathbf{p} - D(\rho)\nabla\rho + \mathbf{f}_d\right], \tag{1.22}$$

$$\partial_t\mathbf{p} = -D_r\mathbf{p} - \frac{1}{2}\nabla\left(v\rho\right) + K\nabla^2\mathbf{p} + \mathbf{f}_p, \tag{1.23}$$

where $\rho(\mathbf{r},t) = \sum_i \delta(\mathbf{r} - \mathbf{R}_i(t))$ and $\mathbf{p}(\mathbf{r},t) = \rho(\mathbf{r},t)\mathbf{P}(\mathbf{r},t) = \sum_i \delta(\mathbf{r} - \mathbf{R}_i(t))\mathbf{u}_i(t)$ are coarse-grained number and polarization densities, respectively, at position $\mathbf{r}$ and time t with $\mathbf{R}_i(t)$ and $\mathbf{u}_i(t)$ being position and velocity-direction of the ith particle respectively, $D(\rho)$ bulk diffusion constant, $v(\rho)$ bulk velocity. $\mathbf{f}_d$ and $\mathbf{f}_p$ Gaussian noises with zero mean and correlations $\langle f_{d\nu}(\mathbf{r},t)f_{d\nu'}(\mathbf{r}',t')\rangle = 2\Delta_d\delta_{\nu\nu'}\delta(\mathbf{r}-\mathbf{r}')\delta(t-t')$ and $\langle f_{p\nu}(\mathbf{r},t)f_{p\nu'}(\mathbf{r}',t')\rangle = 2\Delta_p\delta_{\nu\nu'}\delta(\mathbf{r}-\mathbf{r}')\delta(t-t')$, with $\nu,\nu' = 1,2$ denoting Cartesian components. The strengths of the noise terms are not previously known and are characterized later (see section 2.4.2). Using these two coupled nonlinear differential equation, they calculated the static structure factor in the limit of zero thermal diffusion. Later, Bialke *et al.* derived Eqs. (1.22) and (1.23) *without* the noise terms, starting from many body Smoluchowski equation [35]. They calculated the mean force on a tagged particle due to the surrounding particles to explore the effective evolution equation for that tagged particle. This scheme leads to the well known BBGKY hierarchy of coupled equation where the higher order distribution functions depend explicitly on the lower order distribution functions. By finding an approximate closure, they have finally obtained two free parameters entering in the equation: the force coefficient ζ and

the passive long-time diffusion coefficient D. This force coefficient ζ is responsible for the reduction of the effective swimming speed $v = v_0 - \rho_0\zeta$, and hence the origin of the self trapping, leading to a phase separation.

A crystallization in ABPs is found at sufficiently high density *i.e.*, at clustered state for both Yukawa [33] and WCA [34] interaction potential between particles. This freezing, also known as "active solid" is different in nature from that in passive equilibrium crystallization. The structure of this dense phase is characterized by static structure factor of the cluster which found to be a hexagonal lattice structure. The radial distribution function and the bond-orientational order parameter also indicates the active solid a hexatic. The direction of the self-propulsion force changes continuously due to the rotational diffusion which breaks the local force balance, resulting in defect formation in the active solid.

In many respects, MIPS resembles the equilibrium phase separation familiar in passive systems with attractive interaction potential. This apparent similarity has motivated several groups [31, 40, 48, 69] to map a collection of active Brownian particles (ABPs) onto a passive equilibrium system, interacting via an effective attraction. One important attempt made by Speak *et al.* [48] by deriving an effective, equilibrium-like Cahn-Hilliard equation on large length and time scale, starting from a set of coarse grained time evolution equations of density field and polarization field for ABPs. They also found an effective free energy without "*non integrable*" terms, even in the presence of a true activity, by mapping the ABPs onto a system of passive particles governed by attractive force. On the other hand, Farage *et al.* [69] predicted an effective equilibrium potential directly from bare repulsive interaction potential and self-propulsion speed by a systematic theoretical approach, to explain the role of that effective attraction potential in MIPSs.

An attempt has also made by Cates *et al.* [40, 43] to show the equivalence of ABPs and RTPs. ABPs usually swim at a fixed speed v along a body-axis that rotates by slow angular diffusion with a rotational diffusion constant D_r. On the other hand, RTPs reorients themselves by a sudden and random change in

the direction of their body-axis, with a tumbling rate α. By a phenomenological hydrodynamic study, they claim that ABPs and RTPs could be mapped on each other by $D_r(d-1) \leftrightarrow \alpha$, with d be the dimension. The kinetics of phase separation for these model systems has also been studied intensively [34, 46, 70].

Recently, there is a surge of interest in search of a suitable statistical mechanics framework which could describe macroscopic properties of the SPPs in terms of an intensive thermodynamic variable, such as a chemical potential [40–45, 47–49], pressure [50–55] or an effective temperature [56, 57]. Here we overview some of these interesting works. In a recent study in Ref. [50], Brady *et al.* proposed the concept of a swim pressure (somewhat analogous to a mechanical pressure) exerted by active particles on a confining wall. They also provided an expression for the swim pressure from standard mechanics argument, by showing two distinct parts of it: An 'ideal gas' part and an 'inter-particle collisional pressure'. In another study in Ref. [53], Solon *et al.* derived an expression for a mechanical pressure of active Brownian particles on a wall and found the pressure to be dependent on the properties of the confining wall, unlike pressure in equilibrium systems where mechanical and thermodynamic pressures are the same. Therefore, the authors concluded that there is no *equation of state* for active Brownian particles. However, for torque-free (spherical shape) particles, they showed, both for interacting and non-interacting active Brownian particles, there is an equation of state, *i.e.*, the mechanical pressure is wall independent for torque-free particles. Moreover, in a similar study in Ref. [52], Solon *et al.* evaluated this mechanical pressure in a system of torque-free (spherical) active Brownian particles. There, the pressure have three parts: An 'ideal-gas-like pressure' term, similar to perfect gas equation of state; a 'direct' contribution that depends on the interaction between the particles; an 'indirect' contribution, which depends on the coupling between the self-propulsion forces and the particle interaction forces. This third term is thought to be the most crucial one as it results from a collisional slowdown of particles, directly connecting to the MIPS, which is otherwise absent in the passive systems.

However, a complete framework still remains elusive. In this thesis, we propose a general thermodynamic principle, called additivity, which could enable us to unify fascinatingly broad-ranging phenomena in the systems of self-propelled particles under a unique nonequilibrium thermodynamic theory, directly connecting microscopic fluctuations to the macroscopic properties in the system.

1.4 Macroscopic fluctuation theory

In Sec. 1.2, we discussed about the fluctuations in the stationary states in the large size limit. We are now interested in the study of the dynamics of some conserved-mass transport processes in the thermodynamic limit. We would like to introduce a fluctuating hydrodynamics of coarse-grained variables (such as macroscopic mass density ρ or current J) that will depend on space x and time τ. Since mass remains conserved, therefore, the hydrodynamic equation must be written in the form of a continuity equation,

$$\partial_\tau \rho(x,\tau) + \partial_x J(\rho(x,\tau)) = 0. \tag{1.24}$$

Since the process we consider here are of "gradient type" (*i.e.* local diffusive current can be expressed as a gradient in local observables) [19] with respect to their microscopic evolution, one would expect a non-linear hydrodynamics with current $J = J_D + J_d$. The first part $J_D = -D(\rho)\partial_x\rho$ is the diffusive current and the second part $J_d = \chi(\rho)F$ is the drift current due to a small slowly varying biasing field $F(x)$, with bulk diffusion coefficient $D(\rho)$ and conductivity $\chi(\rho)$ be two transport coefficients.

The hydrodynamic Eq. (1.24) along with the current $J(\rho) = -D(\rho)\partial_x\rho + \chi(\rho)F$ governs the time evolution of density field $\rho(x,\tau)$ deterministically. This deterministic hydrodynamic equation tells that the probability to observe a given time evolution, or, path history, of the hydrodynamic variables ρ and J tends to unity in the thermodynamic limit if that time evolution, or, path history satisfies the deterministic hydrodynamic equation and tends to zero otherwise. We are now

interested in a refined result. We would like to evaluate the probability of rare events, when the path history of the coarse-grained variables deviates from the typical evolution governed by the deterministic macroscopic equation. These rare events are shown with an exponentially weak probability in the system size V, giving rise to a large deviation principle. This approach is called the *macroscopic fluctuation theory* (MFT) which we discuss here.

Most importantly, the macroscopic fluctuation theory (MFT), recently developed by Bertini *et al.* [5, 7, 8], can describe the diffusive systems only through two transport coefficients, the bulk diffusion coefficient $D(\rho)$ and the conductivity $\chi(\rho)$ which depend on the local mass density ρ. For stochastic systems that have an equilibrium state as the time stationary state, Bartini *et al.* developed the following approach to evaluate the large deviation probability of observing a macroscopic current and density profile.

For stochastic systems having Markov property, it is in principle possible to bias the system conditioned to its rare configuration [16, 20, 21]. In other words, the non-stationary large deviation current and density of the original unbiased system becomes the typical current and density for the biased one. To quantify the effect of such a bias, they hypothesised that, the system satisfies a local detailed balance condition, *i.e.*, the biased transition rates from one configuration to other mimics an equilibrium-like detailed balance criterion. For instance, we apply a small constant biasing force field $\mathbf{F} = F\hat{x}$ on a system which possess mass transport on a lattice, and perform a linear-response analysis, with $\hat{x}$ being a unit vector along +ve x axis. The original mass transfer rates $c_{i\to j}$, from site i to j, changes to biased rates $c^F_{i\to j}$ which are now effectively asymmetric due to the biasing force $\mathbf{F}$,

$$c^F_{i\to j} = c_{i\to j}\Phi(\Delta e_{ij}). \tag{1.25}$$

$\Phi(\Delta e_{ij})$ is non-negative function of extra energy cost for transferring mass $\Delta m_{i\to j}$ from site i to j in a particular direction with the mass displacement vector $\delta\mathbf{x}_{ij} = (j-i)a\hat{x}$ and a being the lattice constant. Simply the quantity $\Phi(\Delta e_{ij})$ can be

written as,

$$\Phi(\Delta e_{ij}) = \Delta m_{i\to j}(\mathbf{F}.\delta\mathbf{x}_{ij}). \tag{1.26}$$

We further consider the *local detailed balance hypothesis*, the function Φ to have a form $\Phi(\Delta e) = \exp(\Delta e/2)$ [8, 16]. For small force F, we expand Φ in $O(F)$,

$$\Phi(\Delta e_{ij}) \simeq 1 + \Delta e_{ij}\left[\frac{d\Phi}{d(\Delta e)}\right]_{\Delta e=0} = 1 + \frac{1}{2}\Delta m_{i\to j}(\mathbf{F}.\delta\mathbf{x}_{ij}). \tag{1.27}$$

Now, in presence of a weak bias F, the 'typical' current in biased system will have the form given by

$$J(\rho) = -D(\rho)\partial_x\rho + \chi(\rho)F. \tag{1.28}$$

One can interpret the statement that the weak force F is conditioned to a fluctuation of the original (unbiased) system, quantitatively, in the following way. For the unbiased system, the typical current is $J_D = -D(\rho)\partial_x\rho$ and the observed large deviation current is $J(\rho)$. However, this $J(\rho)$ is also the typical current of conditionally biased system which undergoes typical Gaussian fluctuation around this $J(\rho)$, according to the central limit theorem (CLT). Therefore, the joint probability of large fluctuations of macroscopic density and current profiles $\{\rho(x,\tau), J(x,\tau)\}$ in the original (unbiased) system as well as that probability of the typical fluctuations in the biased system is given by (according to CLT)

$$Prob.(\{\rho(x,\tau), J(x,\tau)\}) \approx \exp\left[-\frac{V}{4}\int d\tau \int dx \frac{\big(J(\rho) + D(\rho)\partial_x\rho\big)^2}{\chi(\rho)}\right] \tag{1.29}$$

with V the system size. One can obtain the density profile distribution by integrating out the current in Eq. (1.29) under the constraint of continuity [Eq. (1.24)], and vice versa.

The joint probability distribution of space-time trajectories of density and current in Eq. (1.29) can be alternatively interpreted in a form of stochastic differential

equations (with multiplicative noise) as written below

$$\left.\begin{aligned} \partial_\tau \rho(x,\tau) = &\quad -\partial_x J(\rho(x,\tau)), \\ J(\rho(x,\tau)) = &\quad -D(\rho)\partial_x \rho + \sqrt{\chi(\rho)}\eta(x,\tau), \end{aligned}\right\} \tag{1.30}$$

with $\rho(x,\tau)$ and $J(\rho(x,\tau))$ are the macroscopic density and current, respectively, of the original (unbiased) system. The quantity $\eta(x,\tau)$ is a coarse-grained noise term - Gaussian, white but multiplicative in nature - in the macroscopic current and is characterized by its zero mean and two-point correlation

$$\langle \eta(x,\tau)\eta(x',\tau')\rangle = \frac{2}{V}\delta(x-x')\delta(\tau-\tau'). \tag{1.31}$$

Starting from the stochastic microscopic dynamics, and using the Markov properties of the stochastic time evolution evolution, one can actually prove the *fundamental equation* Eq. (1.29) in macroscopic fluctuation theory [7, 8] in a broad class of models. We can obtain the large deviation functional $\mathcal{F}[\rho(x)]$ of the density profile $\rho(x,\tau)$, $\mathcal{F}[\rho(x)] = \int dx[f(\rho(x)) - f(\rho_0) - \mu(\rho_0)(\rho(x)-\rho_0)$, with ρ_0 being the global density, by integrating over the current variable $J(x,\tau)$ in Eq. (1.30). This procedure leads to a Hamilton-Jacobi equation [8],

$$\int dx \left[\partial_x\left(\frac{\delta\mathcal{F}}{\delta\rho}\right)\chi(\rho)\left(\frac{\delta\mathcal{F}}{\delta\rho}\right) - \frac{\delta\mathcal{F}}{\delta\rho}\partial_x J_D(\rho)\right] = 0, \tag{1.32}$$

the solution of which, along with appropriate boundary conditions, would provide the large deviation function $\mathcal{F}[\rho(x)]$ [or alternatively a free energy function $f(\rho)$] for density. On a periodic boundary, the above equation leads to an equilibrium-like Einstein relation, $f''(\rho) = D(\rho)/\chi(\rho)$, as discussed below. To see this, one needs to perform a partial integration of the second term in Eq. (1.32) to find that Eq. (1.32) is satisfied by the same LDF $\mathcal{F}[\rho(x)]$, satisfying the following conditions,

$$\partial_x\left(\frac{\delta\mathcal{F}}{\delta\rho}\right) = \partial_x\{f'[\rho(x)] - f'(\rho_0)\}, \tag{1.33}$$

$$\frac{1}{f''(\rho)} = \frac{\chi(\rho)}{D(\rho)}, \tag{1.34}$$

with ρ_0 be the global density of the homogeneous system, $D(\rho)$ and $\chi(\rho)$ are two transport coefficients - bulk diffusion coefficient and the conductivity, respectively. Note that the minimization condition of the LDF $\mathcal{F}[\rho(x) = \rho_0] = 0$ and Eq. (1.33) together provides an expression of the LDF, on a periodic boundary, as given below

$$\mathcal{F}[\rho(x)] = \int dx[f(\rho) - f(\rho_0) - f'(\rho_0)(\rho - \rho_0)]. \tag{1.35}$$

Also note that, a fluctuation response relation can be found as in Eq. (1.7) [see Eq. (2.9) for a nonequilibrium fluctuation response relation], from the functional form of the LDF provided by Eq. (1.35), substituting which in Eq. (1.34), one can obtain an equilibrium-like Einstein relation

$$\sigma^2(\rho) = \frac{\chi(\rho)}{D(\rho)}, \tag{1.36}$$

where $\sigma^2(\rho) = lim_{v\to\infty}(\langle m^2\rangle - \langle m\rangle^2)/v$ is defined as the scaled variance of mass m in a large subsystem of volume v.

When a system obeys the *gradient condition*, one can quite easily identify two transport coefficients - bulk diffusion coefficient $D(\rho)$ and the conductivity $\chi(\rho)$, which quite strikingly satisfy the Einstein relation Eq. (1.36). However, analytically calculating transport coefficients $D(\rho)$ and $\chi(\rho)$ as a function of density ρ from the microscopic dynamics of the systems out of equilibrium is usually difficult. In chapter 4, we identify the expressions of $D(\rho)$ and $\chi(\rho)$ in terms of local observables in a class of simple lattice models of active matters, numerically calculate them as a function of ρ and then verify the existence of an equilibrium-like Einstein relation (ER), which connects number-fluctuation, bulk diffusion coefficient and conductivity.

1.5 Outline of thesis

In this Ph. D. thesis, we explore whether a consistent statistical mechanical framework could be constructed for self-propelled particles (SPPs) systems in general.

Provided the answer is in affirmative, this framework could enable one to unify fascinatingly broad-ranging phenomena in the systems of SPPs under a unique nonequilibrium thermodynamic theory. In particular, we study whether SPP systems possess an equilibrium-like additivity property, which could connect microscopic fluctuations to the macroscopic properties of the system.

Previously the framework of additivity has been successfully applied in explaining various phenomena in a broad class of nonequilibrium mass-transport processes, especially in calculating probability distribution of mass in a large subsystem, leading to a thermodynamic characterization of these systems in terms of an equilibrium-like chemical potential and free energy function. We demonstrate here that, in many of the SPP systems, additivity property can indeed be used to obtain density large deviations in terms of an nonequilibrium chemical potential and the fluctuations can be characterized by an Einstein relation, where fluctuations are related to two transport coefficients - bulk diffusion coefficient and conductivity.

We specifically study particle-number fluctuations in a braod class of systems consisting of interacting SPPs having random self-propulsion velocities, such as (i) active Brownian particles (ABPs), (ii) SPPs with Vicsek-like interactions, and (iii) a class of interacting run-and-tumble particles (RTPs) on a periodic one dimensional lattice.

(i) By using an additivity property and a consequent fluctuation-response relation, we formulate a thermodynamic theory for ABPs, which captures quite well the broad features of nonequilibrium phase transitions from a homogeneous fluid phase to an inhomogeneous phase of coexisting gas and liquid, observed in various studies in the past. We substantiate our claims by analytically calculating subsystem particle-number distributions within additivity and then comparing these distributions with tose obtained from simulations of active Brownian particles (ABPs), consisting of repulsive disks (Weeks-Chandler-Anderson interaction potential) with random self-propulsion velocities. Our analysis provides useful insights into the earlier results, e.g., motility induced phase separation (MIPS) in the SPPs.

(ii) We extend the above formalism to Vicsek model (VM) and its two variants, where the systems consist of polar point-particles with alignment interactions. In these cases, we numerically compute subsystem particle-number distributions in the disordered homogeneous fluid-like phase by using additivity property and compare the subsystem particle-number distributions with those obtained from simulations. We find quite striking agreement between additivity theory and simulations, where the theory captures remarkably well the non-Gaussian features observed in the simulations.

(iii) Furthermore, motivated by the above continuum models, we define a class of active lattice gases on a ring with persistent and long-range hopping of particles, which are hardcore in nature. We map these models exactly onto a class of conserved-mass transport processes where hardcore constrain in the original models is removed, leading to a simpler characterization of these processes. Due to lack of detailed balance, the systems are inherently driven out of equilibrium and cannot be described by the Boltzmann-Gibbs distributions. For some of these lattice models, we derive hydrodynamics and calculate two density-dependent transport coefficients - the bulk diffusion coefficient and conductivity. We compare our hydrodynamic theory with simulations. Then, by using the functional form of the two transport coefficients in a recently developed macroscopic fluctuation theory (MFT), we numerically demonstrate that there exists an equilibrium-like Einstein relation (ER), the earliest known form of the fluctuation-dissipation theorems (FDTs) in equilibrium, which connects number-fluctuation, diffusion coefficient and conductivity even in these nonequilibrium systems. At the end, we compare the bulk diffusion coefficients in these lattice models and investigate the role of diffusivity in the dynamical arrest of particles and cluster formation observed in these systems, which is somewhat analogous to motility induced phase separation (MIPS) reported earlier in the literature.

Chapter 2

Additivity, and density fluctuations in active Brownian particles

2.1 Introduction

In this chapter, [1] we attempt to formulate a thermodynamic theory for a particular class of self-propelled particles, called active Brownian particles (ABPs). The two-dimensional system consists of repulsive (essentially "hard") disks, which move with random self-propulsion velocities. In the regime of homogeneous phase, we study subsystem particle-number distribution $P_{\mathcal{V}}(\mathcal{N})$, the probability that a subsystem of volume $\mathcal{V}$ has $\mathcal{N}$ number of particles. The logarithm of the probability $P_{\mathcal{V}}(\mathcal{N})$, called the density large-deviation function (LDF) or nonequilibrium free energy - analogous to equilibrium free energy function, governs the density fluctuations in the system. The nonequilibrium free energy function thus immediately connects to the standard thermodynamic framework of equilibrium system.

[1] The work reported here is based on the paper "Additivity, density fluctuations and nonequilibrium thermodynamics for active Brownian particles", Subhadip Chakraborti, Shradha Mishra, and Punyabrata Pradhan, Phys. Rev. E **93** 052606 (2016).

We also compare the predictions of additivity, regarding the subsystem particle-number distribution $P_{\mathcal{V}}(\mathcal{N})$ (calculated only in the homogeneous fluid phase), with simulations.

The crucial ingredient of this theory is a nonequilibrium fluctuation-response relation (FR) between compressibility and number-fluctuation or variance $\sigma^2_{\mathcal{V}} = \langle \mathcal{N}^2 \rangle - \langle \mathcal{N} \rangle^2$ (see Eq. 2.5), which is a direct consequence of an additivity property. Provided the functional dependence of the variance $\sigma^2_{\mathcal{V}}(\rho)$ on the particle-number density ρ, we provide a prescription of how, using additivity, one can calculate the distribution function $P_{\mathcal{V}}(\mathcal{N})$.

To illustrate the formalism, we first calculate, within a linearized fluctuating hydrodynamics of the ABPs, the variance $\sigma^2_{\mathcal{V}}(\rho)$ of particle-number in a subsystem of volume $\mathcal{V}$ as a function of density ρ. Then, we use the standard large deviation methods to obtain the large deviation function, or a nonequilibrium free energy density function $f(\rho, Pe)$, and a chemical potential $\mu(\rho, Pe)$, as a function of number density ρ and activity parameter Peclet number Pe. Determination of chemical potential leads to a nonequilibrium equation of state - akin to the equilibrium Van der Waals one. Beyond a critical activity, compressibility $d\rho/d\mu$ becomes negative in a particular density interval, leading to nonmonotonic μ as a function of ρ and hence phase coexistence. In special limits, our theory captures various previous results, e.g., those based on the concept of motility induced phase separation (MIPS) [42–44], indicating the formulation here is indeed consistent with the past studies. Moreover, our analysis suggests that, on a mean-field level, a broad class of self-propelled particles belong to Ising universality.

The organization of this chapter is as follows. In section 2.2, we discuss additivity and show how subsystem particle-number distribution can be calculated solely from the knowledge of variance of subsystem particle-number as a function of number density. In section 2.3, we define the model of active Brownian particles and discuss the corresponding fluctuating hydrodynamics. In section 2.4, we calculate, within linearized hydrodynamics, variance of subsystem particle number as a function of density (section 2.4.1) and then characterize noise strengths in

the hydrodynamic equations (section 2.4.2). In section 2.5, using the functional dependence of the variance on density together with additivity, we formulate a thermodynamic theory of active Brownian particles and substantiate the theory by explicitly calculating subsystem particle-number distributions in homogeneous fluid phase of active Brownian particles. Finally, we summarize in section 2.6.

2.2 Framework of additivity

In this section, we discuss an additivity property, which systems having a *finite* correlation length are expected to possess, *irrespective of* whether the systems are *in* or *out* of equilibrium [9–11]. Recently, additivity has been used in nonequilibrium mass-transport processes for calculating mass distributions and characterizing macroscopic properties in terms of equilibriumlike thermodynamic potentials [12, 13]. Below, we discuss how additivity can be used to calculate subsystem particle-number distribution.

First, let us discuss what additivity means in the context of particle-number or density fluctuations in a system. Let us consider N interacting particles in volume V where the total number of particles N is conserved. We divide the system in $\nu = V/\mathcal{V}$ number of identical subsystems, each having volume $\mathcal{V}$, and ask what could be the form of the joint probability distributions for the subsystem particle-numbers $\{\mathcal{N}_i\} \equiv \{\mathcal{N}_1, \mathcal{N}_2, \ldots, \mathcal{N}_\nu\}$. Provided that the subsystem size is much larger than spatial correlation length ξ, $\mathcal{V}^{1/d} \gg \xi$ in d dimensions, additivity implies that the subsystems are statistically almost independent and therefore, to a very good approximation, the joint subsystem particle-number distribution can be written in a product form [9–11],

$$\mathcal{P}[\{\mathcal{N}_i\}] \simeq \frac{\prod_{k=1}^{\nu} W_{\mathcal{V}}(\mathcal{N}_k)}{Z(N,V)} \delta\left(\sum_k \mathcal{N}_k - N\right), \tag{2.1}$$

in the thermodynamic limit of $N, V \to \infty$ with density $\rho = N/V$ fixed. In Eq. 2.1, $W_{\mathcal{V}}(\mathcal{N}_k)$ is an unknown weight factor, which depends on the subsystem particle-number, and will be determined later. The normalization constant, or the partition sum, $Z(N, V)$ in Eq. 2.1 can be written as

$$Z(N,V) = \sum_{\{\mathcal{N}_i\}} \left[\prod_k W_{\mathcal{V}}(\mathcal{N}_k) \right] \delta \left(\sum_k \mathcal{N}_k - N \right). \tag{2.2}$$

In other words, the property that the joint subsystem particle-number distribution $\mathcal{P}[\{\mathcal{N}_i\}]$ for a system can be approximately written as a product, *i.e.*, subsystems are statistically almost independent, of individual subsystem weight factors $W_{\mathcal{V}}(\mathcal{N}_k)$ is called additivity.

In equilibrium, there is a well-defined thermodynamic prescription, which helps us to calculate the weight factor $W_{\mathcal{V}}(\mathcal{N}_k)$; in equilibrium, $W_{\mathcal{V}}(\mathcal{N}_k)$ can in principle be obtained from the Boltzmann distribution. However, there is no such prescription in nonequilibrium. In fact, in nonequilibrium, the difficulty arises precisely here because, in most cases, the microscopic weights of the configurations in nonequilibrium steady state are a priori unknown. At this scenario, additivity, which originates from the simple physical consideration of statistical independence on the coarse-grained level of large subsystems, could help us to bypass the difficulty. As demonstrated recently in [12, 13], characterization of fluctuation properties on a coarse-grained level, one may not actually require to obtain the steady-state weights of all microscopic configurations. In fact, obtaining coarse-grained probability weights on a larger scale (much larger than the microscopic correlation length scale) would suffice to characterize the macroscopic properties of the system, provided that additivity as in Eq. 2.1 holds.

It is important to note that the weight factor $W_{\mathcal{V}}(\mathcal{N}_k)$ depends only on the subsystem particle-number $\mathcal{N}_k$ and subsystem volume $\mathcal{V}$. Now, provided that Eq. 2.1 holds, probability distribution function $P_{\mathcal{V}}(\mathcal{N}) \equiv \text{Prob}[\mathcal{N}_k = \mathcal{N}]$ for large $\mathcal{V}$ can

be written as [9–12],

$$\begin{aligned} P_{\mathcal{V}}(\mathcal{N}) &\simeq W_{\mathcal{V}}(\mathcal{N})\frac{Z(N-\mathcal{N},V-\mathcal{V})}{Z(N,V)} \\ &= \frac{W_{\mathcal{V}}(\mathcal{N})e^{\mu(\rho)\mathcal{N}}}{\mathcal{Z}}, \end{aligned} \tag{2.3}$$

where $\mu(\rho)$ is a nonequilibrium chemical potential,

$$\mu(\rho) = \frac{df}{d\rho}, \tag{2.4}$$

$f(\rho)$ is a nonequilibrium free energy density function with $Z(N,V) \simeq \exp[-Vf(\rho)]$ and $\mathcal{Z} = \sum_{\mathcal{N}} W_{\mathcal{V}}(\mathcal{N}) \exp(\mu\mathcal{N})$ is the normalization constant. Importantly, free energy density function $f(\rho)$, or equivalently the large deviation function (LDF) which controls the density fluctuations, and chemical potential $\mu(\rho)$ can now be obtained from a fluctuation-response relation (FR) between compressibility and fluctuation [9–12],

$$\frac{d\rho}{d\mu} = \sigma^2(\rho), \tag{2.5}$$

where

$$\sigma^2(\rho) = \lim_{\mathcal{V}\to\infty} \frac{(\langle\mathcal{N}^2\rangle - \langle\mathcal{N}\rangle^2)}{\mathcal{V}}, \tag{2.6}$$

the scaled variance of subsystem particle-number $\mathcal{N}$. The above fluctuation-response relation is analogous to the equilibrium fluctuation-dissipation theorem and follows directly from Eq. 2.1; for details, see Appendix A. The explicit expression of chemical potential $\mu(\rho)$ and free energy density function $f(\rho)$ are obtained by integrating Eq. 2.5 w.r.t. density ρ,

$$\mu(\rho) = \int \frac{1}{\sigma^2(\rho)} d\rho + c_1, \tag{2.7}$$

and, upon further integration,

$$f(\rho) = \int \mu(\rho) d\rho + c_2, \tag{2.8}$$

where c_1 and c_2 are arbitrary integration constants. Therefore, the fluctuation-response relation Eq. (2.5) can be rewritten as,

$$\frac{1}{f''(\rho)} = \sigma^2(\rho). \tag{2.9}$$

We now show, following [14, 18], that the weight factor $W_{\mathcal{V}}(\mathcal{N})$ and, consequently, the particle-number distribution can indeed be calculated using the above chemical potential and free energy function. First we write Laplace transform (discrete) of the partition sum $Z(N,V)$ as

$$\begin{aligned}
\tilde{Z}(s,V) &= \sum_{N=0}^{\infty} e^{-sN} Z(N,V) \\
&= \sum_{N=0}^{\infty} e^{-sN} \sum_{\{\mathcal{N}_k\}} \left[\prod_{k=1}^{\nu=\mathcal{V}/V} W_{\mathcal{V}}(\mathcal{N}_k) \right] \delta \left(\sum_k \mathcal{N}_k - N \right) \\
&= \prod_{k=1}^{\nu} \left[\sum_{\mathcal{N}_k=0}^{\infty} e^{-s\mathcal{N}_k} W_{\mathcal{V}}(\mathcal{N}_k) \right] = \left[\tilde{W}_{\mathcal{V}}(s) \right]^{\nu},
\end{aligned}$$

where Laplace transform of the weight factor $W_{\mathcal{V}}(\mathcal{N})$ is written as $\tilde{W}_{\mathcal{V}}(s) = \sum_{\mathcal{N}=0}^{\infty} e^{-s\mathcal{N}} W_{\mathcal{V}}(\mathcal{N})$. Now approximating $\tilde{Z}(s,V) = \sum_{N=0}^{\infty} e^{-sN} Z(N,V) \simeq \int_0^{\infty} dN Z(N,V) e^{-sN}$ where we replace the sum by an integral and then, using $Z(N,V) \simeq \exp[-V f(\rho)]$ (by definition), we get

$$e^{-\nu h_{\mathcal{V}}(s)} \equiv V \int e^{-V[f(\rho)+s\rho]} d\rho \simeq [\tilde{W}_{\mathcal{V}}(s)]^{\nu}.$$

where the function $h_{\mathcal{V}}(s)$ is obtained from Legendre transform of free energy density function,

$$h_{\mathcal{V}}(s) = \mathcal{V}[\mathbf{inf}_{\rho}\{f(\rho) + s\rho\}], \tag{2.10}$$

The weight factor $W_{\mathcal{V}}(\mathcal{N})$ can, in principle, be calculated by evaluating the following integral on the complex s-plane along a suitably chosen contour C: $W_{\mathcal{V}}(\mathcal{N}) = 1/(2\pi i) \int_C \exp[-h_{\mathcal{V}}(s) + \mathcal{N}s] ds$. Although, for finite $\mathcal{V}$, the explicit calculation of the weight factor may be difficult, the calculation, for large subsystem sizes

$\mathcal{V} \gg \xi$, simplifies as the function $-(1/\mathcal{V}) \ln W_{\mathcal{V}}(\mathcal{N})$ is related to $h_{\mathcal{V}}(s)/\mathcal{V}$ by Legendre transformation [18]. Therefore, in leading order of $\mathcal{N} \gg 1$ and $\mathcal{V} \gg \xi^d$, the function $-(1/\mathcal{V}) \ln W_{\mathcal{V}}(\mathcal{N})$ is nothing but the free energy density function $f(\mathcal{N}/\mathcal{V})$, implying

$$W_{\mathcal{V}}(\mathcal{N}) \simeq \exp[-\mathcal{V} f(\mathcal{N}/\mathcal{V})]. \tag{2.11}$$

Consequently, the subsystem particle-number distribution can be written as

$$P_{\mathcal{V}}(\mathcal{N}) \simeq \frac{e^{[-\mathcal{V} f(\mathcal{N}/\mathcal{V}) + \mu(\rho)\mathcal{N}]}}{\mathcal{Z}}, \tag{2.12}$$

where $\mathcal{Z}(\mu, V)$ is the normalization constant.

2.3 Model and fluctuating hydrodynamics

To illustrate our theory in a particular model system of self-propelled particles, we study fluctuations in a system of interacting active Brownian particles (ABPs) in two dimensions (2D). We consider N particles in a $2D$ periodic box of size $V = L \times L$. At time t, the system is specified by position $\mathbf{R}_i(t)$ and self-propulsion direction $\phi_i(t)$ of ith particle with $i = 1, \ldots, N$. The system evolves in time through the following over-damped Langevin equations [34], for the positions $\{\mathbf{R}_i(t)\}$

$$\dot{\mathbf{R}}_i = -\beta D_0 \mathbf{F}_i + v_0 \mathbf{u}_i + \sqrt{2D_0}\vec{\eta}_i^T$$

and for the orientations $\{\phi_i(t)\}$ of the velocity vectors

$$\dot{\phi}_i = \sqrt{2D_r}\eta_i^R,$$

where $\beta = 1/k_B T$ inverse temperature (we set $\beta = 1$), force on ith particle $\mathbf{F}_i = \sum_{j \neq i} \nabla U(|\mathbf{R}_i - \mathbf{R}_j|)$, the WCA interaction potential $U(r) = 4\epsilon[(a/r)^{12} - (a/r)^6] + \epsilon$

if $r < 2^{1/6}a$ and zero otherwise, $\epsilon = \beta^{-1}$, a diameter of the particles, v_0 self-propulsion speed, $\mathbf{u}_i \equiv \{u_{ix}, u_{iy}\} = \{\cos\phi_i, \sin\phi_i\}$ unit vector along instantaneous self-propulsion direction, D_0 and D_r translational and rotational diffusion constant, respectively, and the η's Gaussian white noises with $\langle \eta_i \rangle = 0$ and $\langle \eta_i(t)\eta_j(t')\rangle = \delta_{ij}\delta(t-t')$.

To analytically study particle-number fluctuations in the active Brownian particles, we resort to a fluctuating hydrodynamic description, representing the system on a coarse-grained level. The following hydrodynamic equations, *without* the noise terms, for a density field $\rho(\mathbf{r},t)$ and a polarization density field $\mathbf{p}(\mathbf{r},t)$ has been previously obtained and studied for the active Brownian particles [35, 40, 48],

$$\partial_t \rho = -\nabla.\left[v(\rho)\mathbf{p} - D(\rho)\nabla\rho + \mathbf{f}_d\right], \tag{2.13}$$

$$\partial_t \mathbf{p} = -D_r\mathbf{p} - \frac{1}{2}\nabla\left(v\rho\right) + K\nabla^2\mathbf{p} + \mathbf{f}_p, \tag{2.14}$$

where $\rho(\mathbf{r},t) = \sum_i \delta(\mathbf{r} - \mathbf{R}_i(t))$ and $\mathbf{p}(\mathbf{r},t) = \rho(\mathbf{r},t)\mathbf{P}(\mathbf{r},t) = \sum_i \delta(\mathbf{r} - \mathbf{R}_i(t))\mathbf{u}_i(t)$ are coarse-grained number and polarization densities, respectively, at position $\mathbf{r}$ and time t with $\mathbf{R}_i(t)$ and $\mathbf{u}_i(t)$ being position and velocity-direction of the ith particle respectively, $D(\rho)$ bulk diffusion constant, $v(\rho)$ bulk velocity, $\mathbf{f}_d$ and $\mathbf{f}_p$ Gaussian noises specified below. Note that, to study fluctuations, we have added the noise terms $\mathbf{f}_d$ and $\mathbf{f}_p$ [31] - Gaussian multiplicative noises with zero mean and correlations $\langle f_{d\nu}(\mathbf{r},t) f_{d\nu'}(\mathbf{r}',t')\rangle = 2\Delta_d(\rho)\delta_{\nu\nu'}\delta(\mathbf{r}-\mathbf{r}')\delta(t-t')$ and $\langle f_{p\nu}(\mathbf{r},t) f_{p\nu'}(\mathbf{r}',t')\rangle = 2\Delta_p(\rho)\delta_{\nu\nu'}\delta(\mathbf{r}-\mathbf{r}')\delta(t-t')$, with $\nu,\nu' = 1,2$ denoting Cartesian components. The strengths of the noise terms are not previously known and are characterized later (see section 2.4.2).

When $v(\rho) \neq 0$, the steady-state probability functional $\mathcal{P}[\{\rho(\mathbf{r}), \mathbf{p}(\mathbf{r})\}]$ [75] *neither* has the Boltzmann distribution for the effective probability $\mathcal{P}_d[\{\rho(\mathbf{r})\}] \propto \exp[-\int f[\rho(\mathbf{r})]d^2\mathbf{r}]$ for density, *nor* it is in general known; only in special cases, a strictly local free energy functional $f[\rho(\mathbf{r})]$ can be obtained [42, 43, 49]. However, additivity in Eq. 2.1 requires *neither* the existence of any Boltzmann-like distribution *nor* any prior knowledge of the full steady-state structure; it requires only the existence of a finite correlation length $\xi(\rho)$ (see the relevant length scales $\xi_{0,1,2}$

defined in Eqs. 2.17 and 2.18). When $v = 0$, $\mathcal{P}_d[\{\rho(\mathbf{r})\}]$ can be exactly calculated; for details, see Appendix E.

2.4 Calculation of particle-number fluctuations

2.4.1 Linearized hydrodynamics

As discussed in section 2.2, using the fluctuation-response relation Eq. 2.5, subsystem particle-number distribution $P_{\mathcal{V}}(\mathcal{N})$ for large $\mathcal{V}$ can be determined solely from the variance of particle number, which requires knowledge of only two-point correlation function $c(\mathbf{r}) = \langle\rho(0)\rho(\mathbf{r})\rangle - \langle\rho(\mathbf{r})\rangle^2$. To this end, we transform the variable $\theta(\mathbf{r}, t) = \nabla.\mathbf{p}$ in Eq. 2.14 and, using the standard linear analysis, expand the nonlinear terms in Eqs. 2.13 and 2.14 upto linear order of $\delta\rho$ and $\delta\mathbf{p}$, where $\delta\rho = \rho - \rho_0$, $\delta\mathbf{p} = \mathbf{p} - \mathbf{p}_0$, $\delta\theta = \nabla.(\delta\mathbf{p})$ with ρ_0 and $\mathbf{p}_0 = 0$ average density and polarization fields respectively. Using Fourier transform of $\delta\rho(\mathbf{r}, t)$ and $\delta\theta(\mathbf{r}, t)$ in the linearlized hydrodynamic equations,

$$\delta\tilde{\rho}(\mathbf{q}, \omega) = \int_{\mathbf{r}}\int_{t} e^{-i\mathbf{q}.\mathbf{r}}e^{-i\omega t}\ \delta\rho(\mathbf{r}, t)d\mathbf{r}dt, \tag{2.15}$$

$$\delta\tilde{\theta}(\mathbf{q}, \omega) = \int_{\mathbf{r}}\int_{t} e^{-i\mathbf{q}.\mathbf{r}}e^{-i\omega t}\ \delta\theta(\mathbf{r}, t)d\mathbf{r}dt, \tag{2.16}$$

and proceeding along the lines of Ref. [31], we obtain static structure factor

$$S(\mathbf{q}) = \frac{1}{2\pi}\int_{-\infty}^{\infty}\langle|\delta\tilde{\rho}(\mathbf{q}, \omega)|^2\rangle d\omega \equiv S_1(q) + S_2(q),$$

where

$$S_1(q) = \frac{V\Delta_d(\Sigma_1)^2}{\mathcal{D}\Sigma_0\Sigma_2} + \frac{V\Delta_d q^2}{D_r\Sigma_2}, \tag{2.17}$$

$$S_2(q) = \frac{V\Delta_p v^2}{D_r^2\mathcal{D}\Sigma_0\Sigma_2}, \tag{2.18}$$

an effective diffusivity $\mathcal{D}(\rho) = D + v\alpha/D_r$, $\alpha(\rho) = (v + \rho dv/d\rho)/2$, $\Sigma_{0,1,2}(q) = (1 + q^2\xi_{0,1,2}^2)$ and correlation lengths $\xi_0(\rho) = \sqrt{DK/D_r\mathcal{D}}$, $\xi_1 = \sqrt{K/D_r}$ and

$\xi_2 = \sqrt{(D+K)/D_r}$; for details, see Appendix B. Now the variance $\sigma^2_{\mathcal{V}}(\rho) = \langle \mathcal{N}^2 \rangle - \langle \mathcal{N} \rangle^2$ of particle-number $\mathcal{N} = \int_{\mathcal{V}} \rho(\mathbf{r}) d^2\mathbf{r}$ in a subvolume $\mathcal{V}$ can be written as integrated correlations, $\sigma^2_{\mathcal{V}}(\rho) = \int_{\mathcal{V}} c(\mathbf{r}) d^2\mathbf{r} = S(\mathbf{q}=0)$. By defining a scaled variance $\sigma^2(\rho) = \sigma^2_{\mathcal{V}}/\mathcal{V}$, we finally obtain the variance, albeit within an approximate linearized analysis,

$$\sigma^2(\rho) = \left[\frac{\Delta_d}{\mathcal{D}} + \frac{\Delta_p v^2}{D_r^2 \mathcal{D}} \right], \tag{2.19}$$

which can be related to compressibility $(d\rho/d\mu)$ through the fluctuation-response relation Eq. 2.5. The above linear analysis, though approximate, is expected to be valid in the regime of small fluctuations, i.e., far away from criticality. A similar expression for structure factor was previously obtained in [31], though without the part $S_1(\mathbf{q})$ and without any characterization of the noise strengths Δ_d and Δ_p. The functional dependence of the noise strengths Δ_d and Δ_p on density ρ and self-propulsion speed v_0 will be determined later in 2.4.2. Note that, in r.h.s. of Eq. 2.19, effective diffusivity $\mathcal{D}(\rho)$ appears in denominators of both the terms, which could vanish for suitable parameter values; consequently, both $S_1(\mathbf{q}=0)$ and $S_2(\mathbf{q}=0)$ can separately diverge.

There are two interesting limiting cases of Eq. 2.19, which consistently capture various previous results obtained in the context of motility induced phase separation (MIPS) in self-propelled particles.

Case I. To see that $S_1(\mathbf{q})$ in Eq. 2.19 can have nontrivial effects, we consider the case when the polarization noise vanishes, $\Delta_p = 0$. In that case, the above linear analysis implies that $S_1(0)$ diverges at a critical density, for any Δ_d, whenever $\mathcal{D} = 0$ ($\mathcal{D} < 0$ corresponds phase coexistence) depending on the functional form of $v(\rho)$. This explains why, in the quasistatic case of $\mathbf{p}$ where $\partial_t \mathbf{p} = 0$, $K = 0$ and $\Delta_p = 0$ in Eq. 2.14, the variance $\sigma^2(\rho) \simeq [1/\rho + (1/v)(dv/d\rho)]^{-1}$ obtained from Eq. 2.19 by choosing $\Delta_d = (D + v^2/2D_r)\rho$ as in [42] and assuming $D \ll v^2/2D_r$ (large velocity regime), can be diverging (for details, see Appendix D). Because, chemical potential $\mu(\rho) = \ln(\rho v) + c_1$, obtained using the fluctuation-response relation Eq. 2.5, has a singularity at the critical point where $dv/d\rho = -v/\rho$ and consequently

compressibility $d\rho/d\mu = (d^2f/d\rho^2)^{-1}$ diverges; the spinodal line is provided by the condition $d^2f/d\rho^2 < 0$, which is consistent with the previous observations in various systems of self-propelled particles [42, 49, 52].

Case II. On the other hand, in the absence of density noise, $\Delta_d = 0$ [31], only the second term in the r.h.s. of Eq. 2.19 contributes to

$$\sigma^2(\rho) = \frac{2\Delta_p^0}{D_r}\left[\frac{D}{\rho v^2} + \left(\frac{1}{\rho} + \frac{1}{v}\frac{dv}{d\rho}\right)\right]^{-1} \tag{2.20}$$

as, from the central limit theorem (CLT), the polarization noise strength $\Delta_p \simeq \Delta_p^0\rho$ is proportional to the number of particles present in unit volume (for details, see Appendix C). Integrating fluctuation-response relation Eq. 2.5, we obtain $\mu(\rho) = \ln(\rho v)+\psi(\rho)+c_1$ and $f(\rho) = \int \mu(\rho)d\rho = \rho(\ln\rho-1)+\int^\rho[\ln v(\rho)+\psi(\rho)]d\rho+c_1\rho+c_2$ where $\psi'(\rho) = D/\rho v^2$ and c_1 and c_2 arbitrary constants of integration. Indeed, the above expressions of $\mu(\rho)$ and $f(\rho)$ are quite similar to those obtained for the MIPS in the self-propelled particles (see Case I).

2.4.2 Noise-strengths and fluctuations

The main difficulty to relate fluctuating hydrodynamic equations 2.13 and 2.14 to the microscopic model of active Brownian particles lies in the fact that the noise strengths Δ_d and Δ_p, bulk diffusion constant D and bulk velocity v could depend on density ρ, self-propulsion velocity v_0 (even function of v_0) and possibly on the norm $|\mathbf{p}|$, but their functional forms are not explicitly known. In fact, a systematic derivation of the noise strengths from a microscopic dynamics is a difficult problem and, so far, has not achieved for the active Brownian particles.

In this section, we characterize strengths of the noises in the hydrodynamic equations 2.13 and 2.14, in the leading order of self-propulsion velocity v_0, i.e., when activity is low. To this end, we resort to a near-equilibrium analysis, which, we see later in simulations, however holds surprisingly well even far away from equilibrium where self-propulsion velocity, or the activity, is quite large. We first note that equilibrium compressibility of two-dimensional hard-disk fluid, known

through virial coefficients [76], has an approximate analytic form [77],

$$\left[\sigma^2(\rho)\right]_{v_0=0} = \frac{\Delta_d}{D} \simeq \rho\left(1-\frac{\rho}{\rho_m}\right)^2, \tag{2.21}$$

where $\rho_m \approx 1.15$ close-packing density. Now, we expand Δ_d in the leading order of self-propulsion velocity v_0,

$$\Delta_d(\rho, v_0) \simeq (\Delta_d^0 + \Delta_d^1 v_0^2)\rho\left(1-\frac{\rho}{\rho_m}\right)^2 \tag{2.22}$$

and write $D \simeq D_0$ where Δ_d^0, Δ_d^1 and D_0 are all constants (though not independent). These approximations may be the simplest possible ones, but they are quite good in describing the fluctuations in the active Brownian particles, as supported later in the simulations. As the relation in Eq. 2.21 must be satisfied in the equilibrium limit of $v_0 = 0$, we have $\Delta_d^0/D_0 = 1$. The dependence of D, Δ_d and Δ_p on the norm $|\mathbf{p}|$ is ignored as orientation order $\langle\mathbf{p}\rangle = 0$ throughout remains absent and the polarization fluctuation is expected to be small. Moreover, the polarization noise strength Δ_p, to a good approximation, is expected to have a linear dependence on density,

$$\Delta_p \simeq \Delta_p^0\rho, \tag{2.23}$$

where Δ_p^0 is a constant. This is because the fluctuation $\sigma_{p_x}^2 = \langle p_x^2\rangle - \langle p_x\rangle^2 \sim 2\Delta_p/D_r$ in the x component of polarization density $\mathbf{p}$ can be written as $\sigma_{p_x}^2 = \rho[\langle u_{ix}^2\rangle - \langle u_{ix}\rangle^2] \propto \rho$ (similarly for the y component) where u_{ix} is the x-component of the orientation unit-vector of ith particle and therefore $\Delta_p \propto \rho$ (for details, see Appendix C). Therefore, the scaled variance as in Eq. 2.19 can be written as given below,

$$\begin{aligned}\sigma^2(\rho) &= \left[\frac{(\Delta_d^0 + \Delta_d^1 v_0^2)\rho(1-\lambda\rho)^2}{\mathcal{D}} + \frac{\Delta_p^0\rho v^2}{D_r^2\mathcal{D}}\right] \\ &= \frac{(\Delta_d^0 + \Delta_d^1 v_0^2)D_r^2\rho(1-\lambda\rho)^2 + \Delta_p^0\rho v^2}{D_r^2\mathcal{D}}.\end{aligned} \tag{2.24}$$

Now, using the previous results for the bulk velocity in the active Brownian particles, $v(\rho) \simeq v_0(1-\lambda\rho)$ [35, 48] with $1/\lambda = \rho_m$ close-packing density, in Eq. 2.19,

effective diffusivity in the above equation can be written as

$$\mathcal{D} = D_0 + \frac{v\alpha}{D_r} = D_0 \left[1 + \frac{v_0^2(1-\lambda\rho)(1-2\lambda\rho)}{2D_r D_0}\right],$$

where $\alpha = (1/2)\left[v(\rho) + \rho dv/d\rho\right] = (v_0/2)[1-2\lambda\rho]$. Therefore, the scaled variance in Eq. 2.24 can be written as

$$\begin{aligned} \sigma^2(\rho) &= \rho_m \frac{(A+BP)x(1-x)^2}{1+P(1-x)(1-2x)} \\ &= \rho_m \frac{(1+A_1 v_0^2+BP)x(1-x)^2}{1+P(1-x)(1-2x)} \end{aligned} \tag{2.25}$$

where $x = \lambda\rho = \rho/\rho_m$ is scaled density, the dimensionless parameters A, A_1 and B are defined as

$$A = (1 + A_1 v_0^2); \quad A_1 = \frac{\Delta_d^1}{\Delta_d^0}; \quad B = \frac{2\Delta_p^0}{D_r}, \tag{2.26}$$

and the dimensionless scaled activity parameter

$$P = \frac{v_0^2}{2D_r D_0}. \tag{2.27}$$

It is customary to define another dimensionless parameter, called activity parameter or Peclet number, $Pe = v_0\tau/a$, where the microscopic diffusive time scale $\tau = a^2/D_0$. Now, using a near-equilibrium linear-response relation $D_r = cD_0/a^2$ between the orientation (or the polarization) relaxation rate and the translational diffusion constant [78], we express P in terms of Pe,

$$P \simeq \frac{Pe^2}{2c}, \tag{2.28}$$

where c is a proportionality constant and can be estimated from simulations (see Fig. 2.2(a) and the corresponding discussions later).

At low activity regime $Pe \ll 1$, one can actually reduce the number of parameters in Eq. 2.25, from A_1, B and P to essentially a single parameter P, using a constraint these parameters A_1, B and P must satisfy. It is not difficult to see

that, at low density $x = \rho/\rho_m \to 0$, the particle-number distribution $P_{\mathcal{V}}(\mathcal{N}) = \exp(-\langle\mathcal{N}\rangle)\langle\mathcal{N}\rangle^{\mathcal{N}}/\mathcal{N}!$, for any self-propulsion v_0, must be Poissonian (verified in simulations; see Fig. 2.3). Therefore, the variance at low density must satisfy the constraint $\sigma^2(\rho) = \rho$, implying

$$A_1 v_0^2 + BP = P, \tag{2.29}$$

or $A_1 = (1-B)/2D_rD_0$. Note that Eq. 2.29 is exact in the leading order of self-propulsion velocity v_0. Using Eq. 2.29 in Eq. 2.25, we finally obtain the scaled variance as a function of scaled density $x = \rho/\rho_m$,

$$\sigma^2(\rho) = \rho_m \frac{(1+P)x(1-x)^2}{1+P(1-x)(1-2x)}, \tag{2.30}$$

which essentially represents a one-parameter family of curves (see $\sigma^2(\rho)$ as a function of ρ for various P in Fig. 2.1) with the scaled activity parameter $P \simeq Pe^2/2c$ as in Eq. 2.28. Interestingly, as we find below in the simulations of the active Brownian particles, the form of the variance in Eq. 2.30 indeed captures quite well the broad features of particle-number fluctuations even when activity is moderately large $Pe \gg 1$.

Now we show, using the form of the scaled variance in Eq. 2.30, how the scaled activity parameter P can be estimated from the simulations of the active Brownian particles. This is done essentially by fitting Eq. 2.30 for a suitable choice of the fitting parameter P. In Fig. 2.1, we plot scaled variance σ^2 as a function of $x = \rho/\rho_m$, obtained from simulations for various $Pe = 0$ (magenta triangles), 5 (blue squares), 10 (sky-blue diamonds), 20 (green inverted triangles), 50 (red circles) and 100 (black left-triangles), and then fit the curves with Eq. 2.30 by suitably choosing $P \approx 0$ (magenta dashed line), 0.5 (blue dashed double-dotted line), 2.0 (sky-blue dotted line), 4.3 (green double-dashed dotted line), 8.0 (red solid line) and 10 (black dashed dotted line), respectively. To find the dependence of P on Pe, we numerically calculate P as a function of Pe, by solving for P where we use a particular value of scaled density x and variance σ^2 in Eq. 2.30. In Fig. 2.2(a), we plot P as a function of Pe, for a set of two densities $\rho = 0.26$

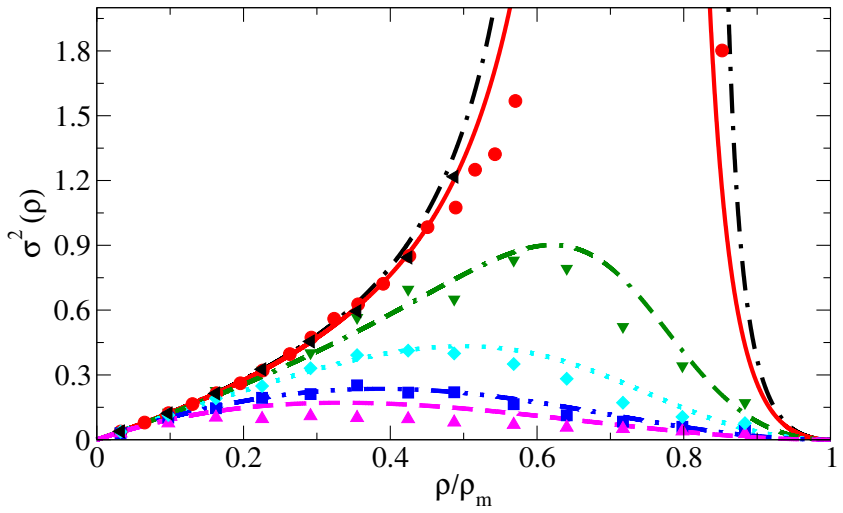

FIGURE 2.1: Simulations in the active Brownian particles. Scaled variance σ^2, for $Pe = 0$ (magenta triangles), 5 (blue squares), 10 (sky-blue diamonds), 20 (green inverted triangles), 50 (red circles) and 100 (black left-triangles), as a function of scaled density ρ/ρ_m, with $\rho_m \approx 1.15$, is compared with Eq. 2.30 with $P \approx 0$ (magenta dashed line), 0.5 (blue dashed double-dotted line), 2.0 (sky-blue dotted line), 4.3 (green double-dashed dotted line), 8.0 (red solid line) and 10 (black dashed dotted line), respectively. Points - simulations, lines - theory.

(green circles) and 0.34 (red squares). The function fits quite well with the form $P \simeq Pe^2/(2c+\kappa Pe^2)$ [see the black solid line in Fig. 2.2(a)] where $c \approx 9$, implying a somewhat larger coarse-grained relaxation rate D_r for the polarization field than that estimated previously [34], and $\kappa \approx 0.1$. In other words, at smaller activity regime $Pe \lesssim 20$, the scaled activity parameter $P \simeq (Pe)^2/2c$ varies quadratically with Pe as in Eq. 2.28. However, for very large activity $Pe \gtrsim 20$, as discussed above, the scaled activity parameter $P \simeq 1/\kappa$ eventually saturates.

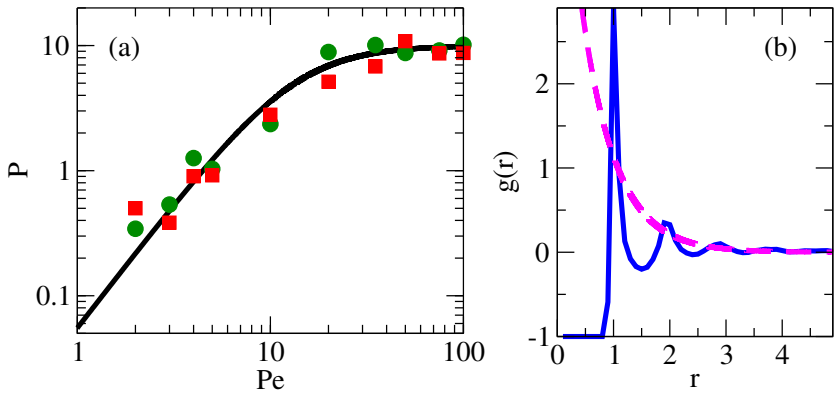

FIGURE 2.2: Panel (a): The scaled activity parameter P (as defined in Eq. 2.30) is plotted as a function of Peclet number Pe for densities $\rho \approx 0.26$ (green circles) and 0.34 (red squares). Panel (b): Pair correlation $g(r)$ (blue solid line) is plotted as a function of distance r for density $\rho \approx 0.5$ and $Pe = 50$; the magenta dashed line (fitting function) shows an exponential decay of the pair correlation function at large distance, with correlation length $\xi \sim 1$ (distance is in unit of diameter a of the particles). Points - simulations, lines - theory with fitting parameter.

2.5 Additivity and nonequilibrium thermodynamics

2.5.1 Chemical potential and free energy function

In this section, we calculate, using the analytic form of the variance in Eq. 2.30, nonequilibrium chemical potential $\mu(\rho)$ and free energy density function $f(\rho)$. We use the fluctuation-response relation Eq. 2.5, change the density variable ρ to a scaled density $x = \rho/\rho_m$ and integrate w.r.t. the scaled density x,

$$\frac{d\rho}{d\mu} = \sigma^2(\rho) \Rightarrow \frac{dx}{d\mu} = \frac{(1+P)x(1-x)^2}{1+P(1-x)(1-2x)}, \tag{2.31}$$

to obtain nonequilibrium chemical potential as a function of the scaled density x,

$$\mu(x) = \frac{1}{1+P}\left[(P-1)\ln(1-x) + (P+1)\ln x + \frac{1}{1-x}\right]$$

which, upon substituting $x = \rho/\rho_m$, gives chemical potential as a function of density ρ

$$\mu(\rho) = \frac{1}{1+P}\left[(P-1)\ln(1-\frac{\rho}{\rho_m}) + (P+1)\ln(\frac{\rho}{\rho_m}) + \frac{1}{1-\frac{\rho}{\rho_m}}\right]. \tag{2.32}$$

Now, integrating chemical potential $\mu(\rho)$ w.r.t. density ρ, we get free energy density function

$$\begin{aligned} f(\rho) &= \int \mu d\rho = \rho_m \int \mu(x) dx \\ &= \rho_m \frac{[P(x-1)-x]\ln(1-x) + x[(P+1)\ln x - 2P]}{1+P}, \end{aligned} \tag{2.33}$$

which has the dimension of density and, upon substituting $x = \rho/\rho_m$, gives free energy density as a function of density ρ.

2.5.2 Subsystem particle-number distributions

Nonequilibrium free energy density function in Eq. 2.33, being a large deviation function, and nonequilibrium chemical potential in Eq. 2.32, together, govern the particle-number fluctuation in the system. Therefore, based on the analytical result of subsystem particle-number distribution in Eq. 2.12 which can be explicitly calculated now using Eqs. 2.30, 2.32 and 2.33 (see section 2.2), we finally test in this section the predictions of additivity concerning density fluctuations in actual simulations of the active Brownian particles. The simulations are performed in the fluid phase, which is much away from criticality, where Eq. 2.30 is expected to hold.

In simulations, we calculate subsystem particle-number distributions $P_{\mathcal{V}}(\mathcal{N})$ in a subsystem ($\mathcal{V} = 9 \times 9$ in units of a) where the rest of the system ($V = 100 \times 100$) acts as a particle *reservoir* of chemical potential $\mu(\rho)$. In Fig. 2.2(b), we plot pair-correlation function $g(\mathbf{r}) = \sum_{i\neq 1}\langle\delta(\mathbf{r} - \mathbf{R}_i(t))\rangle$ as a function of distance r at a moderately high density $\rho \approx 0.5$ and $Pe = 50$ where correlation length

$\xi \sim \mathcal{O}(a)$, much smaller than the subsystem size. In Fig. 2.3, subsystem number-distributions $P_{\mathcal{V}}(\mathcal{N})$ obtained from simulations (points) at $Pe = 50$ are compared with theory Eq. 2.12 (lines) at the corresponding scaled activity $P = 8$, for several densities $\rho \approx 0.11$ (black circles, black dashed line), 0.19 (red triangles, red dashed double-dotted line), 0.26 (magenta diamonds, magenta dotted line), 0.34 (green inverted triangles, green doubled-dashed dotted line), 0.41 (blue squares, blue solid line) and 0.56 (violet asterisks, violet dashed dotted line). Agreement between simulations and theory, even at quite large density $\rho \approx 0.41$, is reasonably good. Note that, provided the variance $\sigma^2(\rho)$ as a function of density ρ (as in Eq. 2.30), there is no fitting parameter in the distribution functions $P_{\mathcal{V}}(\mathcal{N})$ plotted in Figs. 2.3 and 2.4. Expectedly, the distributions are Poissonian at low densities. However, the distributions become increasingly non-Poissonian, or non-Gaussian, with increasing density and activity. To emphasize this point, in Fig. 2.4, we show that, for moderately large density $\rho \approx 0.41$ and large activity $Pe = 50$, the particle-number distribution function $P_{\mathcal{V}}(\mathcal{N})$ in simulations (blue squares) indeed deviates from the corresponding Poisson (black dashed double-dotted line) as well as Gaussian (red dashed line) distributions. Even then, the numerically obtained distribution (blue diamonds) is indeed quite well described by the analytically obtained distribution Eq. 2.12 (blue solid line), thus validating additivity, at least in the homogeneous fluid phase which is sufficiently away from criticality.

However, upon approaching closer to the criticality, some discrepancies arise between analytic theory and simulations, presumably due to the linear analysis of Eqs. 2.13 and 2.14 and finite-size effects. That the linear analysis breaks down at density $\rho \approx 0.56$ is evident from Fig. 2.1 where simulation results (for $Pe = 50$) start deviating from the analytic expressions of Eq. 2.30 (for corresponding $P = 8$). On the other hand, the finite-size effects originate from the facts that the boundary correlations between subsystem and system (due to increasing correlation length) increase while approaching criticality and the ratio between system and subsystem as well as their individual sizes are finite.

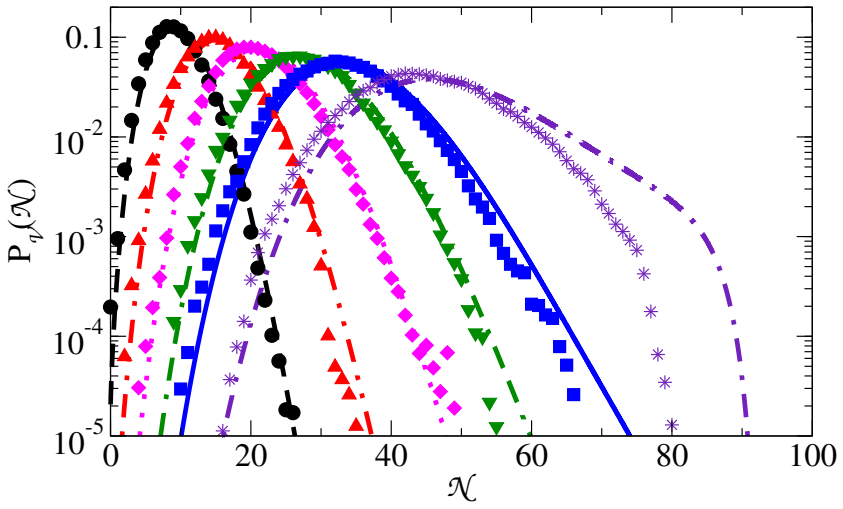

FIGURE 2.3: Subsystem particle-number distributions for activity parameter $Pe = 50$, obtained from simulations (points), are compared with theory Eq. 2.12 (lines) with corresponding scaled activity parameter $P = 8$, for densities $\rho \approx 0.11$ (black circles, black dashed line), 0.19 (red triangles, red dashed double-dotted line), 0.26 (magenta diamonds, magenta dotted line), 0.34 (green inverted triangles, green doubled-dashed dotted line), 0.41 (blue squares, blue solid line) and 0.56 (violet asterisks, violet dashed dotted line).

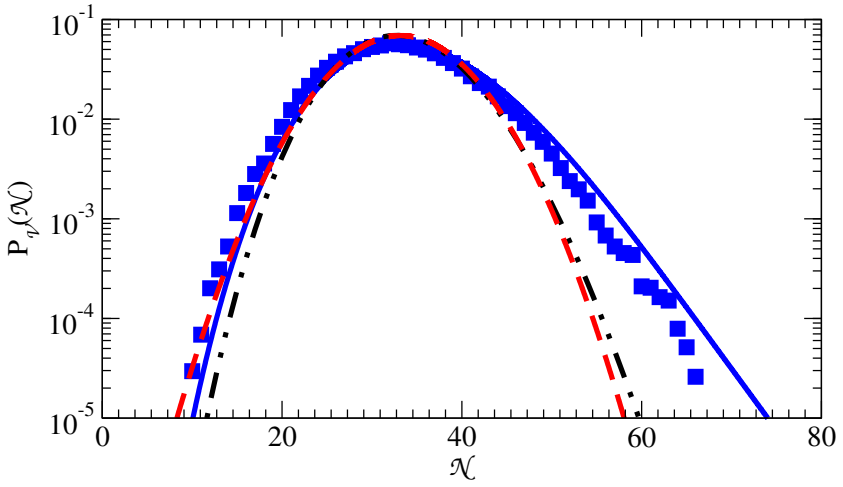

FIGURE 2.4: At moderately large density $\rho \approx 0.41$ and large activity $Pe = 50$, subsystem particle-number distribution $P_\mathcal{V}(\mathcal{N})$ (blue squares), which deviates from Poisson (black dashed double-dotted line) as well as Gaussian (red dashed line) distributions, is quite well captured by theory Eq. 2.12 (blue solid line).

2.5.3 Phase transition

Based on the analysis in the previous sections, one can now formulate a theory of phase transition in the active Brownian particles. We note that the functional form of the scaled variance as in Eq. 2.30 has many interesting implications. In the regime of large activity where Peclet number $Pe \gg 1$ (or $P \gg 1$), the scaled variance $\sigma^2(\rho)$ is independent of P, which is in quite good agreement with simulations (see Fig. 2.1 for $Pe = 50$ and 100) where σ^2 for any ρ almost saturates at large Peclet number. Moreover, the denominator in Eq. 2.30 has two roots

$$x_{2,1} = \frac{3}{4} \pm \frac{\sqrt{P^2 - 8P}}{4P}.$$

In Fig. 2.5(a), we plot the scaled variance (as in Eq. 2.30) and, in Fig. 2.5(b), chemical potential (as in Eq. 2.32) as a function of scaled density $x = \rho/\rho_m$, with $\rho_m \approx 1.15$, for various values of scaled activity $P = 0$, 1, 2, 4, 8, 12 and 15. Below a critical value of the scaled activity $P < P_c = 8$ (corresponding to activity $Pe = 50$ in actual simulations), the variance remains positive in the full interval $0 \leq x \leq 1$. On the other hand, above a critical value of scaled activity $P > P_c$, the variance becomes negative in the interval $x_1 < x < x_2$ and consequently chemical potential becomes nonmonotonic function of density, which is *not* physical and implies onset of phase coexistence. The coexisting densities can, in principle, be calculated using a Maxwell construction on chemical potential $\mu(\rho) = \int^\rho 1/\sigma^2 d\rho$ (Eq. 2.32) or on free energy density function $f(\rho) = \int^\rho \mu d\rho$ (Eq. 2.33). Presently, the Maxwell construction is however not expected to give an accurate estimate of the coexisting densities as our theory (Eq. 2.30 and consequent expressions in Eqs. 2.32 and 2.33) have been derived using a linearized hydrodynamics and a near-equilibrium analysis, which do not capture well the fluctuations in the high activity regime.

Somewhat surprisingly, our theory however predicts quite accurately the critical density ρ_c where compressibility $d\rho/d\mu$ diverges; $\rho_c \approx 0.86$, or critical packing fraction $\phi_c \approx 0.7$, obtained from theory is in excellent agreement with simulations [34]. Moreover, we find that compressibility diverges as $d\rho/d\mu = \sigma^2 \sim 1/(\rho -$

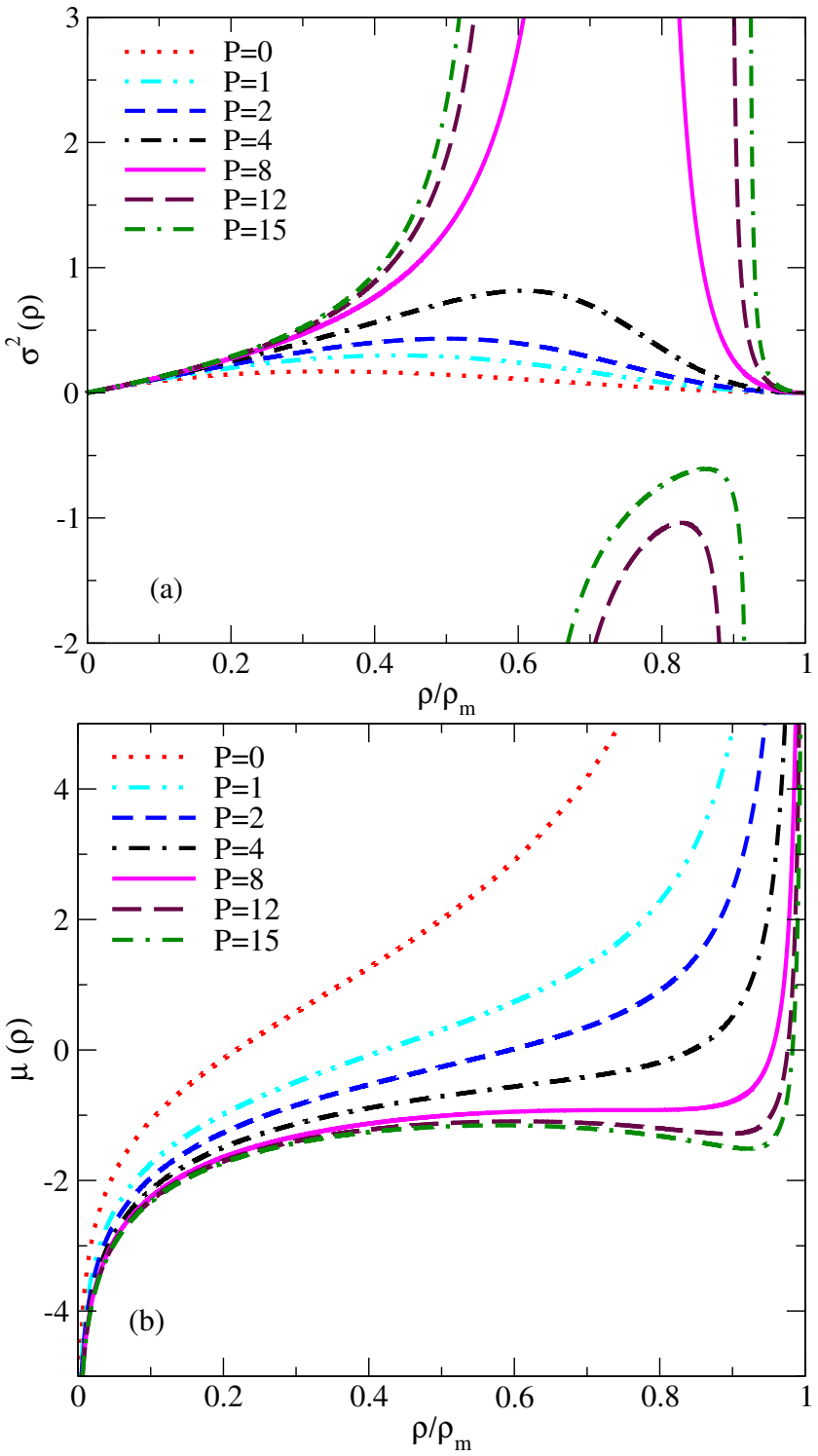

FIGURE 2.5: Scaled variance $\sigma^2(\rho)$ (Eq. 2.30) and corresponding chemical potential $\mu(\rho) = \int^{\rho} 1/\sigma^2 d\rho$ (Eq. 2.32) are plotted in panels (a) and (b), respectively as a function of the scaled density ρ/ρ_m for various values of the scaled activity parameter $P = 0$, 1, 2, 4, 8, 12 and 15. Chemical potential becomes a nonmonotonic function of density beyond a critical value of the scaled activity parameter, $P > P_c = 8$.

$\rho_c)^{\delta-1}$, or equivalently chemical potential vanishes as $\mu \sim (\rho - \rho_c)^{\delta}$, with $\delta = 3$; correlation length diverges as $\xi \sim (\rho - \rho_c)^{-\nu_h}$ with mean-field $\nu_h = 1$. Clearly, on the mean-field level, the exponents are in accordance with Ising universality; P and μ are analogous to temperature and magnetic field, respectively.

2.6 Summary and concluding perspective

In this chapter, using a nonequilibrium fluctuation-response relation - a direct consequence of an additivity property, we formulate a thermodynamic theory for self-propelled particles in the context of a particular model system consisting of active Brownian particles. From the fluctuation-response relation, we demonstrate that subsystem particle-number distributions, which, being related to the density large deviation function and thus analogous to equilibrium free energy, can help us to characterize macroscopic properties in self-propelled particles, in a unified statistical mechanics framework, in terms of a nonequilibrium chemical potential. Analogous to phase transition in equilibrium, as density and activity (Peclet number) increase, chemical potential becomes nonmonotonic function of density, indicating onset of a gas-liquid phase coexistence.

Importantly, the formalism developed here is solely based on characterization of the variance of subsystem particle number, which is directly related to the two-point (equal-time) density correlations or the structure factor. Provided that one calculates the structure factor accurately, our theory can lead to verifiable predictions concerning the density fluctuations. However, analytically calculating structure factor in a many-particle system is not an easy task. To this end, in the first step, we have calculated, though within a linearized fluctuating hydrodynamics, the structure factor in a microscopic model system of active Brownian particles and, consequently, the variance of subsystem particle-number as a function of density. Our studies of fluctuating hydrodynamics provide some insights in characterizing the noises in the hydrodynamic equations, done in the context of active Brownian particles. For this purpose, we have used a near-equilibrium

analysis, which, though approximate, captures reasonably well the broad features of the particle-number fluctuations even in the far-from-equilibrium regime where activity is moderately large.

Furthermore, in the second step, from the functional dependence of the variance of subsystem particle-number on density and then using additivity, we have calculated the subsystem particle-number distribution function and have compared the analytically obtained distribution functions with that obtained from simulations in the active Brownian particles. The agreement between theory and simulations is quite good, except some deviations at the tails. The deviations increase while approaching criticality, indicating the following reasons for these deviations. Firstly, the linear analysis used here breaks down in the regime of high densities and the high activities, where nonlinear effects can induce nontrivial fluctuations; consequently, chemical potential and free energy function obtained from the linear analysis cannot capture the density fluctuations well. Secondly, there can be significant finite-size effects, originating from the increasing boundary correlations between subsystem and system upon approaching criticality and due to the finite ratio between system and subsystem (simulations here are performed upto total particle number $N > 10^4$ and roughly for ratio $1 : 123$ between subsystem and system volumes). Thus, larger scale simulations, though computationally difficult at this stage, would be quite useful for more accurate verification of the predictions of additivity.

For simplicity, here we have restricted ourselves to a particular model system of active Brownian particles. However, the thermodynamic formalism developed here is quite general and could be extended to other active-matter systems, e.g., models with run-and-tumble Bacterial dynamics or Vicsek model [71] and its variants. Moreover, even in the active Brownian particles, it would be quite interesting, though challenging, to go beyond the linear hydrodynamic regime by allowing nonlinear gradient terms (as in [45]) or self-advective terms (as in [71, 74]), which may be relevant in the large activity regime where fluctuations are large.

From the overall perspective, we believe additivity could be the missing link, providing a unified characterization of a broad range of phenomena in the self-propelled particles observed in the past. Also, it will be interesting to explore if additivity holds in the phase with "giant number" fluctuations which many self-propelled particle systems exhibit or in the presence of inhomogeneities, e.g., a confining potential as in a box with hard walls [53], etc.

Chapter 3

Additivity and density fluctuations in Vicsek-like models

3.1 Introduction

In this chapter, we study particle-number fluctuations in another class of model systems of self-propelled particles, namely Vicsek model and two of its variants. The systems consist of point polar particles with alignment interactions and random self-propulsion velocities. The self-propulsion mechanism of the polar particles makes the systems driven out-of-equilibrium, violating detailed balance. Throughout the past several decades, a lot of effort has been made in developing a thermodynamic structure in active-matter systems. However, constructing a suitable statistical mechanics framework in these inherently out-of-equilibrium systems remains elusive. Indeed, the problem is a non-trivial one as the steady-state probability weights of microscopic configurations for such out-of-equilibrium systems are not described by the familiar Boltzmann-Gibbs distributions and are a-priori *not* known. Here, using a equilibrium-like fluctuation-response relation, again a consequence of an additivity property, we calculate subsystem particle-number distributions, solely from the knowledge of particle-number fluctuations in the disordered (homogeneous) state in the Vicsek and Vicsek-like models and

verify the applicability of additivity by comparing numerically calculated (within additivity) subsystem number distributions with those obtained from simulations.

3.2 Framework of additivity

In this section, let us first discuss what additivity means in the context of particle-number fluctuations in a system, which could be driven arbitrarily *far away* from equilibrium. Consider a system of volume V, consisting of N interacting particles where total number N is conserved. We then divide the system in $\nu = V/\mathcal{V}$ number of identical subsystems, each having volume $\mathcal{V}$, and ask what would be the particle-number distributions in one of the subsystems. Provided that the subsystem size is much larger than spatial correlation length ξ, $\mathcal{V}^{1/d} \gg \xi$ in d dimensions, additivity implies that the joint subsystem particle-number distribution has the following product form [9–11],

$$\mathcal{P}[\{\mathcal{N}_k\}] \simeq \frac{\prod_{k=1}^{\nu} W_{\mathcal{V}}(\mathcal{N}_k)}{Z(N,V)} \delta\left(\sum_k \mathcal{N}_k - N\right), \tag{3.1}$$

in the thermodynamic limit of $N, V \to \infty$ with $\rho = N/V$ fixed. In Eq. 3.1, $W_{\mathcal{V}}(\mathcal{N}_k)$ is an unknown weight factor to be determined later, $Z = \prod_k \int d\mathcal{N}_k W_{\mathcal{V}}(\mathcal{N}_k)\delta(\sum_k \mathcal{N}_k - N)$ is the partition sum and $\rho = N/V$ is the number density. Note that the weight factor $W_{\mathcal{V}}(\mathcal{N}_k)$ depends only on the subsystem particle-number $\mathcal{N}_k$ and subsystem volume $\mathcal{V}$. Eq. 3.1 then implies that the probability distribution function $P_{\mathcal{V}}(\mathcal{N}) \equiv \text{Prob}[\mathcal{N}_k = \mathcal{N}]$ can be written for large $\mathcal{V}$ [9–11],

$$P_{\mathcal{V}}(\mathcal{N}) = \frac{1}{\mathcal{Z}} W_{\mathcal{V}}(\mathcal{N}) e^{\mu(\rho)\mathcal{N}}, \tag{3.2}$$

where $\mu(\rho)$ a nonequilibrium chemical potential, $\mathcal{Z}$ normalization constant. The weight factor $W_{\mathcal{V}}(\mathcal{N}) \equiv \exp[-\mathcal{V} f(\mathcal{N}/\mathcal{V})]$, with $f(\rho)$ defined to be a free energy

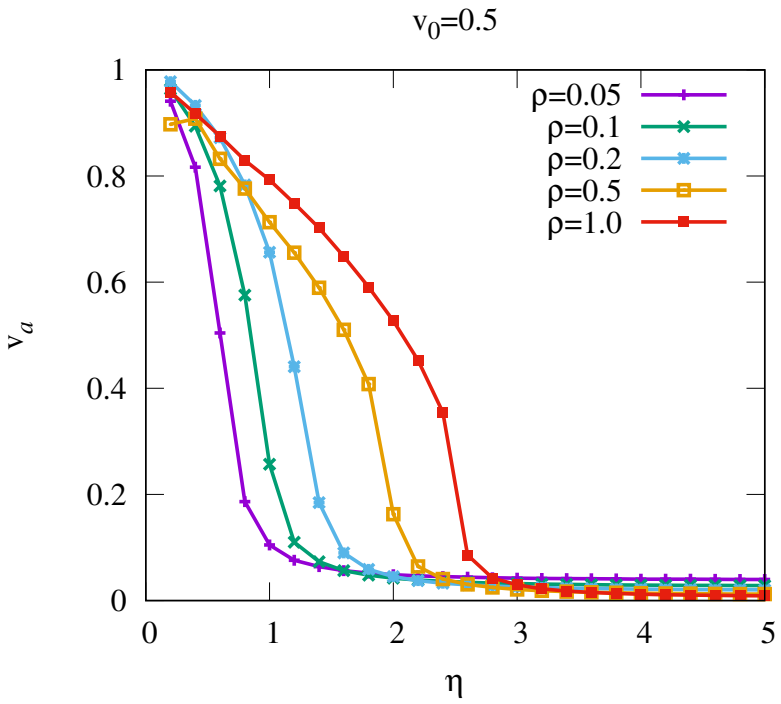

FIGURE 3.1: Order parameter v_a as a function of noise strength η for different densities ρ and fixed self propelled speed $v_0 = 0.5$.

density function, and chemical potential $\mu(\rho)$ can be obtained from a fluctuation-response (FR) relation between compressibility and number-fluctuation [9–14],

$$\frac{d\rho}{d\mu} = \sigma^2(\rho), \tag{3.3}$$

analogous to fluctuation-dissipation theorem in equilibrium, where $\sigma^2(\rho) = (\langle \mathcal{N}^2 \rangle - \langle \mathcal{N} \rangle^2)/\mathcal{V}$ scaled variance of subsystem particle-number $\mathcal{N}$. Thermodynamic potentials $\mu(\rho)$ and $f(\rho)$ are obtained by integrating Eq. 3.3, $\mu(\rho) = \int 1/\sigma^2(\rho) d\rho + c_1$ and $f(\rho) = \int \mu(\rho) d\rho + c_2$ where c_1 and c_2 arbitrary integration constants. Finally, the subsystem particle-number distribution can be written as

$$P_{\mathcal{V}}(\mathcal{N}) \simeq \frac{e^{[-\mathcal{V} f(\mathcal{N}/\mathcal{V}) + \mu(\rho)\mathcal{N}]}}{\mathcal{Z}}, \tag{3.4}$$

where $\mathcal{Z}(\mu, V)$ is the normalization constant.

What remains now is to explicitly calculate the variance $\sigma^2(\rho)$ in the Vicsek model and two of its variants and thereby to characterize fluctuations in terms of chemical

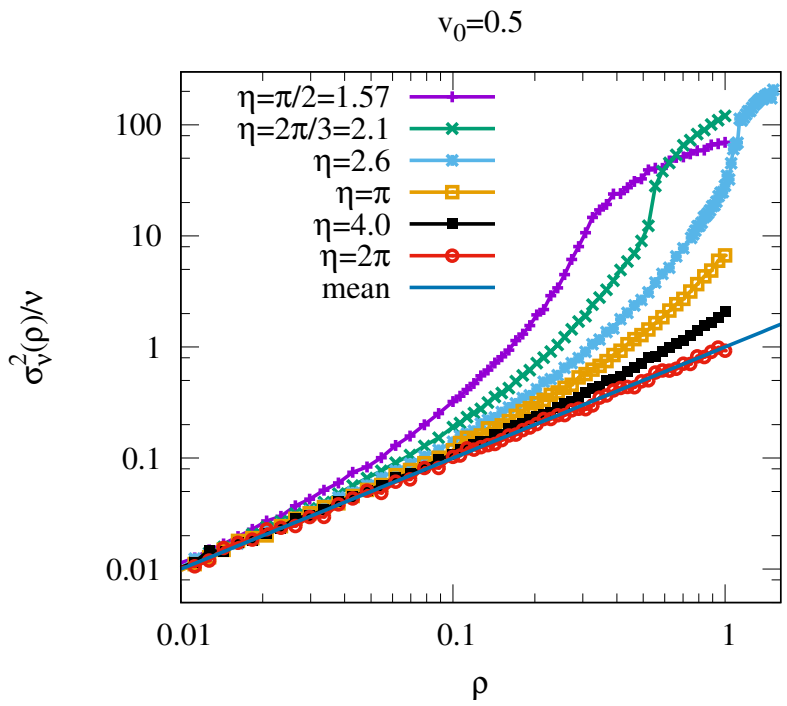

FIGURE 3.2: Top: Subsystem particle number fluctuation $\sigma^2_{\mathcal{V}}(\rho)/\mathcal{V}$ as a function of density ρ for different noise strength η and fixed self propelled speed $v_0 = 0.5$.

potential $\mu(\rho)$, which we address now. Before going into that we should point out, in chapter 2, if one have a careful look at Fig 2.3, the plot of subsystem particle number distribution for active Brownian particles (ABPs), one can notice that for density $\rho = 0.56$, the analytic result (violet dashed dotted line) could not capture the simulation result (violet asterisks) well. There are two arguments which could be the most possible reasons for this deviation. First, we calculated the subsystem particle number fluctuation $\sigma^2(\rho)$ as a function of density field ρ using a linearized theory. This linear analysis could break down at the high density and high activity regime, as a consequence, the chemical potential $\mu(\rho)$ and the free energy function $f(\rho)$ obtained from the linearized theory may not capture the non-linear effects of density fluctuations. Second, the boundary effect of correlation between subsystem and system can cause a significant finite size effect near criticality. So, here we try to overcome these two hurdles to calculate subsystem particle number distribution in Vicsek models.

To illustrate the formalism, we first calculate, in the homogeneous state of Vicsek

models, the variance $\sigma^2_{\mathcal{V}}(\rho)$ of particle-number in a subsystem of volume $\mathcal{V}$ as a function of density ρ from simulation. Given the functional dependence of variance $\sigma^2_{\mathcal{V}}(\rho)$ on density ρ, we use the nonequilibrium fluctuation-response relation [Eq. 3.3], a direct consequence of additivity property, to obtain a equilibrium like chemical potential $\mu(\rho)$. In order to do that, we compute $\sigma^2_{\mathcal{V}}(\rho)$ for sufficiently dense value of ρ so that we can integrate $\sigma^2_{\mathcal{V}}(\rho)$ numerically using standard integration method (Euler method) and get $\mu(\rho)$. Numerical integration [by Euler method] of $\mu(\rho)$ once more with respect to density ρ, will provide a nonequilibrium free energy density $f(\rho)$. Thus, given $\mu(\rho)$ and $f(\rho)$ as functions of density ρ, using Eq. (3.2), additivity property leads to subsystem particle-number distribution function $P_{\mathcal{V}}(\mathcal{N})$, the probability that a subsystem of volume $\mathcal{V}$ contain $\mathcal{N}$ number of particles. We compare this subsystem particle number distribution with the same calculated directly from the microscopic simulation of the model, to verify the additivity property. To check whether there is a finite size effect, we calculate the subsystem particle-number distribution for different subsystem sizes. Now, the logarithm of the subsystem particle-number distribution $P_{\mathcal{V}}(\mathcal{N})$, or the large deviation function (LDF), can be written as

$$\begin{aligned} \log[\mathcal{Z}P_{\mathcal{V}}(\mathcal{N})] &\simeq -\mathcal{V}f(\mathcal{N}/\mathcal{V}) + \mu(\rho)\mathcal{N}, \\ \Rightarrow \frac{1}{\mathcal{V}}\log[\mathcal{Z}P_{\mathcal{V}}(\mathcal{N})] &\simeq -f(\mathcal{N}/\mathcal{V}) + \mu(\rho)\frac{\mathcal{N}}{\mathcal{V}}, \\ \Rightarrow \frac{1}{\mathcal{V}}\log[\mathcal{Z}P_{\mathcal{V}}(\mathcal{N})] &\simeq -f(\rho) + \rho\mu(\rho_0), \end{aligned} \tag{3.5}$$

where $\mathcal{Z}(\mu, V)$ is the normalization constant. For better understanding, we use the notation $\rho = \mathcal{N}/\mathcal{V}$ the local density and ρ_0 the global density of the system in Eq. (3.5). Note that, the RHS of Eq. (3.5) is independent of subsystem size $\mathcal{V}$ and hence the LHS of Eq. (3.5) would be unchanged for different $\mathcal{V}$. This is the key to check whether there is a finite size effect in the results.

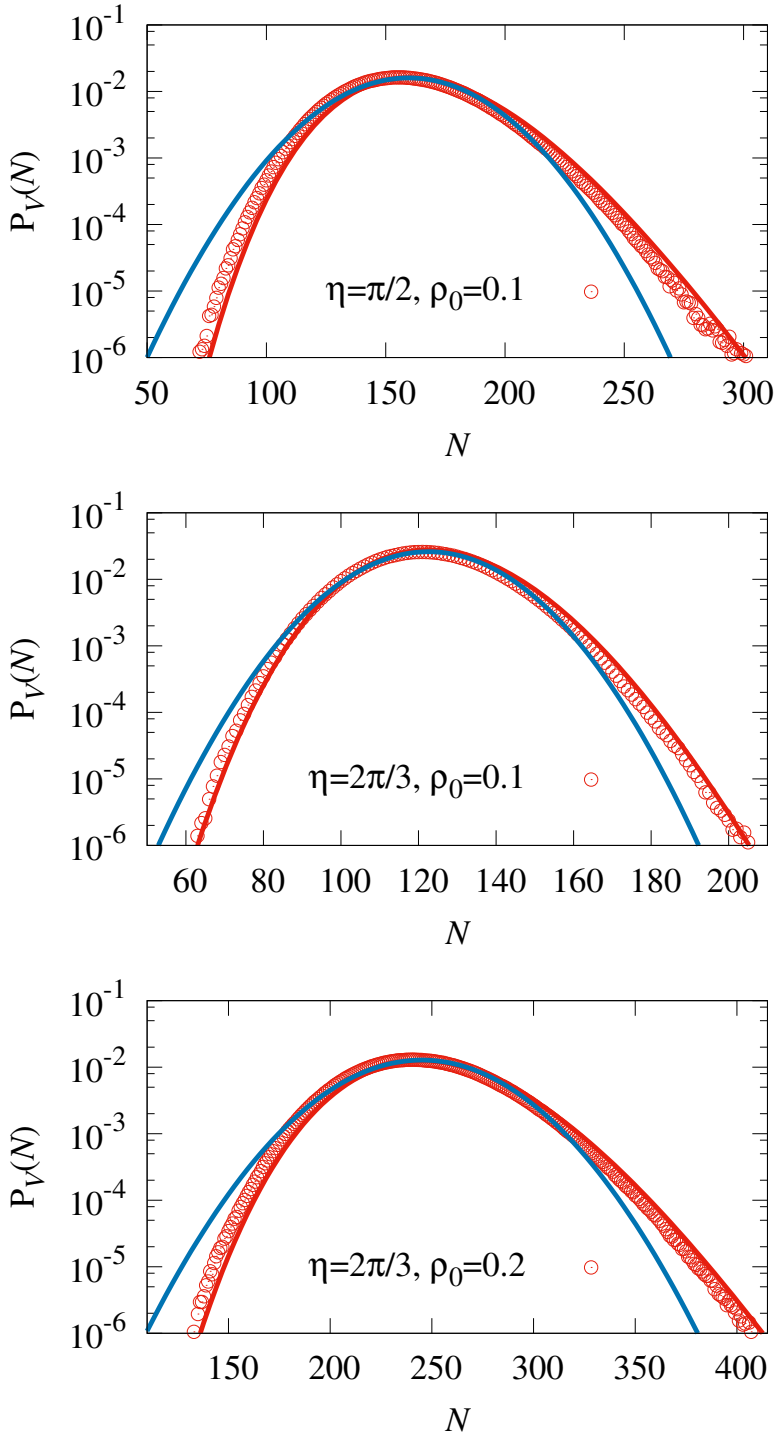

FIGURE 3.3: (Vicsek model) We plot subsystem particle number distribution $P_{\mathcal{V}}(\mathcal{N})$ with $\mathcal{N}$. Red lines- additivity results, red points- simulation results and blue lines- corresponding Gaussian plots. Top panel: $\eta = \frac{\pi}{2}$ and $\rho_0 = 0.1$; middle panel: $\eta = \frac{2\pi}{3}$ and $\rho_0 = 0.1$; bottom panel: $\eta = \frac{2\pi}{3}$ and $\rho_0 = 0.2$.

3.3 Number fluctuations in Vicsek Model

Vicsek model was the first simplest model of self-propelled particles [71] where N polar point particles are moving in a periodic square box of size $V = L \times L$. At any discrete time t, the system is specified by position $\mathbf{r}_i(t)$ and self-propulsion direction $\theta_i(t)$ of ith particle with $i = 1, \ldots, N$. The particles follow their neighbours by averaging the directions of motion of all neighbouring particles within a circle of radius R. They also make some errors in direction in attempting to follow their neighbour of amount $\Delta\theta_i(t)$. $\Delta\theta_i(t)$ is uniform and white noise with $\langle \Delta\theta_i(t) \rangle = 0$ and $\langle \Delta\theta_i(t) \Delta\theta_j(t') \rangle = \eta\ \delta_{ij}\delta_{tt'}$. The equations of motion for $\mathbf{r}_i(t)$ and $\theta_i(t)$ are given below.

$$\theta_i^R(t) = \arctan\left[\frac{\langle \sin\theta_j(t)\rangle_i^R}{\langle \cos\theta_j(t)\rangle_i^R}\right] \tag{3.6}$$

$$\theta_i(t+1) = \theta_i^R(t) + \Delta\theta_i(t) \tag{3.7}$$

$$\mathbf{r}_i(t+1) = \mathbf{r}_i(t) + v_0[\cos\theta_i(t+1), \sin\theta_i(t+1)]\Delta t \tag{3.8}$$

where the average in Eq (3.6) is over all particles j satisfying $|\mathbf{r}_j(t) - \mathbf{r}_i(t)| < R = 1$, v_0 is the self propelled speed and we set discrete time step $\Delta t = 1$. At large density ρ and/or small η, the particles tend to move in the same spontaneously selected direction indicating a phase transition. This phase transition is characterized by determining the absolute value of the average normalized velocity of all particles

$$v_a = \frac{1}{N v_0} \left| \sum_{i=1}^{N} \mathbf{v}_i \right|. \tag{3.9}$$

v_a is the orientation order parameter for the ordered to disordered phase transition. Clearly v_a will take value 1 when all the particles in the system are moving in the same direction and it is zero when all the particles are oriented in completely random direction.

In Fig. 3.1 we plot v_a as a function of noise strength η for different densities ρ [= 0.05, 0.1, 0.2, 0.5 and 1.0] and fixed self propulsion speed $v_0 = 0.5$. For a particular density, if we go from lower η to higher η, we see a sudden, significant change in

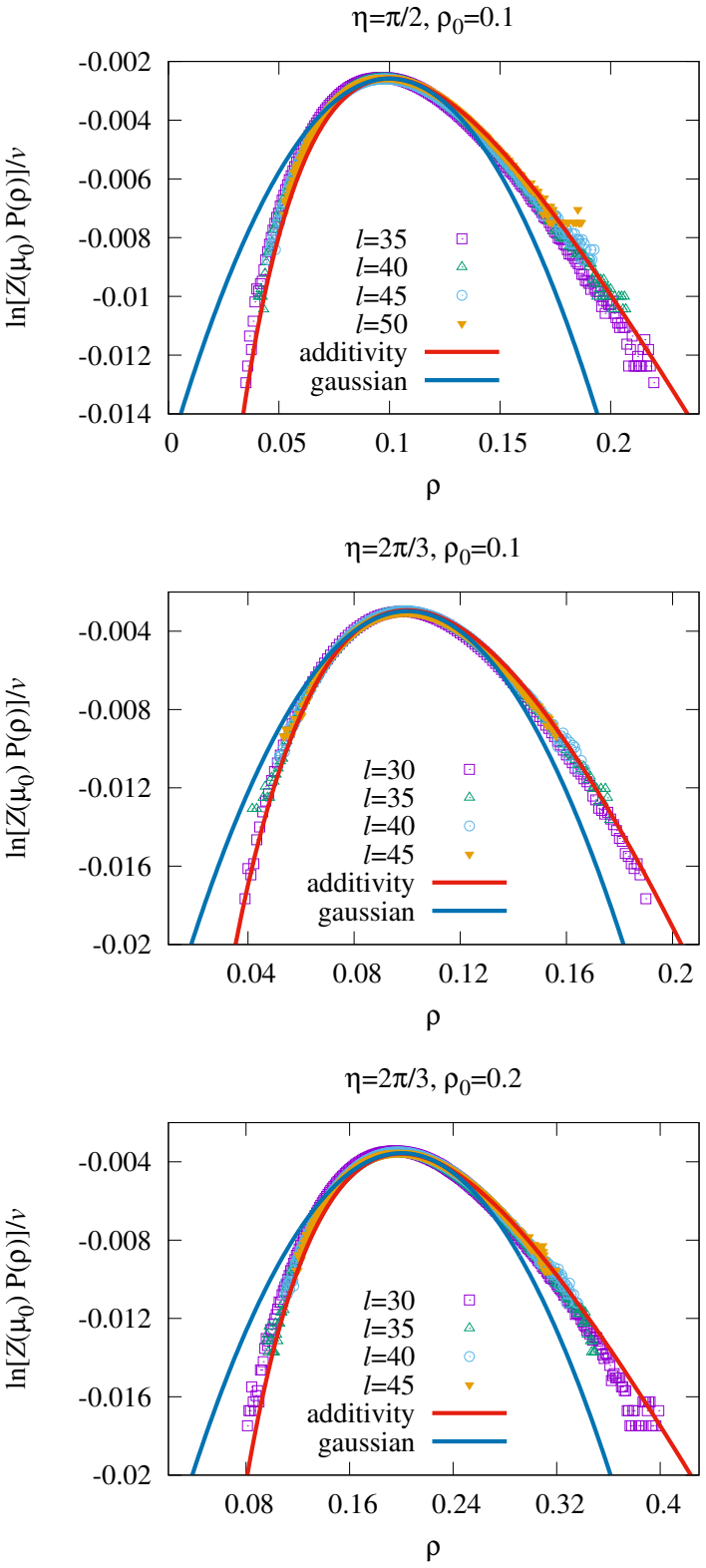

FIGURE 3.4: (Vicsek model) We plot the scaled distribution function $\frac{1}{\mathcal{V}}\log[\mathcal{Z}P_{\mathcal{V}}(\mathcal{N})]$ [Eq. (3.5)] calculated from simulation, as a function of density $\rho = \mathcal{N}/\mathcal{V}$ for different subsystem sizes. Red lines- additivity results, points- simulation results and blue lines- corresponding Gaussian plots. Top panel: $\eta = \frac{\pi}{2}$ and $\rho_0 = 0.1$; middle panel: $\eta = \frac{2\pi}{3}$ and $\rho_0 = 0.1$; bottom panel: $\eta = \frac{2\pi}{3}$ and $\rho_0 = 0.2$.

v_a after a critical $\eta = \eta_c$ indicating an order to disorder phase transition. Note that critical noise strength η_c increases with density ρ which indicates an obvious physical situation that at high density, the alignment interaction rate between particles is higher *i.e.* they will try to order themselves more, for which, one need more noise η to make them disordered. For this reason, the critical noise strength $\eta_c(\rho)$ is an increasing function of density ρ.

Now we take a small subsystem of size $\mathcal{V}$ and calculate scaled particle number fluctuation $\sigma^2_{\mathcal{V}}(\rho)/\mathcal{V}$ in that subsystem. The similar nature like in order parameter plot, could be observed when we plot $\sigma^2_{\mathcal{V}}(\rho)/\mathcal{V}$ in Fig. 3.2 as a function of density ρ for different noise strengths η [$=\pi/2,\ 2\pi/3,\ 2.6,\ \pi,\ 4.0$, and 2π] and a fixed self propulsion speed $v_0 = 0.5$. Here also we get a divergence in $\sigma^2_{\mathcal{V}}(\rho)/\mathcal{V}$ around a critical $\rho = \rho_c$ [for $\eta = \pi/2,\ 2\pi/3$ and 2.6] indicating an order to disorder transition. For the other higher noise values [$\eta = \pi$ and 4.0] we expect similar transition which is not in the plot due to computation difficulty. Note that $\eta = 2\pi$ is the highest possible noise strength in this system. So, for $\eta = 2\pi$, the particles can not feel each other, whatever be the density ρ. In this special case, the subsystem particle number distribution $P_{\mathcal{V}}(\mathcal{N})$ should be Poisson distribution, of which the variance (red circles with line in Fig. 3.2) would be equal to the mean (dark blue line in Fig. 3.2). The critical density $\rho_c(\eta)$ is an increasing function of noise strength η which is the outcome of the necessity of higher density to break the rotational symmetry when the noise is stronger.

To check additivity, we simulate the microscopic model [Eqs. (3.6), (3.7) and (3.8)] and compute variance of particle number $\sigma^2_{\mathcal{V}}(\rho)$ in a subsystem ($\mathcal{V} = 25 \times 25$ in units of interaction radius R) where the rest of the system ($V = 300 \times 300$ in units of interaction radius R) acts as a particle reservoir of chemical potential $\mu(\rho)$. We calculate $\sigma^2_{\mathcal{V}}(\rho)$ for sufficiently dense value of ρ [$\delta\rho = 2.5 \times 10^{-3}$]. Then we integrate $\sigma^2_{\mathcal{V}}(\rho)$ numerically using standard integration method (Euler method) and get the equilibrium like chemical potential $\mu(\rho)$ as a function of density ρ. Numerically integrating $\mu(\rho)$ once more [by Euler method] with respect to density ρ, we get a nonequilibrium free energy density $f(\rho)$. We use $\mu(\rho)$ and $f(\rho)$ as functions of density ρ in Eq. (3.2) to calculate, using additivity, the subsystem particle-number

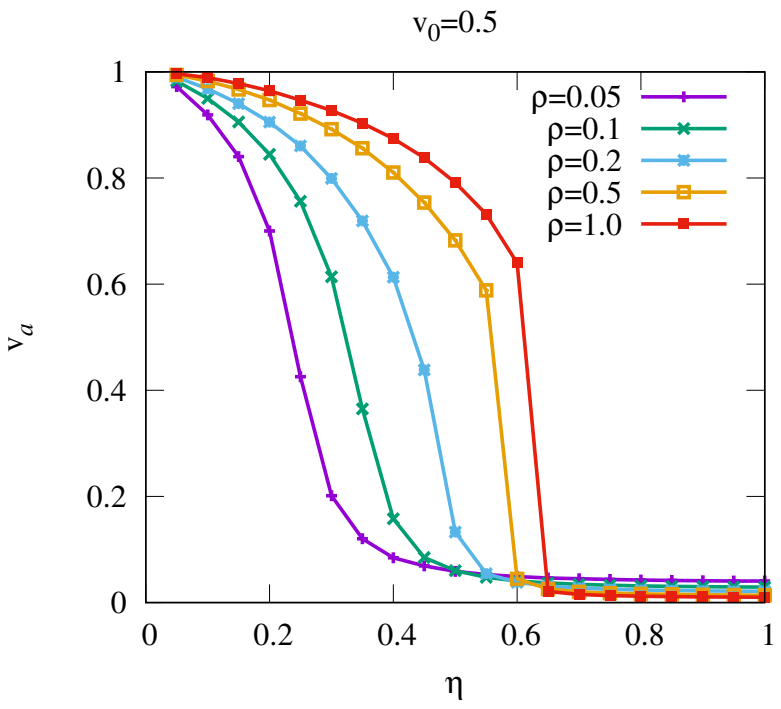

FIGURE 3.5: Order parameter v_a as a function of noise strength η for different densities ρ and fixed self propelled speed $v_0 = 0.5$.

distribution function $P_{\mathcal{V}}(\mathcal{N})$, the probability that a subsystem of volume $\mathcal{V}$ contain $\mathcal{N}$ number of particle. We compare this subsystem particle number distribution with the same calculated directly from the microscopic simulation of the model, to verify the additivity property. In Fig. 3.3 we plot the subsystem particle number distributions for different parameter regime (keeping self propulsion velocity fixed at $v_0 = 0.5$). In the top panel, we plot at $\eta = \pi/2$ and global density $\rho_0 = 0.1$; in middle panel, we keep ρ_0 fixed at 0.1 and change η to $2\pi/3$; and finally in the bottom panel, we fix η at $2\pi/3$ and set ρ_0 at 0.2. In all the panels, red circles are the simulation results and red lines are the additivity results and they agree quite well. The most interesting part of our theory is, we are calculating the distribution solely from the second moment, which is possible only for the Gaussian distribution. We plot in all panels of Fig. 3.3, the corresponding Gaussian distributions (the blue lines) and surprisingly, they differ significantly from the simulation results (red circles). Therefore, our additivity results capture the non-Gaussian feature very well *i.e.* the distribution could be calculated from variance using additivity, even if the distribution is non-Gaussian.

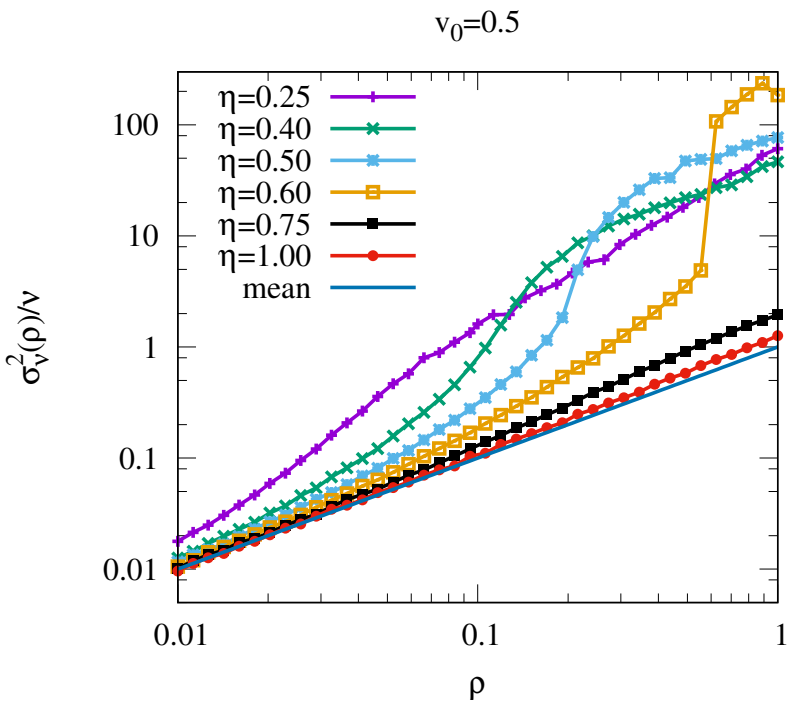

FIGURE 3.6: Top: Subsystem particle number fluctuation $\sigma^2_{\mathcal{V}}(\rho)/\mathcal{V}$ as a function of density ρ for different noise strength η and fixed self propelled speed $v_0 = 0.5$.

Now it is time to check whether there is a finite size effect in the results. In order to do that, in Fig. 3.4, we plot the large deviation function [LHS of Eq. (3.5)] calculated from simulation, for several subsystem sizes $\mathcal{V} = 30$, 35, 40, 45 and 50 [points in Fig. 3.4], for three sets of parameter values $\{\eta, \rho_0\} = \{\pi/2, 0.1\}$, $\{2\pi/3, 0.1\}$, $\{2\pi/3, 0.2\}$, and self propulsion velocity $v_0 = 0.5$. Notice that the LDF for different $\mathcal{V}$ calculated from simulation (points) fall on each other and agree well with the same calculated using additivity (red lines). Here also we plot the corresponding LDF for Gaussian distributions (blue lines) and see that our additivity results capture the non-Gaussian feature quite good.

3.4 Number fluctuations in variant - I of Vicsek Model

The model is same as Vicsek's model, with the only change in the way noise is incorporated in the system. In Vicsek's model, a particle makes an error when it is trying to take the new direction which it has calculated perfectly. This type of noise is called angular noise. Chate *et. al.* [79] argued that, errors could be made by a particle when it is estimating the average direction of all the neighboring particles. When the average direction is calculated, it follow that direction without any error. So, the error is incorporated in each component of the average direction, for which this noise is called vector noise. The updated equations of motion are given by,

$$\theta_i(t+1) = \arctan\left[\frac{\langle \sin\theta_j(t)\rangle_i^R + \eta \sin\xi_i(t)}{\langle \cos\theta_j(t)\rangle_i^R + \eta \cos\xi_i(t)}\right] \tag{3.10}$$

$$\mathbf{r}_i(t+1) = \mathbf{r}_i(t) + v_0[\cos\theta_i(t+1), \sin\theta_i(t+1)]\Delta t \tag{3.11}$$

where, $\xi_i(t)$ is uniform and white noise $\in [-\pi, \pi]$ and noise strength $\eta \in [0, 1]$. We set micro time step $\Delta t = 1$, interaction radius $R = 1$ and self propulsion speed $v_0 = 0.5$. At large density ρ and/or small η, the particles show a phase transition from orientationaly disordered state to ordered state. The orientation order parameter v_a [Eq. (3.9)] for the phase transition, plays the same role here. It takes value 1 when all the particles are perfectly ordered and it is zero when they are completely disordered.

We plot v_a as a function of noise strength η in Fig. 3.5 for different densities ρ [= 0.05, 0.1, 0.2, 0.5 and 1.0] and fixed self propulsion speed $v_0 = 0.5$. Here we see a more sharper change in v_a after a critical $\eta = \eta_c(\rho)$ indicating order to disorder transition. The critical noise strength $\eta_c(\rho)$ is again an increasing function of density ρ.

Next we plot $\sigma^2_{\mathcal{V}}(\rho)/\mathcal{V}$, the scaled particle number fluctuation in a small subsystem of size $\mathcal{V}$ in Fig. 3.6 as a function of density ρ for different noise strengths η (=

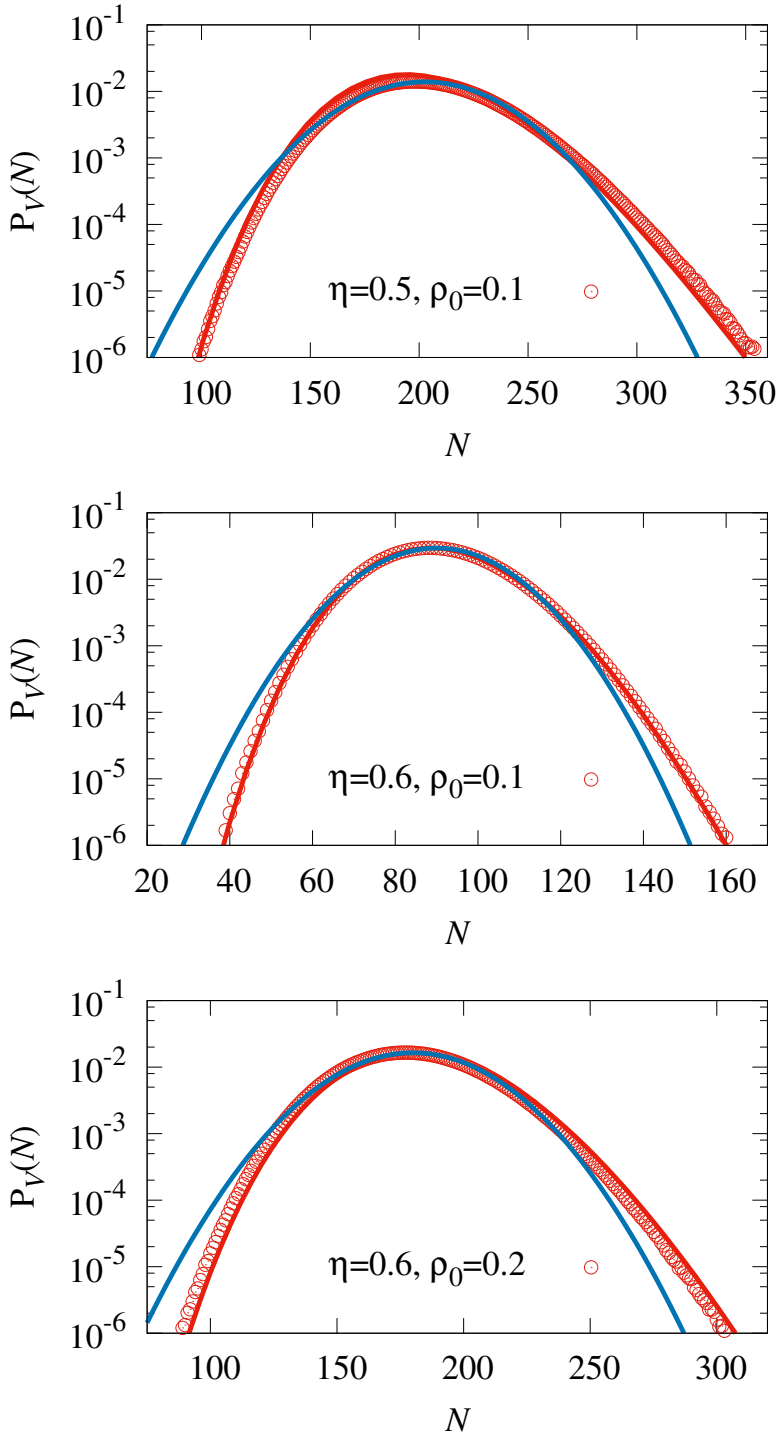

FIGURE 3.7: (Variant - I of Vicsek model) We plot subsystem particle number distribution $P_{\mathcal{V}}(\mathcal{N})$ with $\mathcal{N}$. Red lines- additivity results, red points- simulation results and blue lines- corresponding Gaussian plots. Top panel: $\eta = 0.5$ and $\rho_0 = 0.1$; middle panel: $\eta = 0.6$ and $\rho_0 = 0.1$; bottom panel: $\eta = 0.6$ and $\rho_0 = 0.2$.

0.25, 0.4, 0.5, 0.6, 0.75 and 1.0) and a fixed self propulsion speed $v_0 = 0.5$. Here also we get a divergence in $\sigma^2_{\mathcal{V}}(\rho)/\mathcal{V}$ around a critical $\rho = \rho_c(\eta)$ indicating an order to disorder transition. Note that $\eta = 1.0$ is the highest possible noise strength in this system. Therefore, at $\eta = 1.0$, the particles hardly feel each other and the alignment interaction is dominated by the noise resulting in the subsystem particle-number distribution $P_{\mathcal{V}}(\mathcal{N})$ be a Poisson distribution, of which the variance (red circles with line in Fig. 3.6) would be equal to the mean (dark blue line in Fig. 3.6). Furthermore, the critical density $\rho_c(\eta)$ is an increasing function of noise strength η which explains that one need to increase the density ρ to break the rotational symmetry if the noise strength η is also high.

To verify additivity, we simulate the microscopic model [Eqs. (3.10) and (3.11) and compute variance of particle number $\sigma^2_{\mathcal{V}}(\rho)$ in a subsystem ($\mathcal{V} = 30 \times 30$ in units of interaction radius R) where the rest of the system ($V = 500 \times 500$ in units of interaction radius R) acts as a particle reservoir of chemical potential $\mu(\rho)$. We calculate $\sigma^2_{\mathcal{V}}(\rho)$ as a function of ρ for sufficiently dense value of ρ [$\delta\rho = 3.3 \times 10^{-3}$] which will help us to numerically integrate $\sigma^2_{\mathcal{V}}(\rho)$ twice with respect to density ρ, using Euler method to get first time, an equilibrium like chemical potential $\mu(\rho)$ and second time a nonequilibrium free energy density $f(\rho)$ as a function of density ρ. By using $\mu(\rho)$ and $f(\rho)$ in Eq. (3.2), obtained from additivity, we calculate the subsystem particle-number distribution function $P_{\mathcal{V}}(\mathcal{N})$, the probability that a subsystem of volume $\mathcal{V}$ contain $\mathcal{N}$ number of particle. We compare this additivity result of subsystem particle number distribution with the same calculated directly from the microscopic simulation of the model, to verify the additivity property. In Fig. 3.7 we plot the subsystem particle number distributions for different parameter regime (keeping self propulsion velocity fixed at $v_0 = 0.5$). In the top panel, we plot at $\eta = 0.5$ and global density $\rho_0 = 0.1$; in middle panel, we keep ρ_0 fixed at 0.1 and change η to 0.6; and finally in the bottom panel, we fix η at 0.6 and set ρ_0 at 0.2. In all the panels, red circles are the simulation results and red lines are the additivity results and they agree quite well. Importantly, we are calculating the distribution solely from the second moment, not possible other than the Gaussian distribution. To investigate the non-Gaussian behavior,

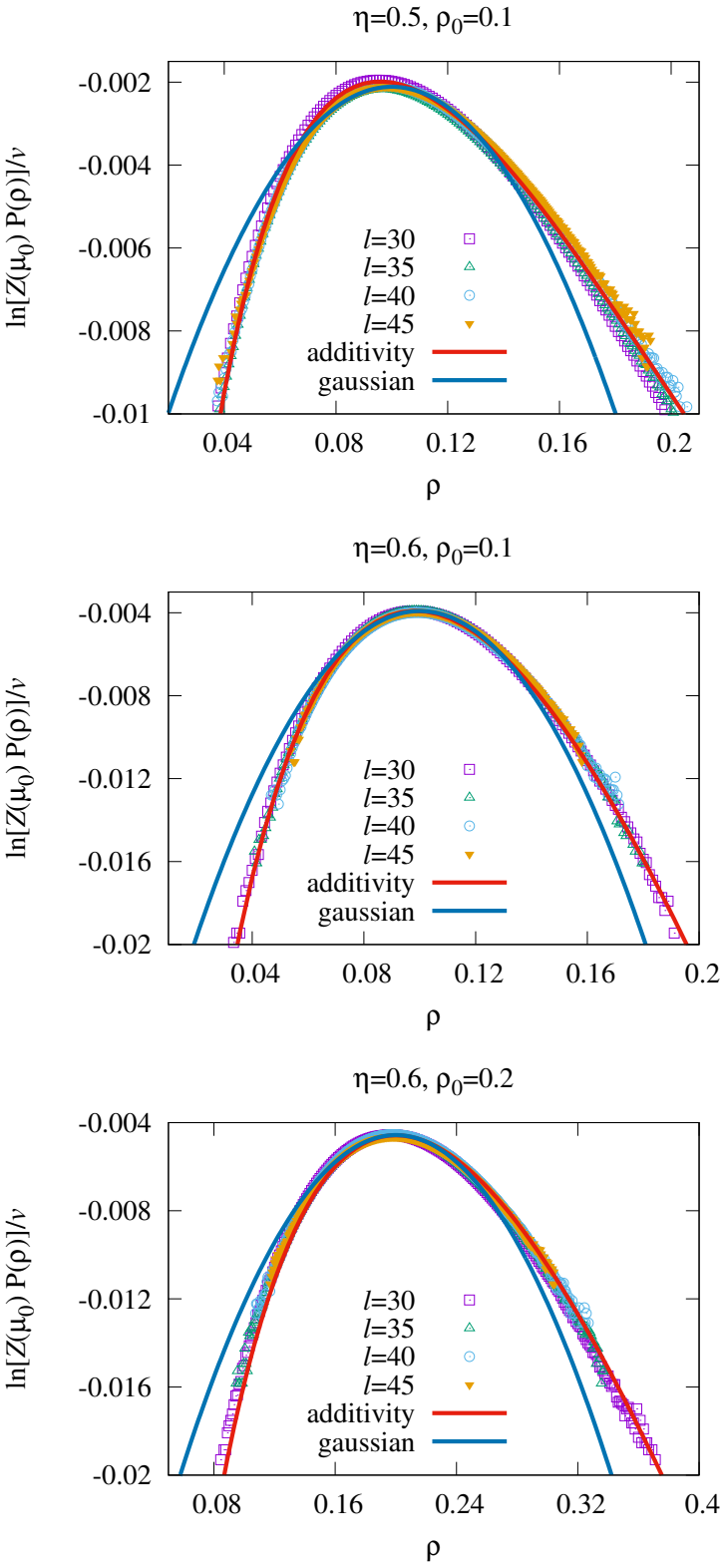

FIGURE 3.8: (Variant - I of Vicsek model) We plot the scaled distribution function $\frac{1}{\mathcal{V}}\log[\mathcal{Z}P_{\mathcal{V}}(\mathcal{N})]$ [Eq. (3.5)] calculated from simulation, as a function of density $\rho = \mathcal{N}/\mathcal{V}$ for different subsystem sizes. Red lines- additivity results, points- simulation results and blue lines- corresponding Gaussian plots. Top panel: $\eta = 0.5$ and $\rho_0 = 0.1$; middle panel: $\eta = 0.6$ and $\rho_0 = 0.1$; bottom panel: $\eta = 0.6$ and $\rho_0 = 0.2$.

we plot in all panels of Fig. 3.7, the corresponding Gaussian distributions (the blue lines) and they clearly differ of an significant amount from the simulation results (red circles). So our additivity results capture the non-Gaussian feature very well *i.e.* the distribution could be calculated from variance using additivity, even if the distribution is non-Gaussian.

Additionally, we examine whether there is a finite size effect in the results. To check that, in Fig. 3.8, we plot the large deviation function [LHS of Eq. (3.5)] calculated from simulation, for several subsystem sizes $\mathcal{V} = 30$, 35, 40 and 45 [points in Fig. 3.8], for three sets of parameter values $\{\eta, \rho_0\} = \{0.5, 0.1\},\ \{0.6, 0.1\},\ \{0.6, 0.2\}$, and self propulsion velocity $v_0 = 0.5$. Notice that the LDF for different $\mathcal{V}$ calculated from simulation (points) fall on each other and agree well with the same calculated from RHS of Eq. (3.5), using additivity (red lines). Here also we plot the corresponding LDF for Gaussian distributions (blue lines) and see that our additivity results capture the non-Gaussian feature quite good.

3.5 Number fluctuations in variant - II of Vicsek model

Depending on the way the noise is incorporated in the system, we introduce another variant of Vicsek model. Here, the model is similar to the previous variant except the components of the vector noise are not same, rather they are chosen independently. The microscopic equations of motion for this model are,

$$\theta_i(t+1) = \arctan\left[\frac{\langle \sin\theta_j(t)\rangle_i^R + \eta \sin\xi_i^1(t)}{\langle \cos\theta_j(t)\rangle_i^R + \eta \cos\xi_i^2(t)}\right] \tag{3.12}$$

$$\mathbf{r}_i(t+1) = \mathbf{r}_i(t) + v_0[\cos\theta_i(t+1), \sin\theta_i(t+1)]\Delta t \tag{3.13}$$

where, $\xi_i^1(t)$ and $\xi_i^2(t)$ are independently chosen uniform and white noises $\in [-\pi, \pi]$ and noise strength $\eta \in [0, 1]$. We set micro time step $\Delta t = 1$, interaction radius $R = 1$ and self propulsion speed $v_0 = 0.5$. We go through the same procedure in this case also and find similar nature of the orientation order parameter v_a and

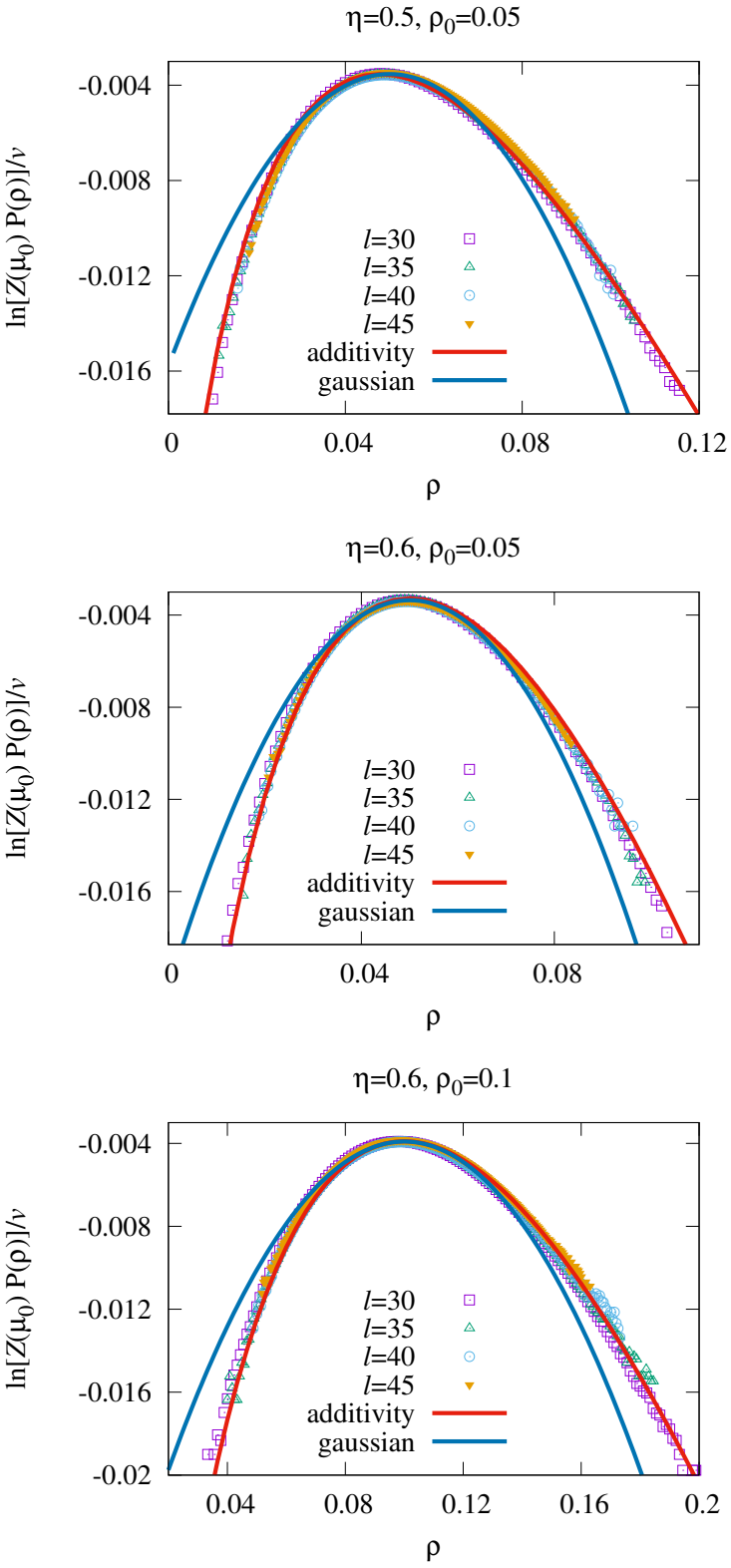

FIGURE 3.9: (Variant - II of Vicsek model) We plot the scaled distribution function $\frac{1}{\mathcal{V}}\log[\mathcal{Z}P_{\mathcal{V}}(\mathcal{N})]$ [Eq. (3.5)] calculated from simulation, as a function of density $\rho = \mathcal{N}/\mathcal{V}$ for different subsystem sizes. Red lines- additivity results, points- simulation results and blue lines- corresponding Gaussian plots. Top panel: $\eta = 0.5$ and $\rho_0 = 0.05$; middle panel: $\eta = 0.6$ and $\rho_0 = 0.05$; bottom panel: $\eta = 0.6$ and $\rho_0 = 0.1$.

$\sigma^2_{\mathcal{V}}(\rho)/\mathcal{V}$, the scaled particle number fluctuation in a small subsystem of size $\mathcal{V}$ as a function of density ρ. Therefore, we directly go to the verification of additivity property in this model.

We compute scaled variance of particle number $\sigma^2_{\mathcal{V}}(\rho)/\mathcal{V}$ in a subsystem of size $\mathcal{V} = 30 \times 30$ (in units of interaction radius R) with the actual system size $V = 500 \times 500$ (in units of interaction radius R), by simulating the microscopic model [Eqs. (3.12) and (3.13)]. Then we follow the same formalism (perform the same analysis) like in previous two models to find an equilibrium like chemical potential $\mu(\rho)$ and a free energy density $f(\rho)$ as a function of density ρ. Using $\mu(\rho)$ and $f(\rho)$ in Eq. (3.5), we calculate the large deviation function from additivity for three sets of parameter values $\{\eta, \rho_0\} = \{0.5, 0.05\}$, $\{0.6, 0.05\}$, $\{0.6, 0.1\}$, and self propulsion velocity $v_0 = 0.5$, which we call the additivity results (red lines in Fig. 3.9). On the other hand we calculate the LDF [using LHS of Eq. (3.5)] directly from simulation, for several subsystem sizes $\mathcal{V} = 30$, 35, 40 and 45 for same three sets of parameter values and plot them in Fig. 3.9 (points). Strikingly, the simulation results (points) fall on each other for different subsystem sizes and also they agree with the additivity results (red lines) reasonably well for all three sets of parameters. The corresponding LDF for Gaussian distributions (blue lines) are also plotted to convince that our additivity results capture the non-Gaussian feature quite good.

3.6 Summary

In this chapter, by using a non-equilibrium fluctuation-response relation - a consequence of an additivity property, we exactly compute the density large-deviation functions in the Vicsek model and its two variants in the disordered homogeneous phase, where average velocity of particles vanishes and there is no macroscopic current in the system (though, microscopically, the systems still remain out-of-equilibrium, due to violation of detailed balance). Comparison between

our results and simulations strongly suggests that all three models with Vicsek-like interactions studied here possess an equilibrium-like thermodynamic structure in the disordered phase, where the large-deviation functions are governed by an equilibrium-like chemical potential and free-energy function.

More specifically, we have extended the statistical mechanics formalism based on equilibrium-like additivity property to other self-propelled-particle systems, such as the Vicsek model (VM) and its two variants, consisting of polar point-particles with alignment interactions. The two variants of the Vicsek model differ from the original one in the way the noise term is incorporated in the system. All three classes of models exhibit a disorder-to-order phase transition as the global particle-number density is increased or the noise strength is decreased. The critical noise strength depends on the density, and vice versa. We first exactly compute the scaled variance of subsystem particle-number as a function of density distributions in the disordered fluid-like phase. Provided additivity property holds, one could then calculate the subsystem particle-number distributions. By using a non-equilibrium fluctuation-response relation between fluctuation and compressibility, we obtain these subsystem number distributions (large deviation functions) and compare them with those calculated from simulations. Indeed, we find a striking agreement between simulations and additivity theory, which captures remarkably well the non-Gaussian features observed in these distributions.

Importantly, our studies brings to the fore the two following interesting open issues, which would provide further insights into the problem of characterizing large-scale structure of self-propelled particles in general. (i) It remains to be seen whether additivity can predict the properties of the ordered phase in self-propelled particles, many of which exhibit giant number fluctuations. (ii) So far, in our studies, the connection between the static structure (as characterized through additivity property) and the dynamic structure (as characterized through transport properties) is not clear. However, calculating the transport coefficients, like the diffusion coefficients and conductivity, is not an easy task in continuum models. Presumably, the task is much easier in the lattice version of these models, which is introduced and calculations of the transport coefficients are carried out in the next chapter,

where, motivated by the active-matter systems studied so far in the thesis, we introduce a broad class of activated lattice gases.

Chapter 4

Hydrodynamics of active lattice gases: Persistent and long-range hopping

4.1 Introduction

As discussed in Secs. 1.3.3 and 1.3.4 in Chapter 1, *motility induced phase separation* (MIPS) is an important aspect of the clustering phenomena, which are observed in active-matter or self-propelled-particle systems (such as active Brownian particles) in spite of the repulsive interactions present among the particles (unlike in an equilibrium phase separations, which happen in the presence of attractive interactions among particles). As discussed in the innumerable studies in the past [31, 34, 42, 43], MIPS is thought to be the mechanism responsible for formation of clusters in self-propelled particle systems. In these active-matter systems (e.g., active Brownian particles and run-and-tumble particles), particles, even *without* alignment interactions and only having random self-propulsion velocities, show on a coarse-grained level effective reduction of particle motion and thus becomes phase separated.

The mechanism for the MIPS could be understood through the competition between the tumbling rate or rotational diffusion constant D_r and collision rate of particles, which plays a key role here. If the latter rate is much higher than the former one, a particle, which might have just resided on a boundary of a cluster, eventually gets trapped by other particles colliding with it, even before it could come out of the cluster. Consequently, the particle becomes part of the cluster. In other words, there is a flux towards the denser region of the system, which effectively reduces the bulk diffusion coefficient, thus creating an instability and promoting clustering or phase separation in the system. Therefore it is perhaps expected that the bulk diffusion coefficient would play an important role in the process of phase separations in active-matter systems.

However, calculating the transport coefficient like diffusivity in non-equilibrium systems, such as active matters, is a difficult task and has not been studied much in the literature in the past. In this chapter, we explore the nature of the bulk diffusion coefficient in non-equilibrium conserved-mass transport processes on a periodic ring, where each site is associated with discrete (non-negative) masses on a lattice and has unbounded occupancy. Interestingly, as we demonstrate in the following sections, these models can be mapped exactly onto several one dimensional lattice gases of self-propelled particles with hardcore exclusion. Therefore, the unbounded-mass and exclusion versions of active lattice models studied here are two completely equivalent descriptions.

Throughout the past several decades, fluctuation-response relations in systems driven out of equilibrium have drawn a lot of interest [1–3]. One of these relations, valid in out-of-equilibrium systems, is an equilibrium-like Einstein relation between fluctuation (e.g., variance of subsystem mass/particle-number) and response (e.g., transport coefficients) [7, 8, 16, 17]. The *Einstein relation* (ER) [80], irrespective of the details of inter-particle interactions, is quite universal in equilibrium systems, where detailed balance is obeyed. Indeed, the ER is one of earliest known form of the *fluctuation-dissipation theorems* (FDTs) in equilibrium statistical physics. It connects two transport coefficients, bulk diffusion coefficient $D(\rho)$ and conductivity

$\chi(\rho)$, as

$$D(\rho) = \frac{\chi(\rho)}{\sigma^2_{eq}(\rho)}, \tag{4.1}$$

where

$$\sigma^2_{eq}(\rho) = lim_{v\to\infty}\frac{(\langle n_v^2\rangle_{eq} - \langle n_v\rangle^2_{eq})}{v} \tag{4.2}$$

is the scaled variance of particle number n_v in a sub-volume v, and ρ is local number density. The FDTs, including the ER, could be proved using a linear response theory [81].

Alternatively, the Einstein relation can be proved using steady-state balance condition between diffusive and drift currents, which may be present in a system. The following argument is valid irrespective of the fact whether the system is in or out of equilibrium. Only condition we use is that the macroscopic bulk current vanishes in the system. Let us consider a one-dimensional system whose first half is kept at an external potential V_1 and the second half is kept in another external potential V_2. This difference in the potential will apply an small force field $\mathbf{F} = F\hat{x}$ between two halves of the system as $V_2 - V_1 = \Delta V = -\int F dx$. In the equilibrium, the effective chemical potentials of the two halves must equalize as given below

$$\mu(\rho_1) + V_1 = \mu(\rho_2) + V_2, \tag{4.3}$$

where ρ_1 and ρ_2 are densities of the first and second halves of the system, respectively. The canonical chemical potential $\mu(\rho) = df(\rho)/d\rho$, where $f(\rho)$ is the canonical free energy density, in the absence of any external force. Alternatively, across a spatial interval Δx, Eq. (4.3) can be written as,

$$\begin{aligned} \frac{\Delta\mu}{\Delta x} &= -\frac{\Delta V}{\Delta x} = F, \\ \Rightarrow \frac{d\mu}{dx} &= F, \end{aligned} \tag{4.4}$$

in the limit of $\Delta x \to 0$. Now, in the limit of $F \to 0$, the diffusion current $J_D = -D(\rho)d\rho/dx$ and the drift current $J_d = \chi(\rho)F$ would cancel each other, so that the total current in the system becomes zero. Therefore, in the small force

limit, the condition $J_D + J_d = 0$ would imply

$$\begin{aligned} D(\rho)\frac{d\rho}{dx} &= \chi(\rho)F, \\ \Rightarrow D(\rho)\frac{d\rho}{dx} &= \chi(\rho)\frac{d\mu}{dx}, \end{aligned} \tag{4.5}$$

by substituting F from Eq. (4.4). Now, using the chain rule $d\mu/dx = (d\mu/d\rho)\,(d\rho/dx)$ and the equilibrium fluctuation-response relation $d\rho/d\mu = \sigma^2(\rho)$ [Eq. (1.6)], one can rewrite Eq. (4.5) as

$$\sigma^2(\rho) = \frac{\chi(\rho)}{D(\rho)}, \tag{4.6}$$

which is the Einstein relation as in equilibrium. The crucial argument here lies in the fact that the force can be related to the spatial gradient of a chemical potential, which is a direct consequence of additivity property, which a system, irrespective of whether in or out of equilibrium, may possess. In the following sections, we demonstrate that many of the active lattice gases introduced in this thesis indeed satisfy an equilibrium-like Einstein relation.

However, characterizing the bulk properties by calculating diffusivity, conductivity, and density fluctuations in systems far from equilibrium is, in general, a difficult problem as the steady-state probabilities of microscopic configurations are *not* described by the Boltzmann-Gibbs distributions. There have been several phenomenological field theories, based on symmetries present in the system, which have been studied in the past. However, these theories cannot capture exact nature of fluctuations, and therefore the fluctuation relations, possible in the systems. In this situation, deriving hydrodynamics of these out-of-equilibrium active-matter systems, from its underlying microscopic dynamics, would be very much desirable and could provide some useful insights into the diverse phenomena observed in such systems.

Interestingly, in the literature [7–12, 14, 15, 19, 82–85], there are several studies, which indicate that there can be fluctuation-response relations, even in non-equilibrium steady states (NESSs), analogous to the fluctuation-dissipation theorems (FDTs) in equilibrium. Particularly, the ER has been found in several model

systems [86–88] having a NESS. Recently, Das *et al.* [16] and Chatterjee *et al.* [17] have obtained a hydrodynamics structure starting from microscopic dynamics in a broad class of non-equilibrium mass transport processes. These authors have found that the transport coefficients obey an equilibrium-like ER in the steady states. Motivated by these studies, we now attempt to explore the hydrodynamic structure in active-matter systems and to check whether there exists an ER in such systems too.

We now briefly review some previous works done on lattice versions of self-propelled particles. In one of the earliest studies, Evans *et al.* [91] proposed a system of self-propelled particles on a periodic lattice, where particles are interacting through alignment interactions similar to that in the Vicsek model [71]. The authors found a phase transition from a homogeneous fluid phase to a inhomogeneous coexising phase of fluid and a condensate, where a finite fraction of total number of particles forms a single cluster or a flock. They also found that the condensate can have alternating velocities with a random change in either of the two directions possible in one dimension. Later, a generalized version of the above lattice model, as discussed in Ref. [92] exhibits transition between several flocking regimes, such as, homogeneous flocks and appearance of dipole structures in the flocks, etc. These regimes were investigated numerically as well as in a mean-field theory. In another study of *two* run-and-tumble particles on a one dimensional lattice, Slowman *et al.* in Ref. [93, 94] found an exact expression for the steady-state probability distribution of relative distance between the two particles. Here, the steady-state distribution has three regimes at different relative distances: A small distance regime due to a dynamical arrest between the two particles facing each other on adjacent sites, a intermediate regime where the distribution falls off exponentially, and an extended regime at large distances where a saturation is found in the distribution. In a recent study of a *single* run-and-tumble in a one dimensional system in continuum [95], the exact probability distribution of the position of the particle has been calculated in the long-time limit in an infinite domain. Interesingly, the distribution is multi-modal in nature. Moreover, in a finite domain with bounding

walls at two sides, there is formation of peaks at the boundaries, in the steady state.

In the following sections, we introduce two different classes of models of active-matter systems on a one-dimensional periodic lattice, which have signature of clustering (in several models, particle motion slows down with increasing activity), and study hydrodynamics of these lattice systems. Even in one dimension, these models have nontrivial probability weights in their steady states, which are a-priori unknown. The one-dimensional lattice gases with hardcore exclusion, we introduce here, can be mapped exactly onto models with discrete masses where lattice sites have unbounded occupancies (no constraint of hardcore exclusion). For some of these unbounded mass models, we derive hydrodynamics, starting from the underlying microscopic dynamics, and consequently we calculate the bulk diffusion coefficient $D(\rho)$ and conductivity $\chi(\rho)$ as a function of local mass density ρ. Moreover, we verify whether there exists an equilibrium-like ER,

$$\sigma^2(\rho) = \frac{\chi(\rho)}{D(\rho)}, \tag{4.7}$$

where $\sigma^2(\rho) = lim_{v\to\infty}(\langle m^2\rangle - \langle m\rangle^2)/v$ is the scaled variance of mass m in a large subsystem of volume v. Note that all the above quantities are calculated in a nonequilibrium steady state. The transport coefficients $D(\rho)$ and $\chi(\rho)$ are defined below.

Hydrodynamics and definition of transport coefficients: Since the total mass in the system is conserved, the hydrodynamic time-evolution equation must be written in the form of a continuity equation,

$$\partial_\tau \rho(x,\tau) + \partial_x J(\rho(x,\tau)) = 0, \tag{4.8}$$

which governs the time evolution of density field $\rho(x,\tau)$ with x and τ being suitably rescaled position and time, respectively. Since the process we consider here are of "gradient type", *i.e.*, local diffusive current can be expressed as a gradient of some local observable [19], one would expect a non-linear drift-diffusion kind of

hydrodynamic equation with total current $J = J_D + J_d$ will have two contributions. The first part $J_D = -D(\rho)\partial_x\rho(x,\tau)$ is the local diffusive current and the second part $J_d = \chi(\rho)F$ is the drift current due to a small externally applied biasing force-field of magnitude F (which, for simplicity, is taken to be constant throughout).

Calculation of conductivity: To check the ER, one requires to calculate conductivity in the system as in a standard linear response theory for equilibrium systems. To this end, we apply a small constant biasing force field $\mathbf{F} = F\hat{x}$, with $\hat{x}$ being a unit vector along +ve x axis and then calculate current in the limit F small. The original mass transfer rates $c_{i\to j}$ (*i.e.*, when $F = 0$), from site i to j, changes to the biased rates $c^F_{i\to j}$ (when $F \neq 0$), which are now effectively asymmetric due to the applied small biasing force $\mathbf{F}$,

$$c^F_{i\to j} = c_{i\to j}\Phi(\Delta e_{ij}). \tag{4.9}$$

$\Phi(\Delta e_{ij})$ is a non-negative function of an (extra) energy cost for transferring mass $\Delta m_{i\to j}$ from site i to j in a particular direction with the mass displacement vector $\delta\mathbf{x}_{ij} = (j-i)a\hat{x}$ and a being the lattice constant. Simply the quantity $\Phi(\Delta e_{ij})$ can be written as,

$$\Phi(\Delta e_{ij}) = \Delta m_{i\to j}(\mathbf{F}.\delta\mathbf{x}_{ij}). \tag{4.10}$$

In macroscopic fluctuation theory, the function Φ is chosen to have a form $\Phi(\Delta e) = \exp(\Delta e/2)$ [8, 16], where the modified rates satisfy a local detailed balance condition. Now, for small force F, we expand Φ in $O(F)$,

$$\Phi(\Delta e_{ij}) \simeq 1 + \Delta e_{ij}\left[\frac{d\Phi}{d(\Delta e)}\right]_{\Delta e=0} = 1 + \frac{1}{2}\Delta m_{i\to j}(\mathbf{F}.\delta\mathbf{x}_{ij}). \tag{4.11}$$

In the following subsections, we introduce two kinds of lattice models, motivated by the run-and-tumble particles (RTPs) and active Brownian particles (ABPs), and map them exactly onto two symmetric conserved-mass transport processes on a periodic ring. We try to derive hydrodynamics for these systems from the microscopic description, using the modified biased rate [as in Eq. (4.9)] along with Eq. (4.11). Moreover, we calculate the transport coefficients for the models, which

have the gradient property, and then we verify an equilibrium-like Einstein relation (ER). Finally, we compare the bulk diffusion coefficients, calculated in both these models, and investigate the role of diffusivity in the dynamical arrest of particles, observed in many of these systems (analogous to that proposed previously in the literature in the context of MIPS).

4.2 Lattice models with persistent hopping

We define a lattice version of interacting run-and-tumble particles [40, 42, 43], where the system evolves in continuous time. We consider N persistent random walkers with hardcore interactions (a site can be occupied by at most one particle) on a periodic lattice of L sites. An arrow or a spin is associated with each of the particles. As the system we consider in the thesis is one dimensional, the spin can only be pointed either leftward or rightward (spin can have $2d$ possible directions in d dimensions). Therefore, a configuration is specified by occupancy and spin variables of all particles. A particle moves with unit rate along its current spin direction to its nearest neighbour site, provided the site is empty. With a tumbling rate D_r, a particle can go into a tumbling state: In the tumbling state, the spin of the particle is flipped with probability p (in this step, the spin remains the same with probability $1-p$). The limit of $D_r \to 0$ would correspond to completely persistent motion and the opposite limit of large D_r would correspond to a simple exclusion process on a periodic lattice. Note that $p = 1/2$ and $p = 1$ can be related to two recently studied model systems as discussed in Refs. [93, 94] (an on-lattice model) and [95] (an off-lattice model), respectively.

Now, in one dimension, the exclusion process described above can be mapped exactly onto an unbounded mass model with discrete masses. Consider the exclusion process of N particles on a ring $\mathcal{R}$ of L lattice sites. Suppose the number of holes in between i^{th} and $(i+1)^{th}$ particle is m_i. So, the total number of holes in the system $L - N = \sum_i m_i$. The spin of the i^{th} particle on $\mathcal{R}$ is denoted by $\tilde{S}_i$. $\tilde{S}_i$ takes value $+1$ or -1 when the direction of the spin associated with i^{th} particle is

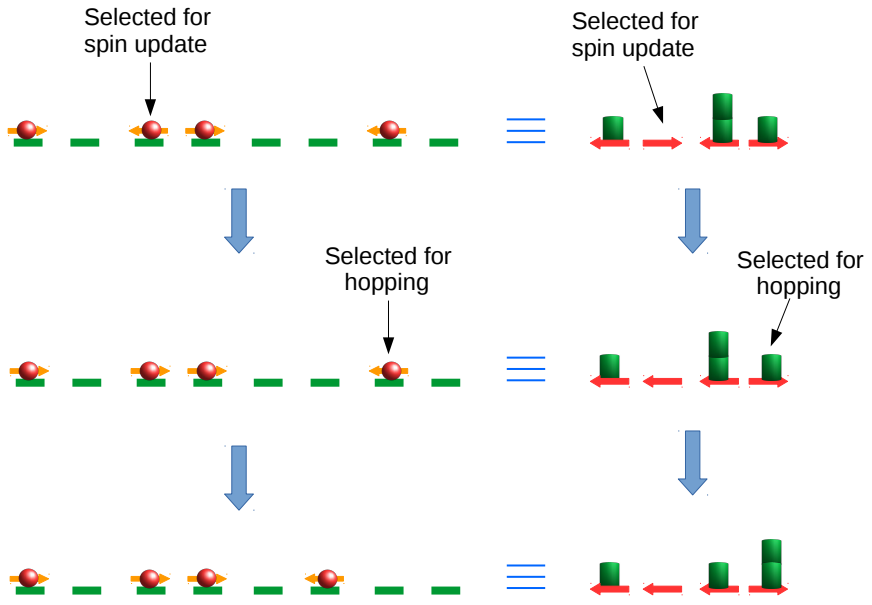

FIGURE 4.1: Exact mapping between one dimensional lattice model of persitent hardcore particles and the corresponding unbounded mass model.

rightward or leftward, respectively. We construct a new ring $\mathcal{R}'$ consisting of L' sites, with $L' = N$. For every i^{th} particle on ring $\mathcal{R}$, we construct a site labeled by i, at ring $\mathcal{R}'$. Now we put mass m_i at i^{th} site of ring $\mathcal{R}'$ so that the total mass $M = \sum_i m_i = L - N$. On ring $\mathcal{R}'$, the spin of i^{th} site $S_i = -\tilde{S}_i$. S_i also takes value $+1$ or -1 when the spin associated with i^{th} site is rightward or leftward, respectively. Thus every particle-hole-spin configuration on $\mathcal{R}$ maps onto a unique mass configuration on $\mathcal{R}'$.

Now we specify the correspondence between the particle dynamics on $\mathcal{R}$ and the mass dynamics on $\mathcal{R}'$. In Fig. 4.1 we give an elaborate example of this mapping and the corresponding dynamics. i is the particle index on $\mathcal{R}$ and site index on $\mathcal{R}'$. There is a crucial difference in mapping of dynamics for left jump and right jump of particles in this model. So we explain the mapping for both the jumps one by one. Suppose there are m_{i-1} holes on the right side of $(i-1)^{th}$ particle and m_i holes on the right side of i^{th} particle on the ring $\mathcal{R}$. Consider the i^{th}

particle of $\mathcal{R}$ is chosen randomly, $\tilde{S}_i = +1$, and the right neighboring site of it is empty. Then the i^{th} particle will jump to its right neighboring site making $m_{i-1} \to m_{i-1} + 1$ and $m_i \to m_i - 1$. Similarly on ring $\mathcal{R}'$, i^{th} site is chosen, $m_i > 0$, and $S_i = -1$. So, a single unit of mass is chipped off from i^{th} site and is transferred to its left nearest neighbor site [$(i-1)^{th}$ site] by changing the mass $m_{i-1} \to m_{i-1} + 1$ and $m_i \to m_i - 1$. Now if, on ring $\mathcal{R}$, i^{th} particle is chosen, $\tilde{S}_i = -1$, and the left neighboring site of it is empty. Then the i^{th} particle will jump to its left neighboring site making $m_{i-1} \to m_{i-1} - 1$ and $m_i \to m_i + 1$. Similarly on ring $\mathcal{R}'$, i^{th} site is chosen, $m_{i-1} > 0$, and $S_i = +1$. So, a single unit of mass is chipped off from $(i-1)^{th}$ site and is transferred to i^{th} site by changing the mass $m_{i-1} \to m_{i-1} - 1$ and $m_i \to m_i + 1$.

To express the above processes in a concise way, we write down the following stochastic update rules of mass $m_i(t)$ at i^{th} site at time t in an infinitesimal time-interval dt,

$$m_i(t+dt) = \begin{cases} m_i(t) - 1 & \text{prob. } a_i \delta_{S_i,-1} dt \\ m_i(t) - 1 & \text{prob. } a_i \delta_{S_{i+1},1} dt \\ m_i(t) + 1 & \text{prob. } a_{i+1} \delta_{S_{i+1},-1} dt \\ m_i(t) + 1 & \text{prob. } a_{i-1} \delta_{S_i,1} dt \\ m_i(t) & \text{prob. } 1 - [a_i \delta_{S_i,-1} + a_i \delta_{S_{i+1},1} + \\ & \qquad a_{i+1} \delta_{S_{i+1},-1} + a_{i-1} \delta_{S_i,1}] dt, \end{cases} \tag{4.12}$$

where $a_i = 1 - \delta_{m_i,0}$ ($a_i = 0$ or 1) is an indicator function for the occupancy of site i, *i.e.*, $a_i = 1$ if site i has at least one unit of mass (occupied) and $a_i = 0$ otherwise. Similar update rules for spin $S_i(t)$ at site i at time t in an infinitesimal time-interval dt can be written as given below,

$$S_i(t+dt) = \begin{cases} -S_i(t) & \text{prob. } D_r p dt \\ S_i(t) & \text{prob. } D_r(1-p) dt \\ S_i(t) & \text{prob. } 1 - D_r dt. \end{cases} \tag{4.13}$$

In the following sections, we work with the unbounded-mass versions (where occupancy is unbounded) of active lattice gases. It is advantageous to work with the unbounded versions as, unlike in the exclusion version, the spatial correlations in the unbounded versions in many cases are negligibly small and therefore the mean-field theory can capture various properties of the models remarkably well.

4.2.1 Particle-number fluctuations

Using the update rules as in Eqs. (4.12) and (4.13), the time evolution equation of the 2^{nd} moment $\langle m_i^2(t)\rangle$ at steady state can be written as

$$\begin{aligned}
\langle m_i^2\rangle = \quad & \langle (m_i^2 - 2m_i + 1)a_i\delta_{S_i,-1}\rangle + \langle (m_i^2 - 2m_i + 1)a_i\delta_{S_{i+1},1}\rangle \\
& + \langle (m_i^2 + 2m_i + 1)a_{i+1}\delta_{S_{i+1},-1}\rangle + \langle (m_i^2 + 2m_i + 1)a_{i-1}\delta_{S_i,1}\rangle \\
& + \langle m_i^2\rangle - \langle m_i^2(a_i\delta_{S_i,-1} + a_i\delta_{S_{i+1},1} + a_{i+1}\delta_{S_{i+1},-1} + a_{i-1}\delta_{S_i,1})\rangle, \\
\Rightarrow \quad & -2\langle m_i a_i\delta_{S_i,-1}\rangle + \langle a_i\delta_{S_i,-1}\rangle - 2\langle m_i a_i\delta_{S_{i+1},1}\rangle + \langle a_i\delta_{S_{i+1},1}\rangle \\
& + 2\langle m_i a_{i+1}\delta_{S_{i+1},-1}\rangle + \langle a_{i+1}\delta_{S_{i+1},-1}\rangle + 2\langle m_i a_{i-1}\delta_{S_i,1}\rangle + \langle a_{i-1}\delta_{S_i,1}\rangle = 0.
\end{aligned}$$

We consider the mass variable, occupancy and the spin variable are independent of each other. So, within this mean-field approximation, the above equation can be written as

$$\begin{aligned}
& -2\langle m_i a_i\rangle\langle\delta_{S_i,-1}\rangle + \langle a_i\rangle\langle\delta_{S_i,-1}\rangle - 2\langle m_i a_i\rangle\langle\delta_{S_{i+1},1}\rangle + \langle a_i\rangle\langle\delta_{S_{i+1},1}\rangle \\
& + 2\langle m_i\rangle\langle a_{i+1}\rangle\langle\delta_{S_{i+1},-1}\rangle + \langle a_{i+1}\rangle\langle\delta_{S_{i+1},-1}\rangle \\
& + 2\langle m_i\rangle\langle a_{i-1}\rangle\langle\delta_{S_i,1}\rangle + \langle a_{i-1}\rangle\langle\delta_{S_i,1}\rangle = 0, \\
\Rightarrow \quad & -2\rho\frac{1}{2} + A\frac{1}{2} - 2\rho\frac{1}{2} + A\frac{1}{2} + 2\rho A\frac{1}{2} + A\frac{1}{2} + 2\rho A\frac{1}{2} + A\frac{1}{2} = 0, \\
\Rightarrow \quad & -\rho + A + \rho A = 0, \\
\Rightarrow \quad & A = \frac{\rho}{1+\rho}, \qquad (4.14)
\end{aligned}$$

with $A = \langle a_i\rangle$ and density $\rho = \langle m_i\rangle$.

Similarly, the time evolution equation of the 3^{rd} moment $\langle m_i^3(t)\rangle$ at steady state, within mean-field limit, can be written as,

$$\begin{aligned}
\langle m_i^3\rangle = \quad & \langle (m_i^3 - 3m_i^2 + 3m_i - 1)a_i\delta_{S_i,-1}\rangle + \langle (m_i^3 - 3m_i^2 + 3m_i - 1)a_i\delta_{S_{i+1},1}\rangle \\
& + \langle (m_i^3 + 3m_i^2 + 3m_i + 1)a_{i+1}\delta_{S_{i+1},-1}\rangle + \langle (m_i^3 + 3m_i^2 + 3m_i + 1)a_{i-1}\delta_{S_i,1}\rangle \\
& + \langle m_i^3\rangle - \langle m_i^3(a_i\delta_{S_i,-1} + a_i\delta_{S_{i+1},1} + a_{i+1}\delta_{S_{i+1},-1} + a_{i-1}\delta_{S_i,1})\rangle, \\
\Rightarrow \quad & -3\langle m_i^2 a_i\delta_{S_i,-1}\rangle + 3\langle m_i a_i\delta_{S_i,-1}\rangle - \langle a_i\delta_{S_i,-1}\rangle \\
& -3\langle m_i^2 a_i\delta_{S_{i+1},1}\rangle + 3\langle m_i a_i\delta_{S_{i+1},1}\rangle - \langle a_i\delta_{S_{i+1},1}\rangle \\
& +3\langle m_i^2 a_{i+1}\delta_{S_{i+1},-1}\rangle + 3\langle m_i a_{i+1}\delta_{S_{i+1},-1}\rangle - \langle a_{i+1}\delta_{S_{i+1},-1}\rangle \\
& +3\langle m_i^2 a_{i-1}\delta_{S_i,1}\rangle + 3\langle m_i a_{i-1}\delta_{S_i,1}\rangle - \langle a_{i-1}\delta_{S_i,1}\rangle \\
\Rightarrow \quad & -3\langle m^2\rangle + 3\rho - A + 3\langle m^2\rangle A + 3\rho A + A = 0 \\
\Rightarrow \quad & \langle m^2\rangle = \frac{\rho(1+A)}{(1-A)}
\end{aligned} \tag{4.15}$$

Using Eqs. (4.14) and (4.15) we can calculate the scaled subsystem number fluctuation (within the mean-field limit) as a function of density ρ

$$\begin{aligned}
\sigma^2(\rho) &= \langle m^2\rangle - \rho^2 \\
&= \frac{\rho(1+A)}{(1-A)} - \rho^2 \\
&= \rho(1+\rho)
\end{aligned} \tag{4.16}$$

Note that, the scaled variance $\sigma^2(\rho)$ in Eq. (4.16) does not depend on tumbling rate D_r. To check that, we perform Monte Carlo simulations of unbounded mass model to obtain scaled variance $\sigma^2(\rho)$ of subsystem mass and plot them in Fig. 4.2 for different tumbling rate $D_r = 0.05$ (blue), 0.3 (green) and 1.0 (magenta) along with the mean-field result (yellow line). One could see from the above plots that the mean-field theory captures qualitative features in simulations quite well only when the value of D_r is reasonably large.

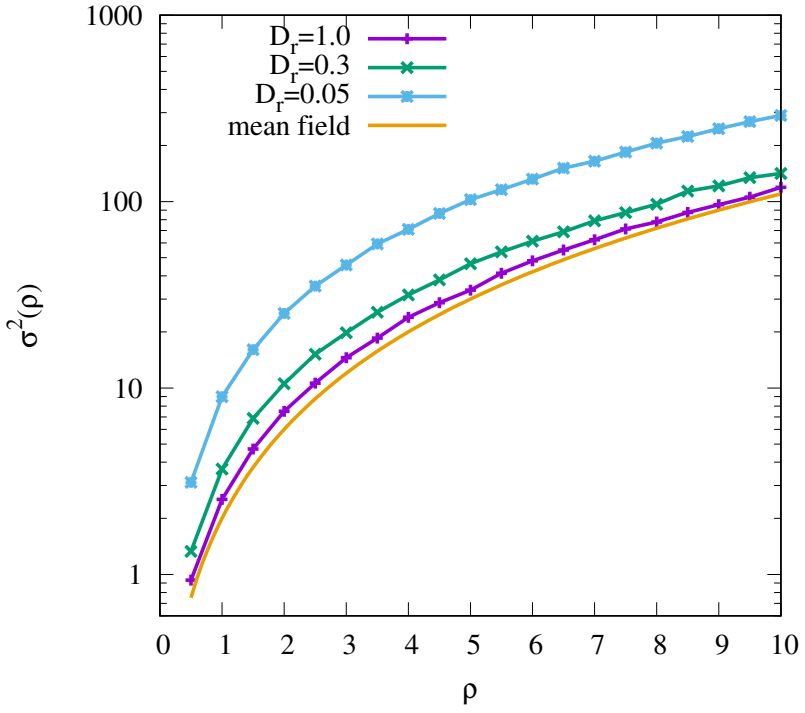

FIGURE 4.2: Scaled variance $\sigma^2(\rho)$ is plotted as a function of density ρ for different tumbling rates $D_r = 0.05$ (blue), 0.3 (green), and 1.0 (magenta) along with the mean-field result [given by Eq. (4.16)] (yellow line).

4.2.2 Hydrodynamics

As we discussed in the introduction, to calculate the transport coefficients, especially the conductivity $\chi(\rho)$, we need to bias the system by a small constant biasing force $\mathbf{F}$ which modifies the original mass-hopping rate. Here we define W as the single mass chipping rate. Combining Eqs. (4.9) and (4.11), the biased mass transfer rate from site i to j becomes,

$$c^F_{i,j} = c^F_{i\to j} = c_{i\to j}\left[1 + \frac{1}{2}\Delta m_{i\to j} F(j-i)a\right], \tag{4.17}$$

with $\Delta m_{i\to j}$ the transferred mass from from site i to j and lattice spacing $a = 1$. We set all the rates for unbiased system to unity in Eq. (4.12). So the biased mass

transfer rates are,

$$W^F_{i,i+1} = 1 + \frac{F}{2} \tag{4.18}$$

$$W^F_{i,i-1} = 1 - \frac{F}{2} \tag{4.19}$$

$$W^F_{i+1,i} = 1 - \frac{F}{2} \tag{4.20}$$

$$W^F_{i-1,i} = 1 + \frac{F}{2} \tag{4.21}$$

Therefore, the biased evolution equation of mass $m_i(t)$ at i^{th} site at time t after an infinitesimal time-interval dt is given by,

$$m_i(t+dt) = \begin{cases} m_i(t) - 1 & \text{prob. } W^F_{i,i-1} a_i \delta_{S_i,-1} dt, \\ m_i(t) - 1 & \text{prob. } W^F_{i,i+1} a_i \delta_{S_{i+1},1} dt, \\ m_i(t) + 1 & \text{prob. } W^F_{i+1,i} a_{i+1} \delta_{S_{i+1},-1} dt, \\ m_i(t) + 1 & \text{prob. } W^F_{i-1,i} a_{i-1} \delta_{S_i,1} dt, \\ m_i(t) & \text{prob. } 1 - \Sigma_1 dt, \end{cases} \tag{4.22}$$

with $\Sigma_1 = W^F_{i,i-1} a_i \delta_{S_i,-1} + W^F_{i,i+1} a_i \delta_{S_{i+1},1} + W^F_{i+1,i} a_{i+1} \delta_{S_{i+1},-1} + W^F_{i-1,i} a_{i-1} \delta_{S_i,1}$.

The evolution equation of spin $S_i(t)$ at i^{th} site at time t remains the same and is given by,

$$S_i(t+dt) = \begin{cases} -S_i(t) & \text{prob. } D_r p dt \\ S_i(t) & \text{prob. } D_r(1-p) dt \\ S_i(t) & \text{prob. } 1 - D_r dt. \end{cases} \tag{4.23}$$

Time evolution equation of average mass, or mass density, $\langle m_i \rangle(t) = \rho_i(t)$ at site i and at time t, can be written as

$$\begin{aligned}
\frac{\partial \langle m_i \rangle}{\partial t} &= \langle (m_i - 1) W^F_{i,i-1} a_i \delta_{S_i,-1} \rangle + \langle (m_i - 1) W^F_{i,i+1} a_i \delta_{S_{i+1},1} \rangle + \\
&\quad \langle (m_i + 1) W^F_{i+1,i} a_{i+1} \delta_{S_{i+1},-1} \rangle + \langle (m_i + 1) W^F_{i-1,i} a_{i-1} \delta_{S_i,1} \rangle \\
&\quad - m_i \langle [W^F_{i,i-1} a_i \delta_{S_i,-1} + W^F_{i,i+1} a_i \delta_{S_{i+1},1} + W^F_{i+1,i} a_{i+1} \delta_{S_{i+1},-1} + W^F_{i-1,i} a_{i-1} \delta_{S_i,1}] \rangle \\
&= \langle - \left(1 - \frac{F}{2}\right) a_i \delta_{S_i,-1} \rangle + \langle - \left(1 + \frac{F}{2}\right) a_i \delta_{S_{i+1},1} \rangle \\
&\quad + \langle \left(1 - \frac{F}{2}\right) a_{i+1} \delta_{S_{i+1},-1} \rangle + \langle \left(1 + \frac{F}{2}\right) a_{i-1} \delta_{S_i,1} \rangle \\
&= - \langle a_i \delta_{S_i,-1} \rangle - \langle a_i \delta_{S_{i+1},1} \rangle + \langle a_{i+1} \delta_{S_{i+1},-1} \rangle + \langle a_{i-1} \delta_{S_i,1} \rangle \\
&\quad \frac{F}{2} \left[\langle a_i \delta_{S_i,-1} \rangle - \langle a_i \delta_{S_{i+1},1} \rangle - \langle a_{i+1} \delta_{S_{i+1},-1} \rangle + \langle a_{i-1} \delta_{S_i,1} \rangle \right]
\end{aligned}$$

We may again consider the mass variable, occupancy and the spin variable are independent of each other. So, within this mean-field approximation, the above equation can be written as

$$\begin{aligned}
\frac{\partial \langle m_i \rangle}{\partial t} &= - \langle a_i \rangle \langle \delta_{S_i,-1} \rangle - \langle a_i \rangle \langle \delta_{S_{i+1},1} \rangle + \langle a_{i+1} \rangle \langle \delta_{S_{i+1},-1} \rangle + \langle a_{i-1} \rangle \langle \delta_{S_i,1} \rangle \\
&\quad \frac{F}{2} \left[\langle a_i \rangle \langle \delta_{S_i,-1} \rangle - \langle a_i \rangle \langle \delta_{S_{i+1},1} \rangle - \langle a_{i+1} \rangle \langle \delta_{S_{i+1},-1} \rangle + \langle a_{i-1} \rangle \langle \delta_{S_i,1} \rangle \right] \\
&= - \langle a_i \rangle + \frac{1}{2} \langle a_{i-1} \rangle + \frac{1}{2} \langle a_{i+1} \rangle - \langle a_{i+1} \rangle \frac{F}{4} + \langle a_{i-1} \rangle \frac{F}{4} \\
&= - A_i + \frac{1}{2} A_{i-1} + \frac{1}{2} A_{i+1} - F A_{i+1}/4 + F A_{i-1}/4 \qquad (4.24)
\end{aligned}$$

where, $A_i = \langle a_i \rangle$ is a local observable. One can notice that in Eq. (4.24), the local diffusive current J_D can be expressed as a *g*radient (discrete) of the local observable A_i, which is called a "gradient condition". This gradient property helps one to identify the bulk diffusion coefficient and the conductivity, which we discuss next.

First, taking the diffusive scaling limit of Eq. (4.24), $i \to x = i/L$ and $t \to \tau = t/L^2$, and lattice constant $a \to 1/L$, we obtain hydrodynamic time-evolution

equation for the density field $\rho(x,\tau)$,

$$\begin{aligned}
\frac{\partial\rho(x,\tau)}{\partial t} &= \frac{1}{2}\left[A\left(x-\frac{1}{L}\right)+A\left(x+\frac{1}{L}\right)-2A(x)\right] \\
&\quad -\frac{1}{4}\left[A\left(x+\frac{1}{L}\right)-A\left(x-\frac{1}{L}\right)\right]\frac{F}{L} \\
&= \frac{1}{2}\left[\frac{1}{L^2}\frac{\partial^2 A}{\partial x^2}\right]-\frac{1}{4}\left[\frac{2}{L}\frac{\partial A}{\partial x}\right]\frac{F}{L} \\
\Rightarrow \frac{\partial\rho(x,\tau)}{\partial\tau} &= \frac{1}{2}\frac{\partial^2 A}{\partial x^2}-\frac{1}{2}F\frac{\partial A}{\partial x} \\
&= -\frac{\partial}{\partial x}\frac{1}{2}\left[-\frac{\partial A}{\partial x}+AF\right] \\
&= -\frac{\partial}{\partial x}\left[-\frac{1}{2}\frac{\partial A}{\partial\rho}\frac{\partial\rho}{\partial x}+\frac{1}{2}AF\right] \\
&= -\frac{\partial}{\partial x}\left[-D(\rho)\frac{\partial\rho}{\partial x}+\chi(\rho)F\right] \qquad (4.25)
\end{aligned}$$

From Eq. (4.25) one can easily identify (due to its gradient nature) the diffusivity and conductivity, respectively as

$$D(\rho) = \frac{1}{2}\frac{\partial A}{\partial\rho} = \frac{1}{2(1+\rho)^2} \qquad (4.26)$$

$$\chi(\rho) = \frac{1}{2}A = \frac{\rho}{2(1+\rho)} \qquad (4.27)$$

Now the ratio of conductivity $\chi(\rho)$ and bulk diffusion coefficient $D(\rho)$ from Eqs. (4.27) and (4.26) respectively, is given by

$$\frac{\chi(\rho)}{D(\rho)} = \rho(1+\rho) = \sigma^2(\rho) \qquad (4.28)$$

Note that, the expression in Eq. (4.28) is the same as the expression of scaled variance in Eq. (4.16). Therefore, within mean-field theory, the Einstein relation as in Eq. (4.7) is indeed exactly satisfied.

4.2.3 Simulations

One could be interested to compare the mean-field hydrodynamics and simulations, which is done as follows. After substituting the functional form of $D(\rho)$ from Eq. (4.26), the hydrodynamic evolution equation [Eq. (4.25)] of density field $\rho(x,\tau)$ with rescaled position x and rescaled time τ in the limit of biasing force $F = 0$ becomes,

$$\frac{\partial \rho(x,\tau)}{\partial \tau} = -\frac{\partial}{\partial x}\left[-\frac{1}{2(1+\rho)^2}\frac{\partial \rho}{\partial x}\right]. \tag{4.29}$$

We are interested in the evolution of density field $\rho(x,\tau)$ at different times, starting from the initial condition

$$\rho(x,\tau=0) = \rho_0 + \rho_1 \frac{\exp(-x^2/2\Delta_0^2)}{\sqrt{2\pi\Delta_0^2}} \tag{4.30}$$

where we have chosen $\Delta_0 = 10$, ρ_0 (a uniform background density) and ρ_1 (strength of the initial density perturbation) are two constants.

We now numerically integrate Eq. (4.29) by discretizing x and τ (we use Euler method with $\delta x = 1$, $\delta\tau = 10^{-2}$), keeping total particle number fixed. Then we also perform Monte Carlo simulations of the microscopic unbounded-mass model with random sequential updates (which would correspond to a continuous-time dynamics). One Monte-Carlo time unit (each site is updated at rate 1 in simulations) corresponds to unit of time in continuous-time hydrodynamic evolution Eq. (4.29). In simulations, we have generated random initial configurations, which would correspond to the initial density profile as in Eq. (4.30); in simulations, we average over the initial configurations as well as over the trajectories.

In Fig. 4.3, we have compared density profiles obtained by integrating hydrodynamic evolution Eq. (4.29) [lines] and that obtained from Monte Carlo simulations of unbounded mass model [points], at different times $\tau = 500$, 1000, 2500 and 5000, starting from initial condition Eq. (4.30), for different values of tumbling rate $D_r = 0.01$, 0.02, 0.05, 0.3, 1.0 and $D_r \to \infty$. In all panels, we plot the mean-field hydrodynamic evolution of density for different times $\tau = 0$ (magenta

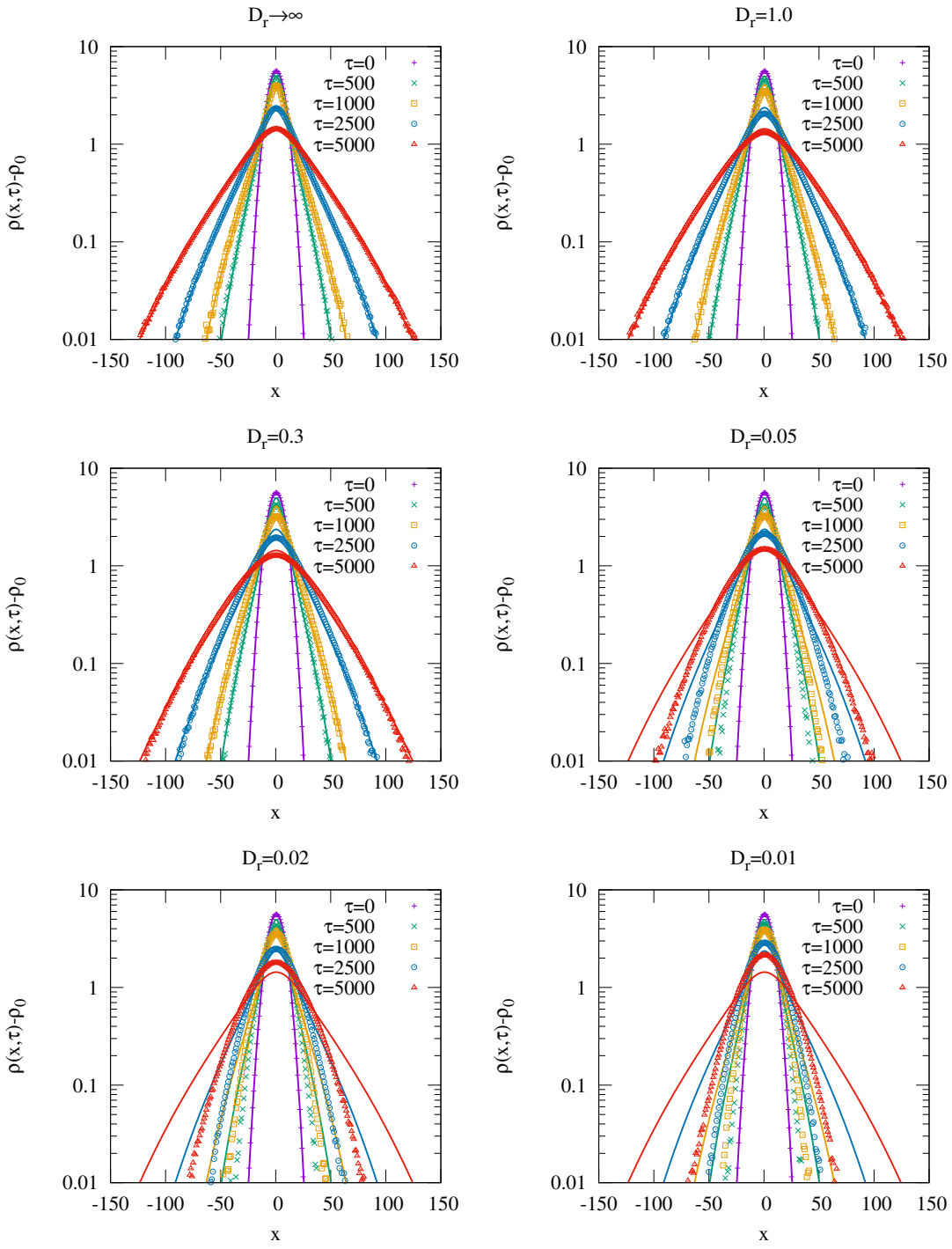

FIGURE 4.3: Comparison between density evolution of mean-field hydrodynamic Eq. (4.29) [lines] and that obtained from simulations [points], at different times $\tau = 0$ (magenta), 500 (green), 1000 (yellow), 2500 (blue) and 5000 (red), for different values of tumbling rate $D_r = 0.01$, 0.02, 0.05, 0.3, 1.0 and $D_r \to \infty$. It shows that mean-field theory can not capture the simulation result at lower value of D_r.

lines), 500 (green lines), 1000 (yellow lines), 2500 (blue lines) and 5000 (red lines). In the limit of tumbling rate $D_r \to \infty$, mean-field hydrodynamics is exact and evidently agrees with the simulation results. Even, at the intermediate values of D_r, mean-field theory captures reasonably well the simulations. However, at very small D_r, deviations from mean-field theory are quite pronounced.

Note that, as this model does not have the gradient property, identifying the transport coefficients analytically as an average over some local observable is not possible and remains to be an open problem. However, using the above method of evolving an initial density profile (for simplicity, taken to be a Gaussian), it is possible to numerically calculate the bulk diffusion coefficient, as discussed in the following sections.

4.2.4 Characterization of density relaxations

In Fig. 4.3, we note that, in the limit of tumbling rate $D_r \to \infty$, mean-field theory is exact. However, mean-field hydrodynamics cannot capture the simulation results at small D_r. Moreover, quite interestingly, the width of the density profile at a particular time τ decreases with decreasing D_r, indicating effective slowing down of particle diffusion and dynamical arrest or clustering. Therefore, to quantify the above observation, we study below in more detail how the width of density spreads over time, calculated from the simulation, for different values of D_r. To this end, we define width of density spreading at time τ as

$$\Delta^2(\tau) = \frac{\sum_{i=-L/2}^{L/2} x_i^2(\tau)(\rho[x_i(\tau)] - \rho_0)}{\sum_{i=-L/2}^{L/2}(\rho[x_i(\tau)] - \rho_0)} \tag{4.31}$$

with L be the system size. We plot $\Delta^2(\tau)$ with time τ for tumbling rate $D_r = 0.01$ (red), 0.02 (yellow), 0.05 (blue), 0.3 (green) and 1.0 (magenta) in the upper panel of Fig. 4.4. It clearly shows that the rate of increment of $\Delta^2(\tau)$ decreases with D_r which signifies clustering of masses in the system. To provide a more quantitative description, we define two quantities as follows. An effective hop length is defined simply as $l_{hop} = 1/D_r$, which, in the original exclusion version of the model, is

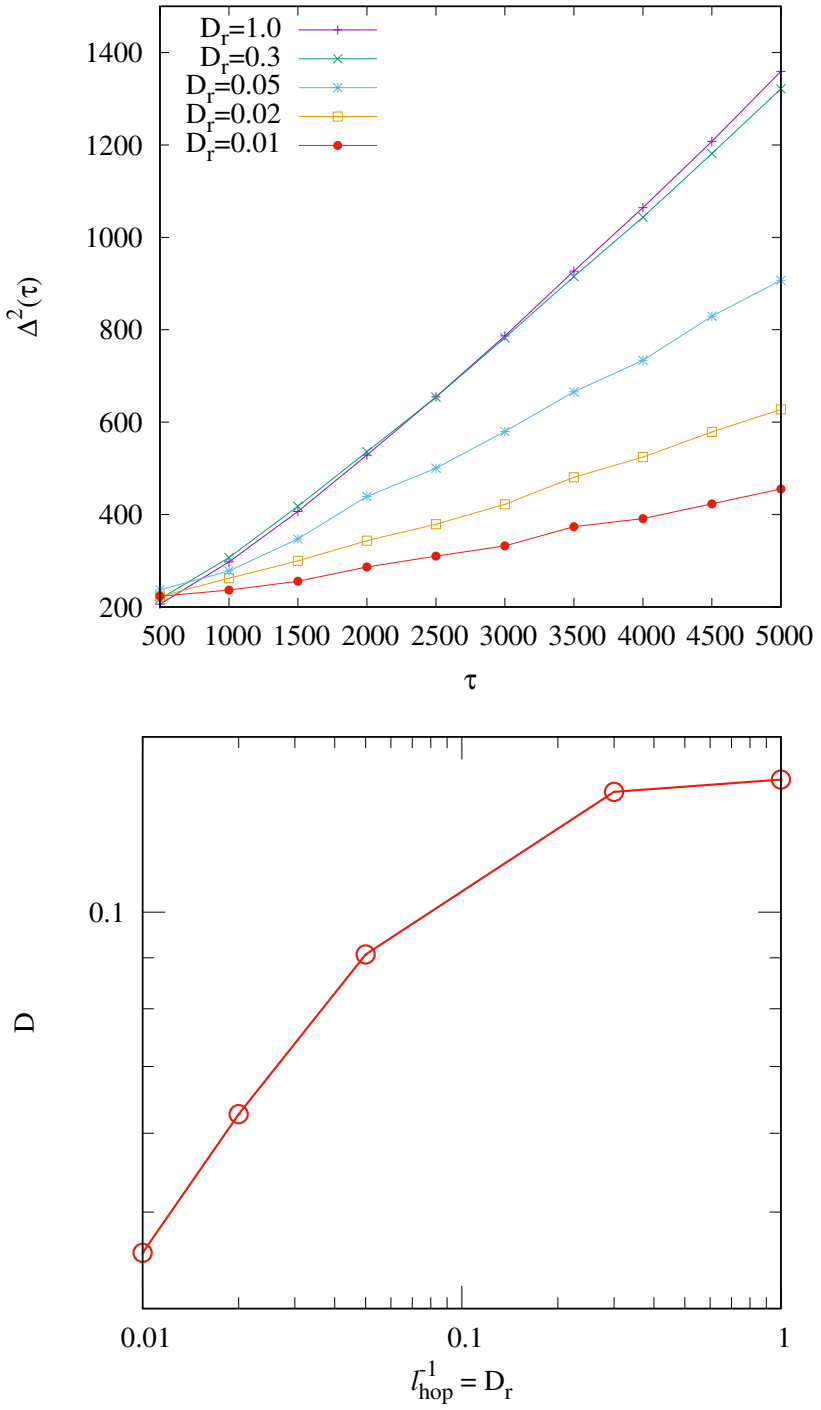

FIGURE 4.4: Upper panel: Width of density $\Delta^2(\tau)$ [as defined in Eq. (4.31)] is plotted with time τ for tumbling rate $D_r = 0.01$ (red), 0.02 (yellow), 0.05 (blue), 0.3 (green) and 1.0 (magenta). Lower panel: diffusion coefficient D is plotted with inverse of effective hop length $l_{hop} = 1/D_r$.

a measure of the average distance traversed by a particle between two successive tumbles and, in the unbounded-mass version, is equivalent to the average mass transferred from a particular site during two successive spin flips. Furthermore, in the long-time limit and for large system size, bulk diffusion coefficient can now be defined as given below

$$D = \lim_{\tau \to \infty} \frac{\Delta^2(\tau)}{2\tau}. \tag{4.32}$$

We find, in upper panel of Fig. 4.4, that bulk diffusion coefficient D decreases with increasing l_{hop} and then plot diffusion coefficient D as a function of the inverse of the effective hop length l_{hop} in the lower panel of Fig. 4.4. This particular behaviour demonstrate that bulk diffusivity of masses indeed slows down quite drastically with decreasing tumbling rates and indicates clustering. Clustering of masses in the unbounded-mass version of the model is related to the clustering of holes in the exclusion version model. The formation of hole clusters in exclusion version of the model could also lead to a self trapping of particles analogous to the motility induced phase separation (MIPS) [see Secs. 1.3.3 and 1.3.4 in Chapter 1] observed in many of active-matter systems.

4.3 Lattice models with long-range hopping

In this section we define a lattice gas with both short-range (nearest neighbour) and long-range (with a specified hop length) in a periodic one dimensional lattice. This one dimensional model of active matter evolves in continuous time. Due to hardcore nature of the particles, each site is occupied by at most one particle and they cannot cross each other. We consider N particles on a one dimensional ring of L sites. The update rules are as follows. A site is chosen randomly. If the site is occupied, the selected particle can perform two possible moves; a short hop to one of its neighbours or a long hop with a fixed length, which is somewhat analogous to the displacement of an active persistent particle (see the persistent-hop model in the previous section) during two successive tumbles. The probability of choosing a short or a long hop can be a parameter in the model. If short hop is chosen,

the particle will hop a single lattice spacing, either leftward or rightward, provided that the target site is empty, with equal probability. In the case of long hop, the particle can hop leftward or rightward, with equal probability, with a fixed hop length v. To perform a long hop, the selected particle hops v lattice spacings if the number of vacant sites along the direction of its hop is greater than or equal to v; otherwise, the particle just sits beside the next occupied site along the direction of its hop.

In one dimension, as shown in the previous section for persistent-hop models, the long-range hop model can be mapped exactly onto an unbounded-mass model, where each lattice site is associated with discrete (non-negative) masses. The mapping can be done as follows. Consider a lattice gas of N particles on a ring $\mathcal{R}$ of L lattice sites. Suppose the number of holes in between i^{th} and $(i+1)^{th}$ particle is m_i. So, the total number of holes in the system $L - N = \sum_i m_i$. We construct a new ring $\mathcal{R}'$ consisting of L' sites, with $L' = N$. For every i^{th} particle in ring $\mathcal{R}$, we construct a site labeled by i, at ring $\mathcal{R}'$. Now we put mass m_i at i^{th} site of ring $\mathcal{R}'$ so that the total mass $M = \sum_i m_i = L - N$. Thus every particle-hole configuration on $\mathcal{R}$ maps onto a unique mass configuration on $\mathcal{R}'$.

Now we specify the correspondence between the particle dynamics on $\mathcal{R}$ and the mass dynamics on $\mathcal{R}'$. In Fig. 4.5 we give an elaborate example of this mapping and the corresponding dynamics. i is the particle index on $\mathcal{R}$ and site index on $\mathcal{R}'$. Suppose there are m_i holes on the right side of i^{th} particle and m_{i+1} holes on the right side of $(i+1)^{th}$ particle on the ring $\mathcal{R}$. Consider the $(i+1)^{th}$ particle of $\mathcal{R}$ is chosen randomly and selected for a short hop to right and the right neighboring site of it is empty. Then the $(i+1)^{th}$ particle will jump to its right neighboring site making $m_i \to m_i + 1$ and $m_{i+1} \to m_{i+1} - 1$. Similarly on ring $\mathcal{R}'$, a single unit of mass is chipped off from $(i+1)^{th}$ site and is transferred to its left nearest neighbor site (i^{th} site) changing the mass $m_i \to m_i + 1$ and $m_{i+1} \to m_{i+1} - 1$.

We also have the long hop in exclusion process. Consider once again that there are m_i holes on the right side of i^{th} particle and m_{i+1} holes on the right side of $(i+1)^{th}$ particle on the ring $\mathcal{R}$. Suppose $(i+1)^{th}$ particle on $\mathcal{R}$ is chosen randomly

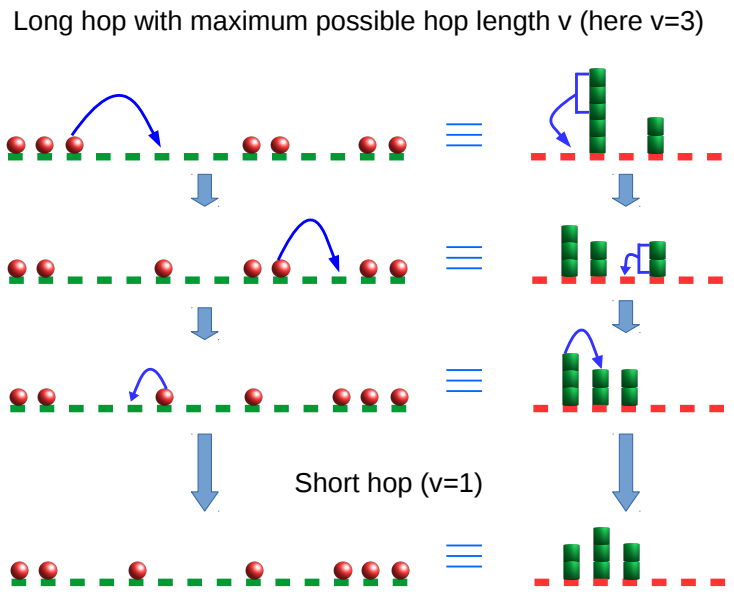

FIGURE 4.5: Exact mapping between one dimensional hardcore lattice gas model with long-range hopping and the corresponding unbounded mass model.

and selected for a long hop to right with a hopping velocity v. If the number of holes to right of $(i+1)^{th}$ particle $m_{i+1} \geq v$, then the $(i+1)^{th}$ particle will jump v sites to right, making $m_i \to m_i + v$ and $m_{i+1} \to m_{i+1} - v$. Otherwise, *i.e.*, if $m_{i+1} < v$ then, the $(i+1)^{th}$ particle will sit just before the $(i+2)^{th}$ particle making $m_i \to m_i + m_{i+1}$ and $m_{i+1} \to 0$. Similarly on ring $\mathcal{R}'$, v unit of mass is chipped off from $(i+1)^{th}$ site and is transferred to its left nearest neighbor site, if the mass at that site $m_{i+1} \geq v$, changing the mass $m_i \to m_i + v$ and $m_{i+1} \to m_{i+1} - v$. For $m_{i+1} < v$, the whole mass at $(i+1)^{th}$ site is chipped off and is transferred to i^{th} site.

Breakdown of Kolmogorov criterion: In Fig. 4.6 we show that in configuration 1, the third particle, at any instant of time, is selected for a long hop towards right with a maximum hop length $v = 3$. As, for this particular configuration, the number of vacant sites in the right of the third particle is one, the particle will jump to the right next site and will reach configuration 2. Now consider the reverse path, *i.e.*, at configuration 2, the third particle is selected for a long hop

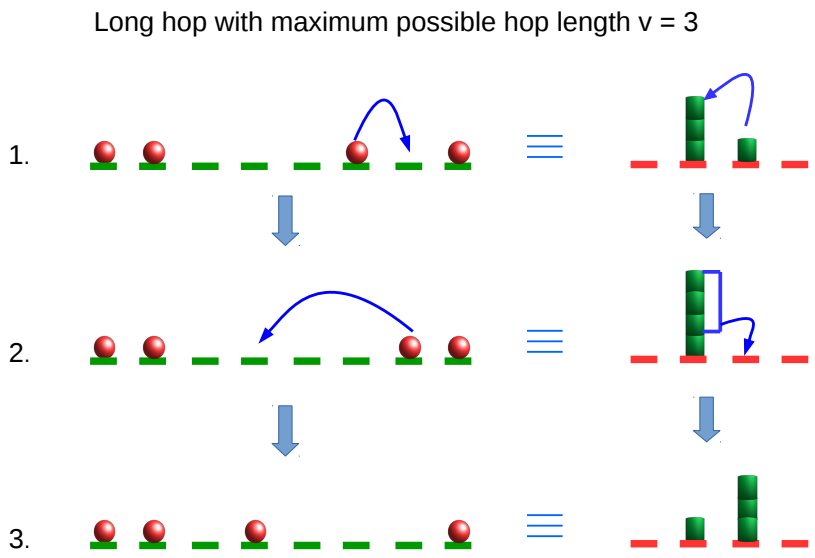

FIGURE 4.6: Breakdown of Kolmogorob criterion in one dimensional lattice model with long-range hopping and in corresponding unbounded mass model.

towards left. It will reach configuration 3 as the number of vacant site in the left of the third particle at configuration 2 is greater than maximum hop length $v = 3$. So going from configuration 2 to configuration 1 by exactly reversing the path is not possible in this model which implies violation of Kolmogorov criterion of equilibrium.

In the following we write down the stochastic time evolution equation of mass $m_i(t)$ at i^{th} site at time t after an infinitesimal time-interval dt,

$$m_i(t+dt) = \begin{cases} m_i(t) - v & \text{prob. } a_i^v dt/2, \\ 0 & \text{prob. } a_i(1-a_i^v)dt/2, \\ m_i(t) - 1 & \text{prob. } a_i dt/2, \\ m_i(t) + 1 & \text{prob. } a_{i-1} dt/4, \\ m_i(t) + 1 & \text{prob. } a_{i+1} dt/4, \\ m_i(t) + m_{i-1}(t) & \text{prob. } a_{i-1}(1-a_{i-1}^v)dt/4, \\ m_i(t) + v & \text{prob. } a_{i-1}^v dt/4, \\ m_i(t) + m_{i+1}(t) & \text{prob. } a_{i+1}(1-a_{i+1}^v)dt/4, \\ m_i(t) + v & \text{prob. } a_{i+1}^v dt/4, \\ m_i(t) & \text{prob. } 1 - \Sigma dt, \end{cases} \tag{4.33}$$

with

$$\Sigma = \frac{1}{2}\left[a_i^v + a_i(1-a_i^v) + a_i\right] + \frac{1}{4}\left[a_{i-1} + a_{i+1} + a_{i-1}(1-a_{i-1}^v)\right] + \frac{1}{4}\left[a_{i-1}^v + a_{i+1}(1-a_{i+1}^v) + a_{i+1}^v\right] \tag{4.34}$$

where $a_i = 1 - \delta_{m_i,0}$ is the occupancy which ensures that the i^{th} site is occupied and a_i^v is another indicator function which ensures that the i^{th} site contains at least v particles.

$$\begin{aligned} a_i^v &= 1 \quad \texttt{if} \quad m_i \geq v \\ &= 0 \quad \texttt{if} \quad m_i < v. \end{aligned}$$

4.3.1 Hydrodynamics

Now we need to bias the system by a small constant biasing force $\mathbf{F}$ to calculate the transport coefficients, especially the conductivity $\chi(\rho)$. This biasing force modifies the original mass-hopping rate according to Eq. (4.17). Here we define B as mass-hopping rate when maximum v mass is transferred and W as the single

mass chipping rate. We set all the rates for unbiased system to unity in Eq. (4.33). So the biased mass transfer rates are,

$$
\begin{aligned}
B^{F_v}_{i,i+1} &= 1 + vF(i+1-i)/2 = 1 + vF/2, && (4.35)\\
B^{F_v}_{i,i-1} &= 1 + vF(i-1-i)/2 = 1 - vF/2, && (4.36)\\
B^{F}_{i,i+1} &= 1 + m_iF(i+1-i)/2 = 1 + m_iF/2, && (4.37)\\
B^{F}_{i,i-1} &= 1 + m_iF(i-1-i)/2 = 1 - m_iF/2, && (4.38)\\
W^{F}_{i,i+1} &= 1 + F(i+1-i)/2 = 1 + F/2, && (4.39)\\
W^{F}_{i,i-1} &= 1 + F(i-1-i)/2 = 1 - F/2, && (4.40)\\
W^{F}_{i-1,i} &= 1 + 1.F(i-i+1)/2 = 1 + F/2, && (4.41)\\
W^{F}_{i+1,i} &= 1 + 1.F(i-i-1)/2 = 1 - F/2, && (4.42)\\
B^{F}_{i-1,i} &= 1 + m_{i-1}F/2, && (4.43)\\
B^{F_v}_{i-1,i} &= 1 + vF/2, && (4.44)\\
B^{F}_{i+1,i} &= 1 - m_{i+1}F/2, && (4.45)\\
B^{F_v}_{i+1,i} &= 1 - vF/2. && (4.46)
\end{aligned}
$$

So, the biased evolution equation of mass $m_i(t)$ at i^{th} site at time t after an infinitesimal time-interval dt becomes,

$$
m_i(t+dt) = \begin{cases}
m_i(t) - v & \text{prob. } a^v_i dt/2\\
0 & \text{prob. } a_i(1-a^v_i)dt/2\\
m_i(t) - 1 & \text{prob. } a_i dt/2\\
m_i(t) + 1 & \text{prob. } W^F_{i-1,i}a_{i-1}dt/4\\
m_i(t) + 1 & \text{prob. } W^F_{i+1,i}a_{i+1}dt/4\\
m_i(t) + m_{i-1}(t) & \text{prob. } B^F_{i-1,i}a_{i-1}(1-a^v_{i-1})dt/4\\
m_i(t) + v & \text{prob. } B^{F_v}_{i-1,i}a^v_{i-1}dt/4\\
m_i(t) + m_{i+1}(t) & \text{prob. } B^F_{i+1,i}a_{i+1}(1-a^v_{i+1})dt/4\\
m_i(t) + v & \text{prob. } B^{F_v}_{i+1,i}a^v_{i+1}dt/4\\
m_i(t) & \text{prob. } 1 - \Sigma' dt
\end{cases} \qquad (4.47)
$$

with

$$\Sigma' = \frac{1}{2}\left[a_i^v + a_i(1-a_i^v) + a_i\right] + \frac{1}{4}\left[W_{i-1,i}^F a_{i-1} + W_{i+1,i}^F a_{i+1}\right]$$
$$+\frac{1}{4}\left[B_{i-1,i}^F a_{i-1}(1-a_{i-1}^v) + B_{i-1,i}^{F_v} a_{i-1}^v + B_{i+1,i}^F a_{i+1}(1-a_{i+1}^v) + B_{i+1,i}^{F_v} a_{i+1}^v\right]. \quad (4.48)$$

Time evolution equation of average mass, or mass density, $\langle m_i\rangle(t) = \rho_i(t)$ at site i and at time t, can be written as,

$$\begin{aligned}
\frac{d\langle m_i\rangle}{dt} &= \frac{1}{2}\left[\langle (m_i(t)-v)a_i^v\rangle + \langle (m_i(t)-1)a_i\rangle\right] \\
&+\frac{1}{4}\left[\langle (m_i(t)+1)W_{i-1,i}^F a_{i-1}\rangle + \langle (m_i(t)+1)W_{i+1,i}^F a_{i+1}\rangle\right] \\
&+\frac{1}{4}\left[\langle (m_i(t)+m_{i-1}(t))B_{i-1,i}^F a_{i-1}(1-a_{i-1}^v)\rangle\right] \\
&+\frac{1}{4}\left[\langle (m_i(t)+v)B_{i-1,i}^{F_v} a_{i-1}^v\rangle + \langle (m_i(t)+m_{i+1}(t))B_{i+1,i}^F a_{i+1}(1-a_{i+1}^v)\rangle\right] \\
&+\frac{1}{4}\left[\langle (m_i(t)+v)B_{i+1,i}^{F_v} a_{i+1}^v\rangle\right] - \frac{1}{2}\langle m_i(t)\left[a_i^v + a_i(1-a_i^v) + a_i\right]\rangle \\
&-\frac{1}{4}\langle m_i(t)\left[W_{i-1,i}^F a_{i-1} + W_{i+1,i}^F a_{i+1} + B_{i-1,i}^F a_{i-1}(1-a_{i-1}^v)\right]\rangle \\
&-\frac{1}{4}\langle m_i(t)\left[B_{i-1,i}^{F_v} a_{i-1}^v + B_{i+1,i}^F a_{i+1}(1-a_{i+1}^v) + B_{i+1,i}^{F_v} a_{i+1}^v\right]\rangle \\
&= \frac{1}{2}\left[\langle -va_i^v\rangle - \langle a_i\rangle\right] + \frac{1}{4}\left[\langle (1+F/2)a_{i-1}\rangle + \langle (1-F/2)a_{i+1}\rangle\right] \\
&+\frac{1}{4}\left[\langle m_{i-1}a_{i-1}(1+m_{i-1}F/2)(1-a_{i-1}^v)\rangle\right] \\
&+\frac{1}{4}\left[\langle v(1+vF/2)a_{i-1}^v\rangle + \langle m_{i+1}a_{i+1}(1-m_{i+1}F/2)(1-a_{i+1}^v)\rangle\right] \\
&+\frac{1}{4}\left[\langle v(1-vF/2)a_{i+1}^v\rangle\right] + \frac{1}{2}\left[-\langle m_i\rangle + \langle m_i a_i a_i^v\rangle\right] \\
\Rightarrow \frac{d\langle m_i\rangle}{dt} &= \frac{1}{4}(\rho_{i-1} + \rho_{i+1} - 2\rho_i) \\
&+\frac{1}{4}\langle (a_{i-1} + a_{i+1} - 2a_i)\rangle + \frac{1}{4}\langle v(a_{i+1}^v + a_{i-1}^v - 2a_i^v)\rangle \\
&-\frac{1}{4}(\langle m_{i+1}a_{i+1}a_{i+1}^v\rangle + \langle m_{i-1}a_{i-1}a_{i-1}^v\rangle - 2\langle m_i a_i a_i^v\rangle) \\
&+\frac{F}{8}(\langle a_{i-1}\rangle - \langle m_{i-1}^2 a_{i-1}a_{i-1}^v\rangle + \langle m_{i-1}^2\rangle + \langle v^2 a_{i-1}^v\rangle) \\
&-\frac{F}{8}(\langle a_{i+1}\rangle - \langle m_{i+1}^2 a_{i+1}a_{i+1}^v\rangle + \langle m_{i+1}^2\rangle + \langle v^2 a_{i+1}^v\rangle) \\
\Rightarrow \frac{\partial \rho_i}{\partial t} &= \frac{1}{4}(g_{i-1} + g_{i+1} - 2g_i) - \frac{1}{8}F(u_{i+1} - u_{i-1}) \qquad (4.49)
\end{aligned}$$

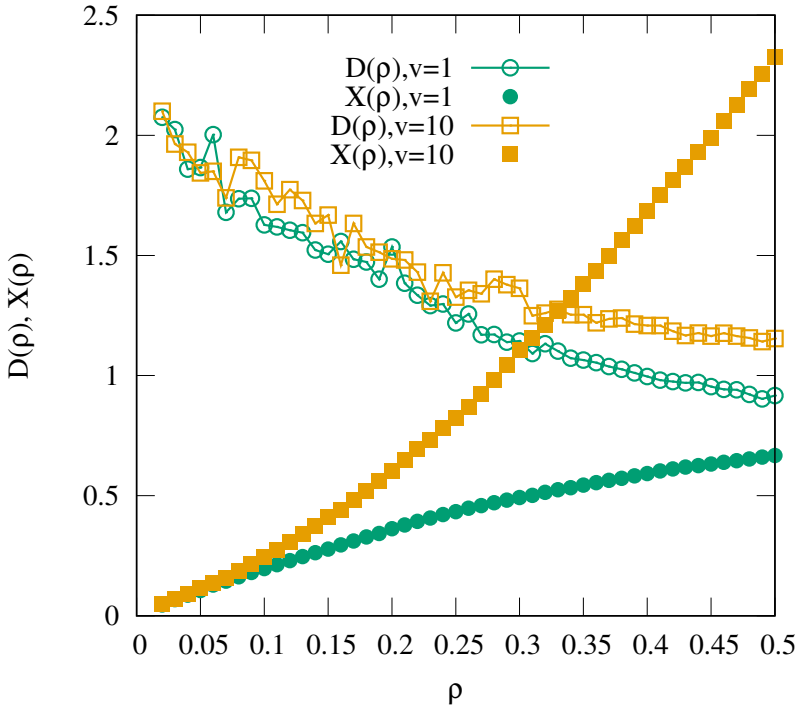

FIGURE 4.7: Two transport coefficients, diffusion coefficient $D(\rho)$ and conductivity $\chi(\rho)$, which are numerically calculated using Eq. (4.54), are plotted as a function of density ρ for velocities $v = 1$ and 10.

where, two local observables g_i and u_i are defined as,

$$g_i = \rho_i + \langle a_i \rangle + v\langle a_i^v \rangle - \langle m_i a_i a_i^v \rangle, \tag{4.50}$$

$$u_i = \langle a_i \rangle - \langle m_i^2 a_i a_i^v \rangle + \langle m_i^2 \rangle + v^2 \langle a_i^v \rangle. \tag{4.51}$$

One can notice that in Eq. (4.49), the local diffusive current J_D can be expressed as a *g*radient (discrete) of the local observable g_i, which is called a "gradient condition". This gradient property is important because it helps one to find the bulk diffusion coefficient and the conductivity.

Now taking the diffusive scaling limit of Eq. (4.49), $i \to x = i/L$ and $t \to \tau = t/L^2$, and lattice constant $a \to 1/L$, we obtain the hydrodynamic equation for the

density field,

$$\begin{aligned}
\frac{\partial \rho(x)}{\partial t} &= \frac{1}{4}\left[g\left(x-\frac{1}{L}\right)+g\left(x+\frac{1}{L}\right)-2g(x)\right] \\
&\quad -\frac{1}{8}\left[u\left(x+\frac{1}{L}\right)-u\left(x-\frac{1}{L}\right)\right]\frac{F}{L} \\
&= \frac{1}{4}\left[\frac{1}{L^2}\frac{\partial^2 g}{\partial x^2}\right]-\frac{1}{8}\left[\frac{2}{L}\frac{\partial u}{\partial x}\right]\frac{F}{L} \\
\Rightarrow \frac{\partial \rho(x)}{\partial \tau} &= \frac{1}{4}\frac{\partial^2 g}{\partial x^2}-\frac{1}{4}F\frac{\partial u}{\partial x}
\end{aligned} \tag{4.52}$$

Therefore,

$$\frac{\partial \rho(x)}{\partial \tau} = -\frac{\partial}{\partial x}\left[-\frac{1}{4}\frac{\partial g}{\partial \rho}\frac{\partial \rho}{\partial x}+\frac{1}{4}uF\right] = -\frac{\partial}{\partial x}\left[-D(\rho)\frac{\partial \rho}{\partial x}+\chi(\rho)F\right]. \tag{4.53}$$

From Eq. (4.53) one can easily identify the bulk diffusion coefficient and conductivity, respectively as

$$D(\rho)=\frac{1}{4}\frac{\partial g(\rho)}{\partial \rho}, \qquad \chi(\rho)=\frac{u(\rho)}{4}. \tag{4.54}$$

In Fig. 4.7, we plot two transport coefficients, bulk diffusion coefficient $D(\rho)$ and conductivity $\chi(\rho)$, calculated from simulation using Eq. (4.54), are plotted as a function of density ρ for velocities $v = 1$ and 10.

Hydrodynamics in the limit $v \to \infty$:

The limiting case of $v \to \infty$ of this model was introdued by Majumdar *et al.* [89] in a conserved-mass aggregation model, which allows for "chipping" (where a single unit of mass is transferred to its nearest neighbor) and "diffusion" (where the whole mass at a particular cite is transferred to its nearest neighbour) of masses. Beyond a critical density, a condensation transition was observed with an infinite aggregate present in the system, in addition to a power law decay of mass distribution in the bulk. However, large-scale hydrodynamic properties of this aggregation (equivalently, long-hop) model was never studied before. In

the following sections, we derive hydrodynamics of the unbounded-mass version (aggregation) of the long-hop model defined in the previous section. We calculate two transport coefficients - the bulk diffusion coefficient and conductivity and explains the clustering mechanism in terms of these coefficients. We would see that clustering mechanism is interestingly different than that observed in the persistent-hop model described before.

According to our description, at $v \to \infty$ limit, mass m_i at any site i is always lesser than v that implies the indicator function a_i^v to be always zero. By putting this condition in Eq. (4.33), the modified mass transfer rates can be written as given below [90],

$$m_i(t+dt) = \begin{cases} 0 & \text{prob. } a_i dt/2, \\ m_i(t)-1 & \text{prob. } a_i dt/2, \\ m_i(t)+1 & \text{prob. } a_{i-1} dt/4, \\ m_i(t)+1 & \text{prob. } a_{i+1} dt/4, \\ m_i(t)+m_{i-1}(t) & \text{prob. } a_{i-1} dt/4, \\ m_i(t)+m_{i+1}(t) & \text{prob. } a_{i+1} dt/4, \\ m_i(t) & \text{prob. } 1-[a_i+(a_{i-1}+a_{i+1})/2]dt, \end{cases} \tag{4.55}$$

Using Eq. (4.55), we can write the time evolution equation of second moment of mass $\langle m_i^2(t)\rangle$ at steady state as,

$$\begin{aligned} \langle m_i^2\rangle &= \langle (m_i^2-2m_i+1)a_i\rangle/2 + [\langle (m_i^2+2m_i+1)a_{i-1}\rangle + \langle (m_i^2+2m_i+1)a_{i+1}\rangle]/4 \\ &+ [\langle (m_i^2+2m_im_{i-1}+m_{i-1}^2)a_{i-1}\rangle + \langle (m_i^2+2m_im_{i+1}+m_{i+1}^2)a_{i+1}\rangle]/4 \\ &+ \langle m_i^2\rangle - \langle m_i^2[a_i+(a_{i-1}+a_{i+1})/2]\rangle, \end{aligned} \tag{4.56}$$

where at steady state, $\langle m_i^n(t+dt)\rangle = \langle m_i^n(t)\rangle$ for any n^{th} moment. Now we calculate in simulations two-point spatial correlation function $C(r) = \langle m_i m_{i+r}\rangle - \rho^2$ and, in Fig. 4.8, plot $C(r)$ for $v = 1$, 10 and ∞ as a function of relative distance r, for global density $\rho = 0.3$. Clearly, $C(r) \to 0$ is vanishingly small for all neighbouring points with $r \geq 1$, which allows us to use a mean-field theory in Eq. (4.56); indeed, a finite-size scaling analysis of two-point correlations suggests that

the mean-field theory is exact. The mean-field theory straighforwardly provides us an expression for the occupation probability $A(\rho) = \langle a \rangle$ as a function of density as given below,

$$A(\rho) = \frac{\rho(1-\rho)}{1+\rho}. \tag{4.57}$$

Similarly, the time evolution equation of third moment of mass $\langle m_i^3(t) \rangle$ at steady state, within the mean-field limit, will provide an expression of second moment $\langle m_i^2 \rangle \equiv \theta_2(\rho)$, which is function of only density ρ, not a function of position i (due to homogeneous systems), and can be written as given below,

$$\theta_2(\rho) = \frac{\rho(1+A(\rho))}{1-A(\rho)-2\rho}. \tag{4.58}$$

Using Eqs. (4.57) and (4.58), one can calculate the scaled subsystem mass fluctuation [14] given by,

$$\begin{aligned} \sigma^2(\rho) &= \theta_2(\rho) - \rho^2 \\ &= \frac{\rho(1+\rho)(1+\rho^2)}{1-2\rho-\rho^2}. \end{aligned} \tag{4.59}$$

To calculate the transport coefficients, bulk diffusion coefficient $D(\rho)$ and conductivity $\chi(\rho)$, we need to derive the hydrodynamics after biasing the system by applying a small constant force of magnitude F. The biased stochastic update equation for mass transport can be obtained from Eq. (4.47) with indicator function $a_i^v = 0$. Using the modified biased rate equations at the limit of $v \to \infty$, one can easily find (following the procedure as in Sec. 4.3.1) the same gradient type hydrodynamic equation as it was in Eq. (4.53), but with a modified form of local observables [see Eqs. (4.50) and (4.51)], given by,

$$g(\rho) = \rho + A(\rho), \tag{4.60}$$

$$u(\rho) = A(\rho) + \theta_2(\rho). \tag{4.61}$$

Then we substitute $A(\rho)$ and $\theta_2(\rho)$ respectively from Eqs. (4.57) and (4.58) in Eqs. (4.60) and (4.61) and use them to find the transport coefficients $D(\rho)$ and

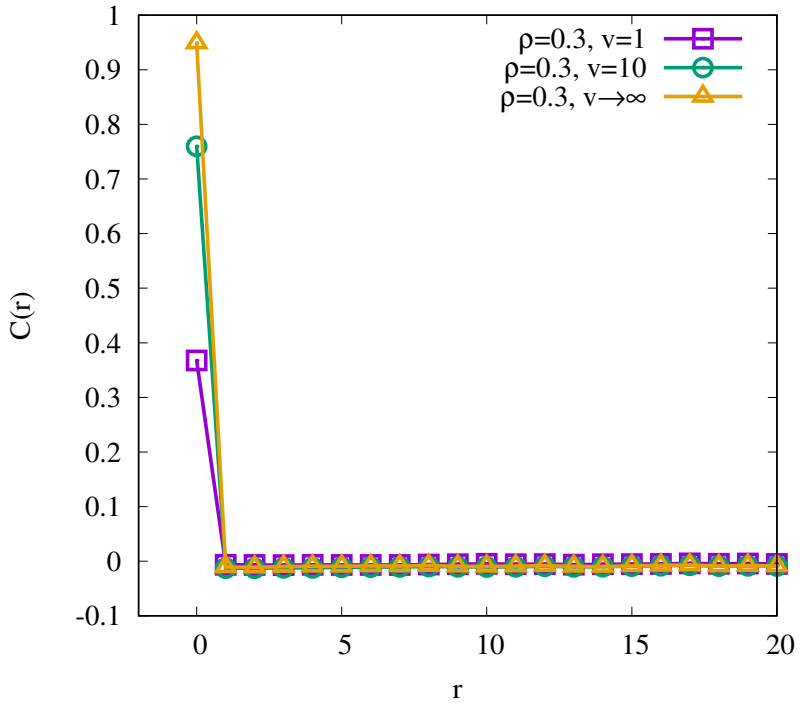

FIGURE 4.8: Mass-mass correlation $C(r) = \langle m_i m_{i+r} \rangle - \rho^2$ is plotted as a function of inter particle distance r for global density $\rho = 0.3$ and velocities $v = 1$, 10 and $v \to \infty$.

$\chi(\rho)$ [see Eq. (4.54)] given by,

$$D(\rho) = \frac{1}{4}\frac{\partial g(\rho)}{\partial \rho} = \frac{1}{2(1+\rho)^2}, \tag{4.62}$$

$$\chi(\rho) = \frac{u(\rho)}{4} = \frac{\rho(1+\rho^2)}{2(1+\rho)(1-2\rho-\rho^2)}. \tag{4.63}$$

Now the ratio of conductivity $\chi(\rho)$ and bulk-diffusion coefficient $D(\rho)$ from Eqs. (4.63) and (4.62) respectively, is given by,

$$\frac{\chi(\rho)}{D(\rho)} = \frac{\rho(1+\rho)(1+\rho^2)}{1-2\rho-\rho^2}. \tag{4.64}$$

Note that, the expression in Eq. (4.64) is the same as the expression of scaled variance in Eq. (4.59). So one can verify that the Einstein relation as in Eq. (4.7) is indeed satisfied in mean-field level at the limit of $v \to \infty$.

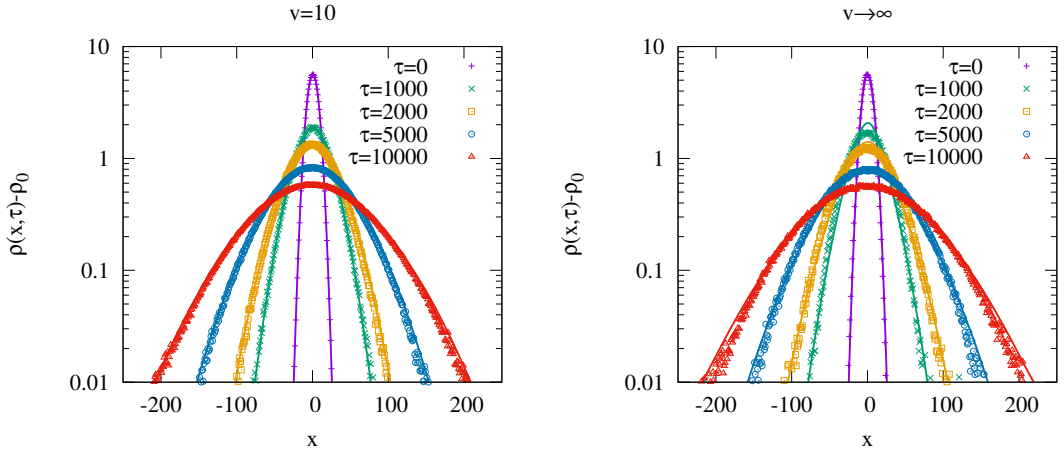

FIGURE 4.9: Comparison between hydrodynamic theory and simulation at different times $\tau = 0$ (magenta), 1000 (green), 2000 (yellow), 5000 (blue) and 10000 (red) starting from initial condition Eq. (4.66), for $v = 10$ and $v \to \infty$. In the left panel, lines are the numerically calculated hydrodynamic evolution of density for $v = 10$, whereas, in the right panel, the lines are the mean-field hydrodynamic evolution plots for $v \to \infty$.

4.3.2 Comparison with simulations

We now verify the hydrodynamics we derived [Eq. (4.52)] by comparing the time evolution of density calculated from theory with that observed in Monte Carlo simulation of the microscopic model for $v = 10$ and $v \to \infty$. The hydrodynamic evolution equation [Eq. (4.52)] of density field $\rho(x, \tau)$ with rescaled position x and rescaled time τ in the limit of biasing force $F = 0$ becomes,

$$\frac{\partial \rho(x,\tau)}{\partial \tau} = \frac{1}{4}\frac{\partial^2 g[\rho(x,\tau)]}{\partial x^2}. \tag{4.65}$$

We are interested in the evolution of density field $\rho(x, \tau)$ at different times, starting from the initial condition

$$\rho(x, \tau = 0) = \rho_0 + \rho_1 \frac{\exp(-x^2/2\Delta_0^2)}{\sqrt{2\pi\Delta_0^2}} \tag{4.66}$$

where we have chosen $\Delta_0 = 10$, ρ_0 (a uniform background density) and ρ_1 (strength of the initial density perturbation) are two constants.

We have numerically integrated Eq. (4.65) by discretizing x and τ (Euler method; $\delta x = 1$, $\delta\tau = 10^{-2}$), keeping the particle number conserved. To integrate Eq. (4.65), for $v = 10$, we first need to determine, from microscopic simulations, the function $g(\rho)$ as a function of density ρ in a small density interval $\delta\rho$. Then one can calculate the value of the local function g at any intermediate density value by using simple linear interpolation method. In case of $v \to \infty$, the method is easier as we already know the functional form of $g(\rho)$ in Eq. (4.60). According to our hydrodynamic theory, determination of $g(\rho)$ as a function of density ρ is sufficient to determine the time evolution of hydrodynamic Eq. (4.65).

We perform Monte Carlo simulations of the microscopic unbounded mass model with random sequential updates (which corresponds to the continuous-time dynamics). One Monte-Carlo time unit (each site is updated at rate 1 in simulations) corresponds to unit of time in Eq. (4.65). In simulations we have generated random initial configurations which would correspond to the initial density profile as in Eq. (4.66); also, in simulations, we have averaged over the initial configurations as well as the trajectories.

In Fig. 4.9, we have compared density profiles obtained by integrating hydrodynamic evolution Eq. (4.65) [lines] and that obtained from Monte Carlo simulations of unbounded mass model [points], at different times $\tau = 0$ (magenta), 1000 (green), 2000 (yellow), 5000 (blue) and 10000 (red) starting from initial condition Eq. (4.66), for $v = 10$ and $v \to \infty$. In the left panel, lines are the numerically calculated hydrodynamic evolution of density for $v = 10$, whereas, in the right panel, the lines are the mean-field hydrodynamic evolution plots for $v \to \infty$. In both plots, the hydrodynamic theory captures the simulation results reasonably well.

4.3.3 Fluctuation, response and Einstein relation

Here we verify an equilibrium-like Einstein relation [Eq. 4.7]. To this end, we first require to calculate two transport coefficients, the bulk diffusion coefficient

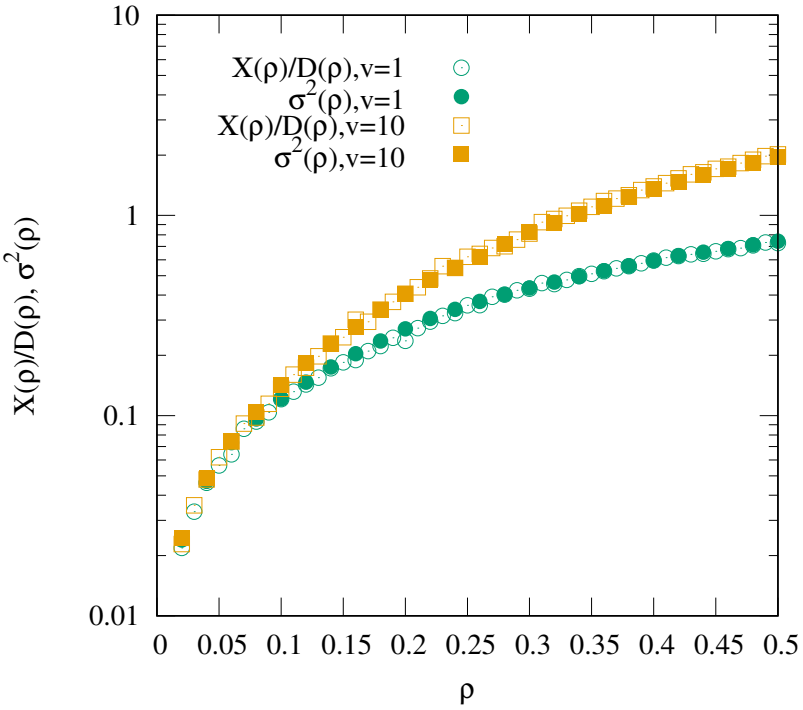

FIGURE 4.10: Scaled subsystem particle number fluctuation $\sigma^2(\rho)$ calculated from simulation, is plotted as a function of density ρ for velocities $v = 1$ (green filled circles) and 10 (yellow filled square). We compare $\sigma^2(\rho)$ with the ratio of two transport coefficients $\chi(\rho)$ and $D(\rho)$, respectively, calculated numerically using Eq. (4.54), for velocities $v = 1$ (green empty circles) and 10 (yellow empty square). It shows existence of an ER in this non-equilibrium model.

$D(\rho)$ and the conductivity $\chi(\rho)$ by using Eq. (4.54). We perform Monte Carlo simulations of unbounded mass-transport models to obtain two local observables $g(\rho)$ and $u(\rho)$ as a function of local density field ρ. The functional forms (numerically obtained) of two local observables lead to the functional forms of $D(\rho)$ and $\chi(\rho)$ using Eq. (4.54). Then we plot the ratio of these two transport coefficients $\chi(\rho)/D(\rho)$ in Fig. 4.10 for two different self propulsion velocities $v = 1$ (green empty circles) and 10 (yellow empty squares). To verify ER, we also compute the scaled variance $\sigma^2(\rho)$ of subsystem mass and plot them in Fig. 4.10 for those two velocities $v = 1$ (green solid circles) and 10 (yellow solid squares). Interestingly, the ratio of the transport coefficients agree quite well with the scaled subsystem mass variance, indicating existence of an ER even in this non-equilibrium model.

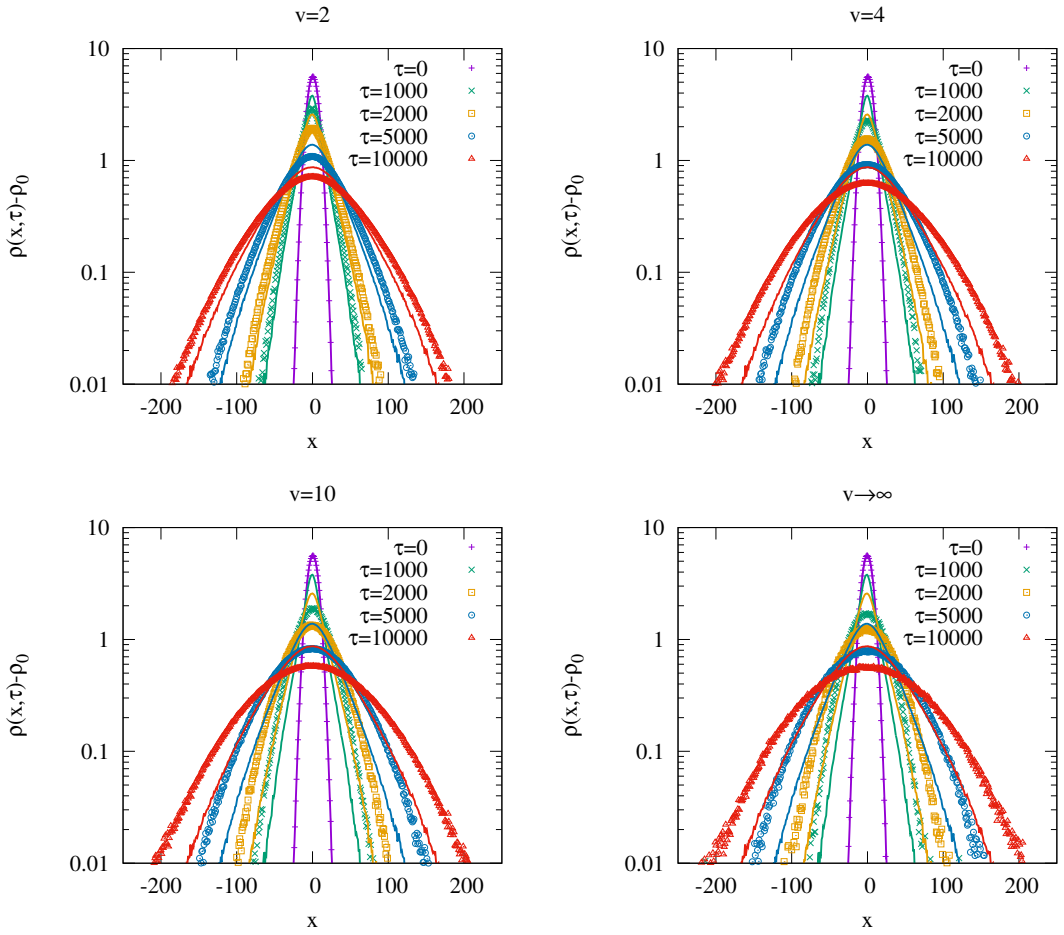

FIGURE 4.11: Density evolution at different times $\tau = 0$ (magenta), 1000 (green), 2000 (yellow), 5000 (blue) and 10000 (red), starting from initial condition Eq. (4.66) for different velocities $v = 2$, 4, 10 and $v \to \infty$ [points] and compare them with that for $v = 1$ (simple exclusion process) [lines] in each panel.

4.3.4 Characterization of density relaxations

In Fig. 4.11, we plot the density evolution at different times $\tau = 0$ (magenta), 1000 (green), 2000 (yellow), 5000 (blue) and 10000 (red), starting from initial condition Eq. (4.66) for different velocities $v = 2$, 4, 10 and $v \to \infty$ [points] and compare them with that for $v = 1$ (simple exclusion process) [lines] in each panel. Note that, the width of density at particular time τ increases with v. Therefore, we need to measure the width of density spreading, observed from the simulation, quantitatively for different values of v, like we did for previous model. To this

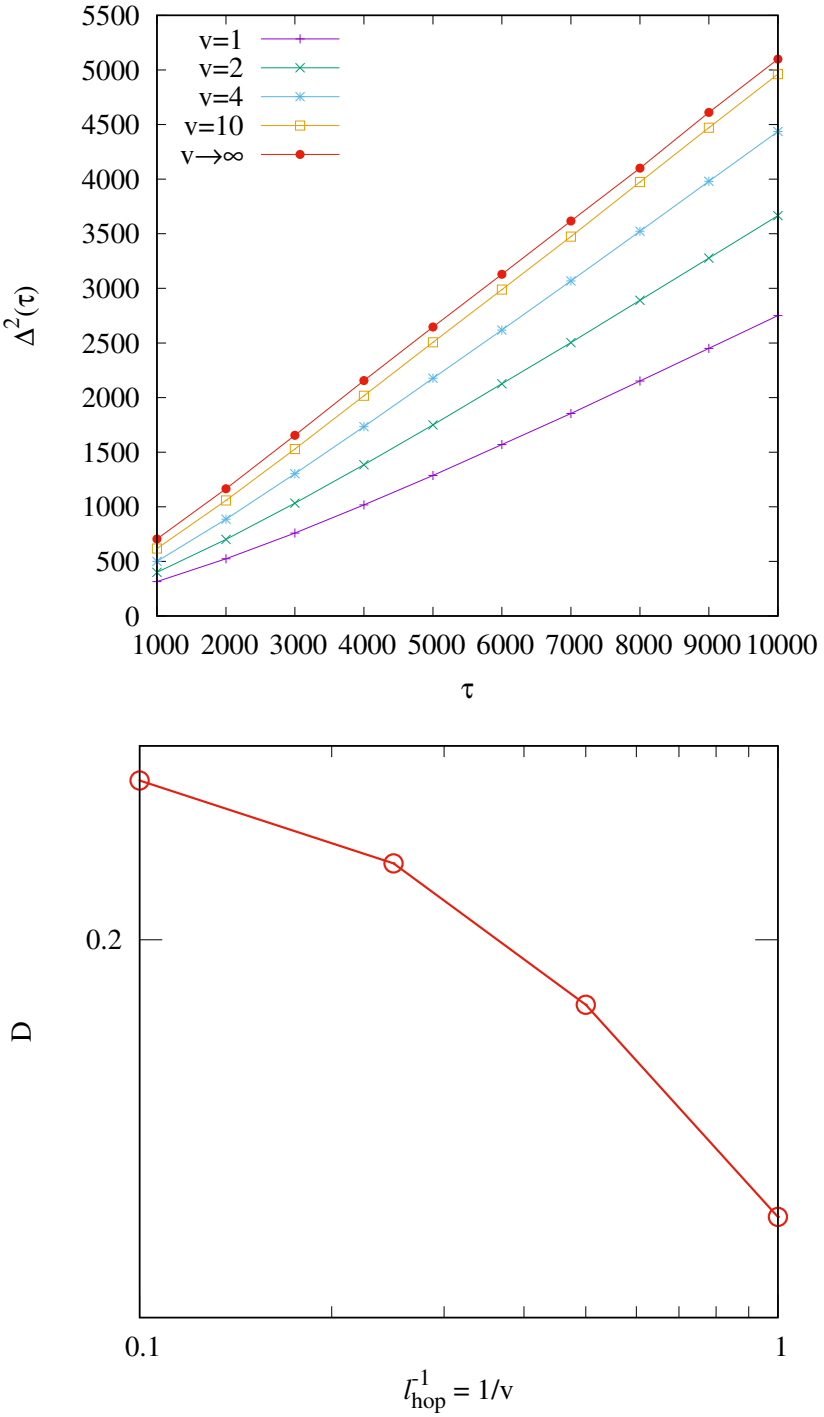

FIGURE 4.12: Upper panel: Width of density $\Delta^2(\tau)$ [as defined in Eq. (4.67)] is plotted with time τ for velocities $v = 1$ (magenta), 2 (green), 4 (blue), 10 (yellow) and $v \to \infty$ (red). Lower panel: diffusion coefficient D is plotted with inverse of effective hop length $l_{hop} = v$.

end, we again define the width of density spreading at time τ

$$\Delta^2(\tau) = \frac{\sum_{i=-L/2}^{L/2} x_i^2(\tau)(\rho[x_i(\tau)] - \rho_0)}{\sum_{i=-L/2}^{L/2}(\rho[x_i(\tau)] - \rho_0)} \tag{4.67}$$

with L be the system size. We plot $\Delta^2(\tau)$ with time τ for velocities $v = 1$ (magenta), 2 (green), 4 (blue), 10 (yellow) and $v \to \infty$ (red), in the upper panel of Fig. 4.12. It shows that the rate of increment of $\Delta^2(\tau)$ increases with v. To provide a quantitative description, we define, as in the case of the persistent model discussed in the previous section, a hop length $l_{hop} = v$ (which equals to the mass transferred during "diffusion" process in the unbounded model), and an diffusion coefficient

$$D = \lim_{\tau\to\infty} \frac{\Delta^2(\tau)}{2\tau}. \tag{4.68}$$

We plot the diffusion coefficient D with inverse of effective hop length l_{hop} in the lower panel of Fig. 4.12 and find D increases with l_{hop}, as seen from the plot in upper panel. This behavior of D is opposite to that we observed in the model with persistent hardcore particles.

4.4 Comparison between persistent-hop and long-hop models

In this section, we compare two quantities, the scaled variance $\sigma^2(\rho)$ of subsystem mass and the bulk-diffusion coefficient D, for persistent-hop and long-hop lattice gases with unbounded occupancy. In the upper panel of Fig. 4.13, we plot $\sigma^2(\rho)$ as a function of density ρ in persistent-hop model for effective hop length $l_{hop} = 1/D_r = 3$ (blue filled circles) and 10 (blue empty circles), and in model with long-hop model for $l_{hop} = v = 3$ (yellow filled squares) and 10 (yellow empty squares). Mass fluctuations in both systems increases with increasing density and the behaviour is qualitatively similar. On the other hand, in the lower panel of Fig. 4.13, we compare the bulk-diffusion coefficient D as a function of the inverse of the effective hop length l_{hop} [i.e., inverse tumbling rate, which is analogous to

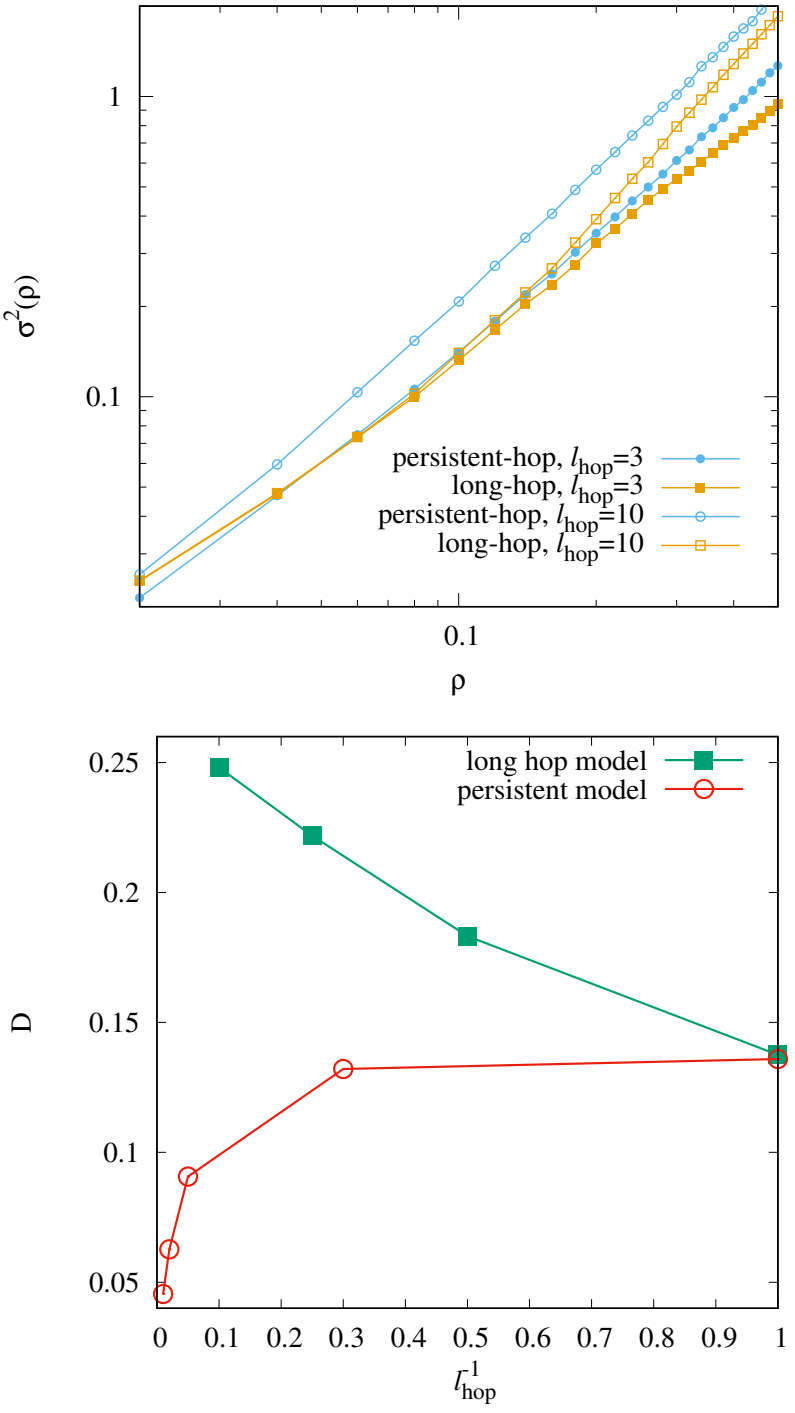

FIGURE 4.13: Upper panel: Comparison between scaled subsystem mass fluctuation $\sigma^2(\rho)$ of persistent model and model with long-range hopping. We plot $\sigma^2(\rho)$ as a function of density ρ of persistent model for effective hop length $l_{hop} = 1/D_r = 3$ (blue filled circle) and 10 (blue empty circle), and of model with long-range hopping for $l_{hop} = v = 3$ (yellow filled square) and 10 (yellow empty square). Lower panel: Comparison between behavior of diffusion coefficient D with inverse of effective hop length l_{hop} of persistent model (red circle) and model with long-range hopping (green square).

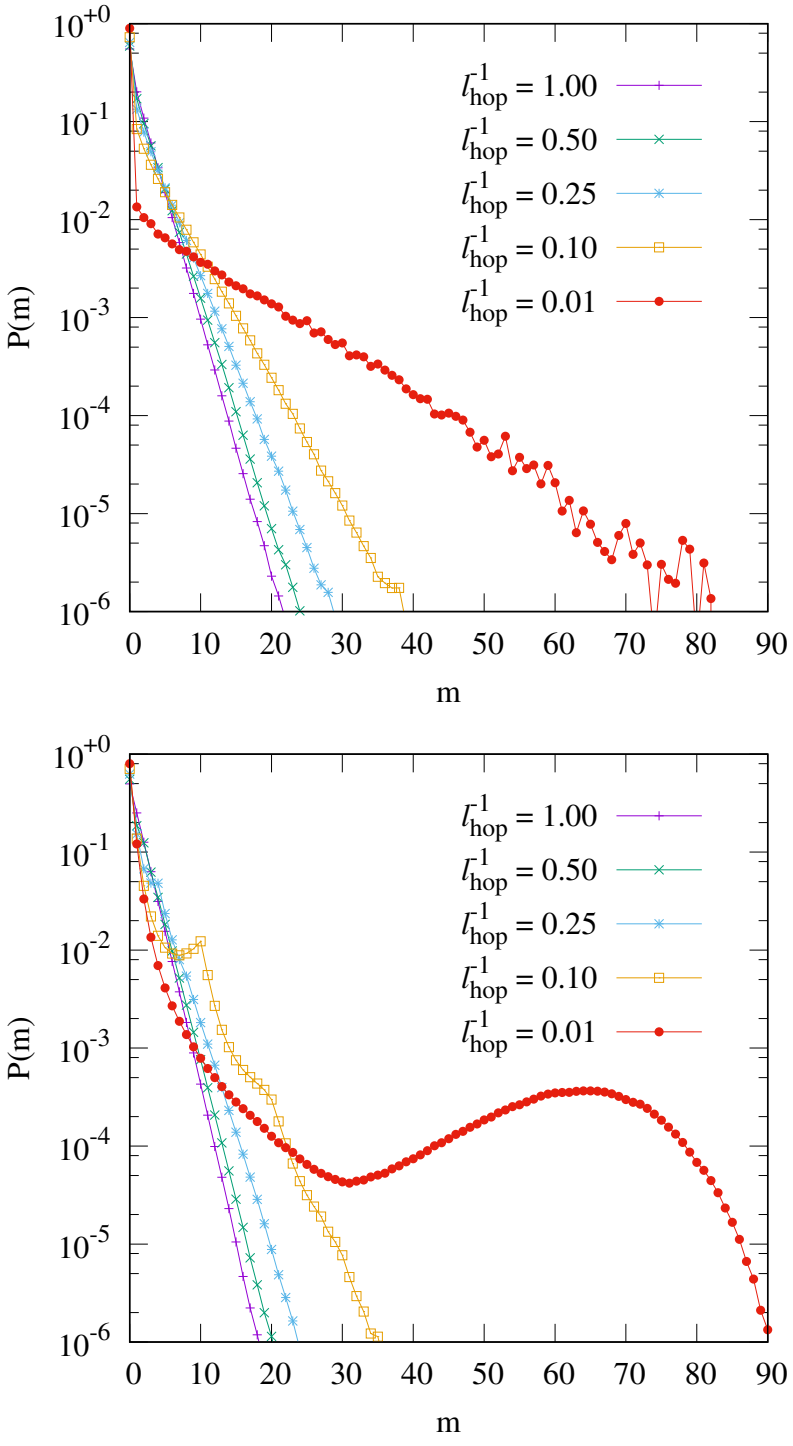

FIGURE 4.14: Single-site mass distribution $P(m)$ (equivalently, cluster size distribution of vacancies, or holes, in the lattice gas version with exclusion constraint) is plotted as a function of mass m at a particular site for different values of $l_{hop}^{-1} = 1.0$ (magenta), 0.5 (green), 0.25 (blue), 0.1 (yellow) and 0.01 (red). Upper panel: Persistent-hop model. Lower panel: Long-hop model. Appearance of the second peak (or mode) in the mass distribution in long-hop model for $v = l_{hop} \to \infty$ indicates the condensate formed in the system. Note that there is no such peak in the distribution in persistent-hop model, indicating there is no phase separation as such. We have taken global mass density $\rho = 1$ in all simulations.

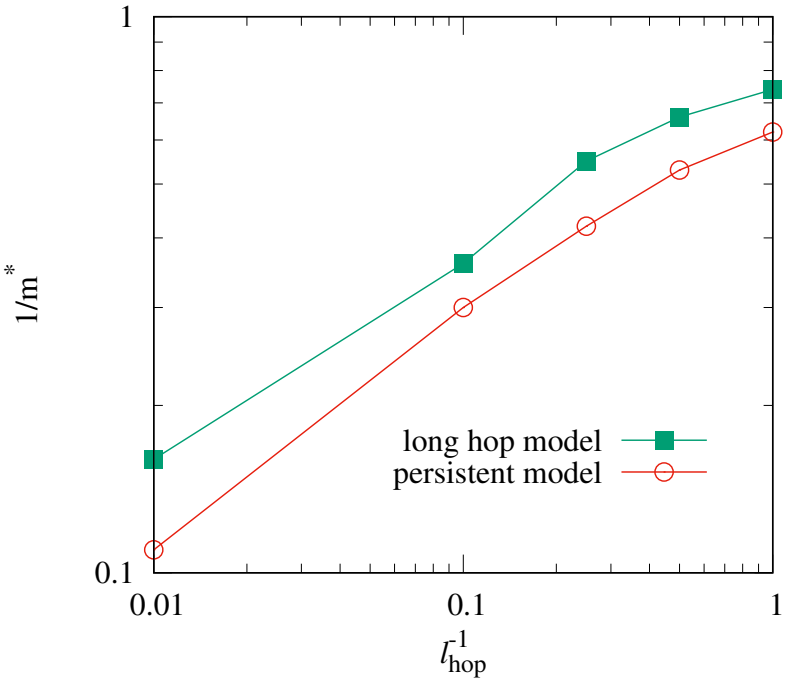

FIGURE 4.15: We calculate the large-mass cut-off m^* in the single-site mass distribution $P(m) \sim \exp(-m/m^*)$ and plot inverse of the cut-off m^* as a function of the inverse of the effective hop length l_{hop} for persistent-hop model (red circles) and long-hop model (green squares). We have taken global mass density $\rho = 1$ in all simulations.

the activity, or the Peclet number, in the model of active Brownian particles; see Eq. (2.27) in chapter 2] in persistent-hop model (red circle) and long-hop model (green square). Clearly, the behavior of diffusivity of masses in the two models is quite contrasting, in the sense that, while the diffusivity in the long-hop model increases with increasing l_{hop}, the diffusivity in the persistent-hop model interstingly decreases with increasing l_{hop}. It is expected that transport coefficients, such as diffusion coefficient here, play an important role in the phase separation, if any. In the persistent-hop model, vanishing diffusivity with increasing effective hop-length l_{hop} (i.e., inverse tumbling rate or the acitivity) indicates aggregation of masses, which would imply clustering of holes (expectedly, also for the particles) in the corresponding lattice gas with exclusion constraint. On the other hand, the mechanism behind clustering in the long-hop model (where a condensation transition happens with infinite range hop $v = \infty$) is due to a large conductivity in the system; indeed, as seen in Eq. (4.63) for $v = \infty$, the conductivity diverges

at the critical point.

For a more detailed investigation of clustering in these models, we also study the single-site mass distributions $P(m)$, i.e., probability distributions of mass at a particular site. In Fig. 4.14, we plot the single-site mass distributions as a function of single-site mass for different values of $l_{hop}^{-1} = 1.0$ (magenta), 0.5 (green), 0.25 (blue), 0.1 (yellow) and 0.01 (red) for persistent-hop model (in upper panel) and long-hop model (in lower panel). Note that, in the long-hop model, there is a peak at large mass, indicating a thermodynamic condensation of mass in the limit of $l_{hop}^{-1} \to 0$ ($v \to \infty$), where a finite fraction of total mass in the system belongs to a single cluster and rest of the total mass is distributed homogeneously. However, in the persistent-hop model (in upper panel), although there are large clusters present in the system, there is no signature of condensation transition in the system. For a more quantitative look, we calculate the cut-off mass to the distributions $P(m) \sim \exp(-m/m^*)$ at large masses and, in Fig. 4.15, plot inverse of the cut-off mass m^* with l_{hop}^{-1}, the inverse hop-length. In both the models, the cut-off mass diverges with increasing hop-length (activity), which implies the presence of strong mass fluctuations and, expectedly, the presence of large clusters in the systems.

4.5 Summary

In this chapter, we have introduced a broad class of active lattice gases on a ring, such as models of run-and-tumble particles (RTPs) with persistent hopping and corresponding models with long-range hopping. We have mapped the models exactly onto a class of conserved-mass transport processes with unbounded-mass occupancy (in contrast to hardcore exclusion constraint in the original models). Due to lack of detailed balance, all these systems are inherently driven out of equilibrium and cannot be described by the familiar equilibrium Boltzmann-Gibbs distributions.

In the models with persistent hopping, we find that the models do not possess the gradient property (that the local current cannot be written as a gradient of a local observable) and therefore the transport coefficients could not be analytically identified as an average of a local observable. Indeed calculating transport coefficients in these models would be a challenging open issue. On the other hand, in the lattice models with long-range hopping, which are shown to have the gradient property, we could derive hydrodynamics, by identifying the transport coefficients in terms of an average of a local observable and then exactly computing the two transport coefficients - the bulk diffusion coefficient and conductivity as a function of particle-number density. We also directly compare our hydrodynamic theory with simulations, which are in excellent agreement with each other. Moreover, by using the functional form of the two transport coefficients, we demonstrate in the models with long-range hop that there indeed exists an Einstein relation (ER), the earliest known form of the fluctuation-dissipation theorems (FDTs) in equilibrium, which connects number-fluctuation, the diffusion coefficient and the conductivity. We note here that, in one dimension, though the models with persistent hopping do not show any phase transition (in spite of signature of clustering), the models with long-range hopping in a particular limit of infinite-range hopping ($v = \infty$) does show condensation transition upon tuning the global particle-number density. Moreover, at the critical density, the conductivity diverges, but the diffusivity remains finite. It would be of interest to explore if the models with persistent hopping, as introduced here in the thesis, would exhibit a phase transition in higher dimensions.

At the end, we calculate the bulk bulk diffusion coefficient through a slightly different, but a direct, route by monitoring the time-evolution of an initial Gaussian density profile at large times. In this way, we can directly investigate the role of bulk diffusion coefficient in clustering phenomena and dynamical arrest of particles [mechanism of which was proposed previously in the literature in the context of motility induced phase transition (MIPS)], observed in many of these systems.

Finally, we compare, in these two classes of models - with persistent and long hop, the scaled variances of subsystem mass as a function of density and the diffusion

coefficients as a function of hop length for these lattice models. Quite interestingly, we observe that, although the qualitative behaviour of the variance in both these models as a function of density is quite similar, but the behaviour of the diffusion coefficients in the models is markedly different as a function of the activity parameters, indicating clustering happens through two contrasting mechanisms: (i) One with the small diffusivity (possibly, vanishing in models in higher dimensions) and (ii) the other with the diverging conductivity. Studies of transport coefficients in self-propelled particles in higher dimensions would provided much desired insights into the nature of cluster and their thermodynamic characterization.

Chapter 5

Summary of the thesis

In this Ph. D. thesis, we formulate a statistical mechanics framework for three classes of self-propelled particles or active matter - (i) active Brownian particles, (ii) particles with Vicsek-like interactions, and (ii) lattice gas versions of interacting run-and-tumble particles. This particular formulation could enable us to unify fascinatingly broad-ranging phenomena in the systems of self-propelled particles under a unique nonequilibrium thermodynamic theory. More specifically, we study whether such nonequilibrium systems possess an equilibrium-like additivity property, which could connect microscopic fluctuations to the macroscopic properties of the system. Previously, additivity has been successfully applied in nonequilibrium mass-transport processes for calculations of probability distribution of mass in a large subsystem and for characterizing macroscopic properties in terms of an equilibrium-like thermodynamic variables like chemical potential and free-energy function. We address here whether the similar thermodynamic structure can be extended to systems of self-propelled particles.

In first chapter, we provide a detailed introduction of active matter systems studied in the literature in the past decades. In second chapter, using an additivity property, we formulate a thermodynamic theory of active Brownian particles in using the set-up of a fluctuating hydrodynamics. We demonstrate that a nonequilibrium fluctuation-response relation - a direct consequence of additivity - can be used to characterize the macroscopic properties in active Brownian particles in terms of a

nonequilibrium chemical potential. As the particle-number density and the activity (or Peclet number) increase, the chemical potential becomes a non-monotonic function of density, indicating onset of a gas-liquid-like phase coexistence. Importantly, the formalism developed here is solely based on characterization of the variance of subsystem particle number as a function of particle-number density, which we have calculated within a linearized fluctuating hydrodynamics. Our studies of fluctuating hydrodynamics have new insights in characterizing the two multiplicative noise terms (density and polarization noises), which appear in the hydrodynamic equations. In the disordered phase, where correlation lengths are small, we have compared simulations results and additivity theory, which captures the subsystem particle-number distributions, especially the non-Gaussian features inherently present in a driven interacting-particle system, reasonably well even in the far-from-equilibrium regime where activity is moderately large.

In third chapter, we verify the applicability of additivity to another class of paradigmatic self-propelled particle systems - the Vicsek model (VM) and its two variants, consisting of polar point-particles with alignment interactions. The two variants differ from the original one in the way noise or stochasticity is incorporated in the system. In all three models, the order parameter, average velocity of particles, go through a disorder-to-order phase transition as the number density is increased or the noise strength is decreased. Moreover, the critical noise strength depends on the density, and vice versa. First we calculate, from simulations, the scaled variance of subsystem particle-number as a function of density in the disordered fluid-like phase. Then, using a non-equilibrium fluctuation-response relation - a consequence of an additivity property, we exactly compute subsystem particle-number distributions, or the density large-deviation functions. Moreover, we compare the theoretically obtained subsystem particle-number distributions with those obtained from simulation and we find quite striking agreement between simulations and additivity theory. Indeed, the theory captures remarkably well the non-Gaussian features observed in these distributions. The fact that the number distributions are determined solely from the knowledge of the variance

as a function of density strongly indicates validity of additivity in the Vicsek-like models.

In fourth chapter, motivated by run-and-tumble particles, we introduce a broad class of active lattice gases with hardcore interactions - (i) persistent-hop models and (ii) long-hop models, and study these models by exactly mapping them onto conserved-mass transport processes with unbounded occupancy (therefore, without any hardcore constraint). Due to lack of detailed balance, these systems are inherently driven out of equilibrium and cannot be described by the familiar equilibrium Boltzmann-Gibbs distributions. For some of these lattice models, we derive hydrodynamics and identify two transport coefficients - the bulk diffusion coefficient and conductivity as a function of density. Moreover, by using the functional form of the two transport coefficients in the lattice gases with long hop, we demonstrate that there exists an Einstein relation (ER), analogous to the earliest known form of the fluctuation-dissipation theorems (FDTs) in equilibrium, which connects number-fluctuation, diffusion coefficient and conductivity. In both persistent-hop and long-hop models, we calculate the bulk-diffusion coefficient by time-evolving a initial Gaussian density profile at larger times and investigate the role of mass diffusivity in the phenomenon of clustering of particles observed in these systems [mechanism of the clustering phenomenon was proposed previously in the context of active Brownian particles is the motility induced phase separation (MIPS)]. Finally we compare the scaled variance of subsystem mass as a function of density and the diffusion coefficients as a function of hop length (analogous to activity in the active Brownian particles) for both these models. Interestingly, we found that, although the behaviour of the scaled variance is qualitatively quite similar, but the behaviour of the diffusion coefficients is quite contrasting in these two models: In models with persistent hopping, diffusivity decreases with increasing effective hop length, on the other hand, in the models with long-range hopping, diffusivity increases with increasing effective hop length.

We believe our studies in this thesis, which explore the connection between the static additivity properties and dynamic properties like transport coefficients in a broad class of self-propelled particles, would provide some useful insights into the

nature of clustering, and, therefore, a complete thermodynamic characterization of interacting self-propelled particles in general.

APPENDIX A: Additivity and fluctuation-response relation

Here we show how additivity, as in 2.1 in the main text, directly leads to the fluctuation-response relation as in Eq. 2.5 in the main text. Provided additivity property is satisifed, the subsystem particle-number distribution can be written , in the thermodynamic limit, as

$$P_{\mathcal{V}}(\mathcal{N}) = \frac{1}{\mathcal{Z}} W_{\mathcal{V}}(\mathcal{N}) e^{\mu\mathcal{N}}, \tag{1}$$

where $\mathcal{W}$ is the weight factor for the respective subsystem, μ is a chemical potential and the normalization constant $\mathcal{Z}$ is given by

$$\mathcal{Z}(\mu) = \sum_{\mathcal{N}=0}^{\infty} W_{\mathcal{V}}(\mathcal{N}) e^{\mu\mathcal{N}}. \tag{2}$$

Now, the average particle number can be calculated by taking a derivative of logarithm of the normalization constant w.r.t. μ,

$$\langle \mathcal{N} \rangle = \frac{d(\ln \mathcal{Z})}{d\mu}. \tag{3}$$

By taking another derivative of Eq. 3 w.r.t. μ, one can immediately relate compressibility to the fluctuation,

$$\frac{d\langle \mathcal{N} \rangle}{d\mu} = \frac{d^2(\ln \mathcal{Z})}{d\mu^2} = \langle \mathcal{N}^2 \rangle - \langle \mathcal{N} \rangle^2, \tag{4}$$

where, in the last step, we have used Eq. 2. Dividing both side of the above equation by the subsystem volume $\mathcal{V}$, we get, in the limit of large $\mathcal{V}$, the fluctuation-response relation as in Eq. 3 in the main text,

$$\frac{d\rho}{d\mu} = \sigma^2, \tag{5}$$

where the scaled variance is defined as

$$\sigma^2 = \lim_{\mathcal{V}\to\infty} \frac{(\langle \mathcal{N}^2\rangle - \langle \mathcal{N}\rangle^2)}{\mathcal{V}}.$$

APPENDIX B: Calculation of Structure factor in the active Brownian particles within linearized fluctuating hydrodynamics

We consider the following fluctuating hydrodynamic equations, as considered in the main text, for self-propelled particles (SPP)

$$\partial_t \rho = -\nabla.\left[v(\rho)\mathbf{p} - D(\rho)\nabla\rho + \mathbf{f}_d\right], \tag{6}$$

$$\partial_t \mathbf{p} = -D_r\mathbf{p} - \frac{1}{2}\nabla\left(\rho v\right) + K\nabla^2\mathbf{p} + \mathbf{f}_p, \tag{7}$$

and perform linear analysis along the lines of Ref. [31]. We transform the variable $\theta(\mathbf{r}) = \nabla.\mathbf{p}$, expand the nonlinear terms upto linear order of $\delta\rho$ and $\delta\mathbf{p}$, where $\delta\rho = \rho - \rho_0$, $\delta\mathbf{p} = \mathbf{p} - \mathbf{p}_0$, $\delta\theta = \nabla.(\delta\mathbf{p})$ with ρ_0 and $\mathbf{p}_0 = 0$ average density and polarization profile, to obtain

$$\partial_t\delta\rho(\mathbf{r},t) = -v(\rho_0)\delta\theta(\mathbf{r},t) + D(\rho_0)\nabla^2\delta\rho(\mathbf{r},t) - \nabla.\mathbf{f}_d, \tag{8}$$

$$\partial_t\delta\theta(\mathbf{r},t) = -D_r\delta\theta(\mathbf{r},t) - \alpha(\rho_0)\nabla^2\delta\rho(\mathbf{r},t) + K\nabla^2\delta\theta(\mathbf{r},t) + \nabla.\mathbf{f}_p, \tag{9}$$

where $\nabla.(v\mathbf{p}) \simeq v\delta\theta$, $\nabla(\rho v) \simeq 2\alpha(\rho_0)\nabla(\delta\rho)$ with

$$2\alpha(\rho_0) = \frac{d}{d\rho_0}[\rho_0 v(\rho_0)] = v(\rho_0) + \rho_0\frac{dv(\rho_0)}{d\rho_0}.$$

Using Fourier amplitudes

$$\delta\tilde{\rho}(\mathbf{q},\omega) = \int_{\mathbf{r}}\int_{t} e^{-i\mathbf{q}.\mathbf{r}}e^{-i\omega t}\ \delta\rho(\mathbf{r},t)d\mathbf{r}dt, \tag{10}$$

$$\delta\tilde{\theta}(\mathbf{q},\omega) = \int_{\mathbf{r}}\int_{t} e^{-i\mathbf{q}.\mathbf{r}}e^{-i\omega t}\ \delta\theta(\mathbf{r},t)d\mathbf{r}dt, \tag{11}$$

and reverting back to global density $\rho_0 = \rho$ (for notational simplicity), Eqs.(8) and (9) can be written as

$$[i\omega + q^2D(\rho)]\delta\tilde{\rho} + v(\rho)\delta\tilde{\theta} = -i\mathbf{q}.\tilde{\mathbf{f}}_d \tag{12}$$

$$\alpha(\rho)q^2\delta\tilde{\rho} - (D_r + Kq^2 + i\omega)\delta\tilde{\theta} = -i\mathbf{q}.\tilde{\mathbf{f}}_p. \tag{13}$$

Solving for the Fourier modes, we get

$$\begin{bmatrix} \delta\tilde{\rho} \\ \delta\tilde{\theta} \end{bmatrix} = -i\mathbf{q}.\begin{bmatrix} q^2D(\rho)+i\omega & v(\rho) \\ \alpha q^2 & -(D_r+Kq^2+i\omega) \end{bmatrix}^{-1}\begin{bmatrix} \tilde{\mathbf{f}}_d \\ \tilde{\mathbf{f}}_p \end{bmatrix}$$

and therefore

$$\delta\tilde{\rho}(\mathbf{q},\omega) = \frac{i}{\det(M)}[(D_r + Kq^2 + i\omega)\mathbf{q}.\tilde{\mathbf{f}}_d + v\mathbf{q}.\tilde{\mathbf{f}}_p] \tag{14}$$

with

$$M = \begin{bmatrix} i\omega + q^2D(\rho) & v(\rho) \\ \alpha q^2 & -(Kq^2 + D_r + i\omega) \end{bmatrix}. \tag{15}$$

Using the noise correlations, $\langle|\mathbf{q}.\tilde{\mathbf{f}}_d|^2\rangle = 2V\Delta_d q^2$, $\langle|\mathbf{q}.\tilde{\mathbf{f}}_p|^2\rangle = 2V\Delta_p q^2$ and $\langle(\mathbf{q}.\tilde{\mathbf{f}}_d^*)(\mathbf{q}.\tilde{\mathbf{f}}_p)\rangle = \langle(\mathbf{q}.\tilde{\mathbf{f}}_d)(\mathbf{q}.\tilde{\mathbf{f}}_p^*)\rangle = 0$, we obtain dynamic structure factor

$$\begin{aligned} S(\mathbf{q},\omega) &= \langle|\delta\tilde{\rho}(\mathbf{q},\omega)|^2\rangle \\ &= \frac{\{\omega^2 + (D_r + Kq^2)^2\}\langle|\mathbf{q}.\tilde{\mathbf{f}}_d|^2\rangle + v^2\langle|\mathbf{q}.\tilde{\mathbf{f}}_p|^2\rangle}{|\det(M)|^2} \\ &= \frac{2q^2V}{|\det(M)|^2}[\Delta_d\{\omega^2 + (D_r + Kq^2)^2\} + \Delta_p v^2] \end{aligned} \tag{16}$$

where

$$|\det(M)|^2 = (\omega^2 - a)^2 + \omega^2 b^2 \tag{17}$$

with

$$a = q^2[D_r\mathcal{D}(\rho) + D(\rho)Kq^2],$$

$$b = D_r + q^2[K + D(\rho)],$$

and

$$\mathcal{D}(\rho) = D(\rho) + v(\rho)\alpha(\rho)/D_r.$$

The Static Structure factor can be computed as $S(\mathbf{q}) = (1/2\pi)\int_{-\infty}^{\infty} S(\mathbf{q},\omega)\ d\omega$. Now using the following equalities,

$$\begin{aligned}\int_{-\infty}^{\infty} \frac{d\omega}{(\omega^2 - a)^2 + \omega^2 b^2} &= \frac{\pi}{ab},\\ \int_{-\infty}^{\infty} \frac{\omega^2 d\omega}{(\omega^2 - a)^2 + \omega^2 b^2} &= \frac{\pi}{b},\end{aligned} \tag{18}$$

we obtain $S(\mathbf{q}) = S_1(\mathbf{q}) + S_2(\mathbf{q})$ where

$$\begin{aligned}S_1(\mathbf{q}) &= V\frac{2q^2\Delta_d}{2\pi}\left[\frac{\pi}{b} + (D_r + Kq^2)^2\frac{\pi}{ab}\right]\\ &= \frac{V\Delta_d q^2}{D_r + q^2(K + D)}\\ &+\frac{V\Delta_d q^2(D_r + Kq^2)^2}{q^2[D_r\mathcal{D} + DKq^2][D_r + q^2(K + D)]}\end{aligned} \tag{19}$$

and

$$\begin{aligned}S_2(\mathbf{q}) &= V\frac{2q^2\Delta_p v^2}{2\pi}\frac{\pi}{ab}\\ &= V\frac{\Delta_p v^2}{[D_r\mathcal{D} + DKq^2][D_r + q^2(K + D)]}.\end{aligned} \tag{20}$$

The structure factor $S(\mathbf{q} = 0) = S_1(0) + S_2(0)$ is related to variance $\sigma^2_{\mathcal{V}}(\rho) = \langle\mathcal{N}^2\rangle - \langle\mathcal{N}\rangle^2$ of number of particles $\mathcal{N} = \int_{\mathcal{V}}\rho(\mathbf{r})\mathbf{dr}$ in a *subvolume* $\mathcal{V}$ which can

be written as

$$\sigma^2_{\mathcal{V}}(\rho) = S(\mathbf{q}=0) = \mathcal{V}\left[\frac{\Delta_d}{\mathcal{D}(\rho)} + \frac{\Delta_p v^2(\rho)}{D_r^2 \mathcal{D}(\rho)}\right], \tag{21}$$

the desired expression in the main text.

APPENDIX C: Polarization fluctuations in the active Brownian particles

As defined in the equations of motion for the active Brownian particles in the main text, $\mathbf{u}_i \equiv \{u_{ix,iy}\} = \{\cos\phi_i, \sin\phi_i\}$ the orientation unit vector for the ith Brownian particle. From the definition of the polarization density $\mathbf{p}(\mathbf{r},t) = \sum_i \delta(\mathbf{r} - \mathbf{R}_i(t))\mathbf{u}_i(t)$, we can express total polarization $\mathbf{P}_{\Delta V}$, in a small volume ΔV, as

$$\mathbf{P}_{\Delta V} = \sum_{i \in \Delta V} \mathbf{u}_i(t) \tag{22}$$

where the sum is over ΔN number of particles in the volume ΔV so that

$$\mathbf{p} = \lim_{\Delta V \to 0} \frac{\mathbf{P}_{\Delta V}}{\Delta V}. \tag{23}$$

Now, using the central limit theorem (CLT), one can estimate the fluctuation or the variance of $\mathbf{P}_{\Delta V} \equiv \{P^x_{\Delta V}, P^y_{\Delta V}\}$, which is the sum of ΔN random variables (i.e., the sum of random orientation unit vectors of ΔN particles in volume ΔV) where the variance of the x and y components of each orientation unit vector $\mathbf{u_i}$, for any i, are calculated to be constant. Consequently, the variance of the x and y components of polarization density $\mathbf{p}$ can be calculated as given below,

$$\begin{aligned}
\sigma^2_{p_{ix}} &= \langle p^2_{ix}\rangle - \langle p_{ix}\rangle^2 \\
&= \lim_{\Delta V \to 0} \frac{\langle (P^x_{\Delta V})^2\rangle - \langle (P^x_{\Delta V})\rangle^2}{\Delta V} \\
&= \lim_{\Delta V \to 0} \frac{\langle \Delta N\rangle}{\Delta V}[\langle u^2_{ix}\rangle - \langle u_{ix}\rangle^2] \propto \rho,
\end{aligned} \tag{24}$$

and similarly

$$\sigma^2_{p_{iy}} \propto \rho. \tag{25}$$

APPENDIX D: Structure factor in the limit of quasistatic polarization field ($\Delta_p = 0$)

In the quasi-static limit of polarization field, by setting $\partial_t \mathbf{p} = 0$, $K = 0$ and polarization noise strength $\Delta_p = 0$ in Eq. 7 and then substituting $\mathbf{p}$ in Eq. 7 [40, 43], we get an effective evolution equation for density field,

$$\begin{aligned} \partial_t \rho &= -\nabla.\left[-v\frac{\nabla(v\rho)}{2D_r} - D\nabla\rho + \mathbf{f}_d\right] && (26)\\ &= -\nabla.[\tilde{v}\rho - \tilde{D}\nabla\rho + \mathbf{f}_d] && (27) \end{aligned}$$

where effective velocity $\tilde{v}(\rho) = -v\nabla v/2D_r$ and effective diffusivity $\tilde{D} = D + v^2/2D_r$. Now we perform linear analysis of fluctuation $\delta\rho = \rho - \rho_0$ around the average density ρ_0,

$$\partial_t \delta\rho = -\nabla.[-\mathcal{D}(\rho_0)\nabla\delta\rho + \mathbf{f}_d] \tag{28}$$

where effective diffusivity

$$\mathcal{D} = \tilde{D} + \frac{\rho v}{2D_r}\frac{dv}{d\rho} = D + \frac{\alpha v}{D_r}, \tag{29}$$

where $\alpha = (v + \rho\frac{dv}{d\rho})/2$. Taking Fourier transform of both sides and solving for density mode,

$$\delta\tilde{\rho}(q,\omega) = \frac{-iq}{i\omega + q^2\mathcal{D}}\tilde{f}_d, \tag{30}$$

we calculate the dynamic structure factor,

$$S(\mathbf{q},\omega) = \langle|\delta\tilde{\rho}(q,\omega)|^2\rangle = \frac{2Vq^2\Delta_d}{\omega^2 + q^4\mathcal{D}^2} \tag{31}$$

and the static Structure factor,

$$S(\mathbf{q}) = \frac{1}{2\pi}\int_{-\infty}^{\infty} S(q,\omega)d\omega = \frac{V\Delta_d}{\mathcal{D}}, \tag{32}$$

which is independent of $\mathbf{q}$, i.e., the two-point correlation function $c(\mathbf{r}) \propto \delta(\mathbf{r})$ and correlation length $\xi = 0$. This is the reason why the linear analysis is exact in this case and provides the variance exactly

$$\sigma^2(\rho) = \frac{\Delta_d}{\mathcal{D}}, \tag{33}$$

which is consistent with an integrability condition in [42] and with the free energy density function $f(\rho)$ satisfying $d^2f/d\rho^2 = 1/\sigma^2(\rho)$. This could be seen if we choose $\Delta_d = \tilde{D}\rho$ as in [42] and we find

$$\sigma^2(\rho) = \frac{\tilde{D}\rho}{\tilde{D} + \frac{\rho v}{2D_r}\frac{dv}{d\rho}} \simeq \frac{v^2\rho/2D_r}{\frac{v^2}{2D_r} + \frac{\rho v}{2D_r}\frac{dv}{d\rho}} = \left[\frac{1}{\rho} + \frac{1}{v}\frac{dv}{d\rho}\right]^{-1}, \tag{34}$$

by assuming $D \ll v^2/2D_r$. Chemical potential $\mu(\rho)$ can be obtained by integrating fluctuation-response relation (Eq. 5 in the main text) w.r.t. density ρ,

$$\mu(\rho) = \int \frac{1}{\sigma^2(\rho)}d\rho = \ln(\rho v) + c_1, \tag{35}$$

c_1 an arbitrary constant of integration.

APPENDIX E: Functional Fokker-Planck Equation and $v = 0$ limit

For a functional Langevin equation (stochastic differential equation) having a general form,

$$\partial_t\rho(\mathbf{r},t) = B[\rho(\mathbf{r},t)] + g(\mathbf{r},t), \tag{36}$$

where $B[\rho(\mathbf{r},t)]$ is a functional of $\rho(\mathbf{r})$ and $g(\mathbf{r},t)$ is a Gaussian noise with correlation

$$\langle g(\mathbf{r},t)g(\mathbf{r}',t)\rangle = G(\mathbf{r},\mathbf{r}')\delta(t-t'), \tag{37}$$

the functional Fokker-Planck equation is given by [75]

$$\begin{aligned}\partial_t\mathcal{P}[\rho(\mathbf{r},t)] &= -\int d^3\mathbf{r}\frac{\delta}{\delta\rho(\mathbf{r})}\{B[\rho(\mathbf{r})]\mathcal{P}[\rho(\mathbf{r},t)]\}\\ &+\frac{1}{2}\int\int d^3\mathbf{r}d^3\mathbf{r}'\left[\frac{\delta^2}{\delta\rho(\mathbf{r})\delta\rho(\mathbf{r}')}G(\mathbf{r},\mathbf{r}')\mathcal{P}[\rho(\mathbf{r},t)]\right]\end{aligned} \tag{38}$$

For simplicity, let us consider only one spatial dimension with Cartesian position coordinate x. Now, we are interested in a Langevin equation having a particular form

$$\dot{\rho} = -\partial_x\left[\rho v - D(\rho)\partial_x\rho + f_\rho\right] \tag{39}$$

where $g(x,t) = \partial_x f_\rho(x,t)$ with noise correlation $\langle f_\rho(x,t)f_\rho(x',t')\rangle = 2\Delta(\rho)\delta(x-x')\delta(t-t')$. Using Eq. 38, the functional Fokker-Planck equation becomes

$$\partial_t\mathcal{P} \;=\; \int dx\frac{\delta}{\delta\rho(x)}\partial_x\left[\rho v - D(\rho)\partial_x\rho - \Delta(\rho)\partial_x\frac{\delta}{\delta\rho(x)}\right]\mathcal{P} \tag{40}$$

For nonzero $v(\rho) \neq 0$, solution of the above Fokker-Planck equation is not in general known. In a special case, when an integrability condition is satisfied $v/D = \partial_x(\delta F/\delta\rho)$ for a functional $F[\rho(x)] = \int f[\rho(x)]dx$, the steady-state solution is given by the Boltzmann form $\mathcal{P} \sim \exp[-F[\rho(x)]$ [42].

When velocity $v(\rho) = 0$, i.e., in equilibrium, the Fokker-Planck equation for the many body probability $\mathcal{P}[\rho(x),t]$ can be shown to always have the Boltzmann form as follows. The Fokker-Planck equation in this case can be written as,

$$\dot{\mathcal{P}} = \int dx\frac{\delta}{\delta\rho(x)}\partial_x\left[-D(\rho)\frac{\partial\rho}{\partial x} - \Delta(\rho)\left(\frac{\delta}{\delta\rho}\right)'\right]\mathcal{P} \tag{41}$$

We start with an ansatz $\mathcal{P} \sim \exp\left[-\int f(\rho)dx\right]$ and, using

$$\left(\frac{\delta\mathcal{P}}{\delta\rho}\right)' = -\mathcal{P}\frac{d^2f}{d\rho^2}\frac{\partial\rho}{\partial x}, \tag{42}$$

in Eq. 41, we obtain $f(\rho)$ as given below,

$$-D(\rho)\frac{\partial\rho}{\partial x}\mathcal{P} - \Delta(\rho)\left(\frac{\delta\mathcal{P}}{\delta\rho}\right)' = 0 \tag{43}$$

$$\Rightarrow \quad -D(\rho)\frac{\partial\rho}{\partial x}\mathcal{P} + \Delta(\rho)\mathcal{P}\frac{d^2f}{d\rho^2}\frac{\partial\rho}{\partial x} = 0 \tag{44}$$

$$\Rightarrow \quad \frac{\partial\rho}{\partial x}\mathcal{P}\left[-D(\rho) + \Delta(\rho)\frac{d^2f}{d\rho^2}\right] = 0 \tag{45}$$

$$\Rightarrow \quad \frac{d^2f}{d\rho^2} = \frac{D(\rho)}{\Delta(\rho)}. \tag{46}$$

Therefore the steady-state probability functional for density fluctuation can be written as $\mathcal{P}[\{\rho(\mathbf{r})\}] \propto \exp[-\int f[\rho(\mathbf{r})]d^2\mathbf{r}]$ where $d^2f/d\rho^2 = [\Delta_d(\rho)/D(\rho)]^{-1}$. This is what is expected from the equilibrium fluctuation-dissipation theorem.

Bibliography

[1] G. Gallavotti and E. G. D. Cohen, Phys. Rev. Lett. **74**, 2694 (1995); D. J. Evans and G. P. Morriss, *Statistical Mechanics of Nonequilibrium Fluids*, Academic Press, New-York (1990).

[2] C. Jarzynski, Phys. Rev. Lett. **78**, 2690 (1997); C. Jarzynski, Phys. Rev. E **56**, 5018 (1997).

[3] G. E. Crooks, Phys. Rev. E **60**, 2721 (1999).

[4] B. Derrida, J. L. Lebowitz, and E. R. Speer, Phys. Rev. Lett. **87**, 150601 (2001); B. Derrida, J. L. Lebowitz, and E. R. Speer, Phys. Rev. Lett. **89**, 030601 (2002); B. Derrida, J. Stat. Mech. **P01030** (2011).

[5] B. Derrida, J. Stat. Mech. **P07023** (2007).

[6] Y. Oono and M. Paniconi, Prog. Th. Phys. Supp. **130**, 29 (1998).

[7] L. Bertini, A. De Sole, D. Gabrielli, G. Jona-Lasinio, and C. Landim, Phys. Rev. Lett. **87**, 040601 (2001).

[8] L. Bertini, A. De Sole, D. Gabrielli, G. Jona-Lasinio and C. Landim, J. Stat. Phys. **107**, 635 (2002); L. Bertini, A. De Sole, D. Gabrielli, G. Jona-Lasinio and C. Landim, Rev. Mod. Phys. **87**, 593 (2015).

[9] G. L. Eyink, J. L. Lebowitz, H. Spohn, J. Stat. Phys **83**, 385 (1996).

[10] E. Bertin, O. Dauchot, and M. Droz, Phys. Rev. Lett. **96**, 120601 (2006).

[11] P. Pradhan, C. P. Amann, and U. Seifert, Phys. Rev. Lett. **105**, 150601 (2010).

[12] S. Chatterjee, P. Pradhan and P. K. Mohanty, Phys. Rev. Lett. **112**, 030601 (2014).

[13] S. Chatterjee, P. Pradhan, and P. K. Mohanty, Phys. Rev. E **91**, 062136 (2015).

[14] A. Das, S. Chatterjee, P. Pradhan, and P. K. Mohanty, Phys. Rev. E **92**, 052107 (2015).

[15] A. Das, S. Chatterjee, and P. Pradhan, Phys. Rev. E **93**, 062135 (2016).

[16] A. Das, A. Kundu, and P. Pradhan, Phys. Rev. E. **95**, 062128 (2017).

[17] S. Chatterjee, A. Das, and P. Pradhan, Phys. Rev. E **97**, 062142 (2018).

[18] H. Touchette, Physics Reports **478**, 1 (2009).

[19] D. Gabrielli, G. Jona-Lasinio, and C. Landim, Phys. Rev. Lett. **77**, 1202 (1996).

[20] C. Giardin, J. Kurchan, and L. Peliti, Phys. Rev. Lett. **96**, 120603, (2006).

[21] A. Kundu, S. Sabhapandit, and A. Dhar, Phys. Rev. E **83**, 031119, (2011).

[22] E. Ben-Jacob, I. Cohen, and H. Levine, Adv. Phys. **49**, 395 (2000); C. Dombrowski, L. Cisneros, S. Chatkaew, R. E. Goldstein, and J. O. Kessler, Phys. Rev. Lett. **93**, 098103 (2004).

[23] S. Hubbard, P. Babak, S. Sigurdsson, and K. Magnusson, Ecol. Model. **174**, 359 (2004).

[24] T. Feder, Phys. Today **60**, 28 (2007); C. Feare, *The Starling* (Oxford University Press, Oxford, 1984)

[25] E. Rauch, M. Millonas, and D. Chialvo, Phys. Lett. A **207**, 185 (1995).

[26] J. Palacci, S. Sacanna, A. P. Steinberg, D. J. Pine, P. M. Chaikin, Science **339**, 936 (2013). H. Jiang, N. Yoshinaga, and M. Sano, Phys. Rev. Lett. **105**, 268302 (2010).

[27] H. H. Wensink, J. Dunkel, S. Heidenreich, K. Drescher, R. E. Goldstein, H. Lowen, and J. M. Yeomans, PNAS **109**, 14308 (2012); J. Dunkel, S. Heidenreich, K. Drescher, H. H. Wensink, M. Bar, and R. E. Goldstein, Phys. Rev. Lett. **110**, 228102 (2013); J. Palacci, C. Cottin-Bizonne, C. Ybert, and L. Bocquet, Phys. Rev. Lett. **105**, 088304 (2010); Fernando Peruani, J. Starruss, V. Jakovljevic, L. Sogaard-Andersen, A. Deutsch, and M. Bar, Phys. Rev. Lett. **108**, 098102 (2012).

[28] S. Mishra, A. Baskaran, and M. C. Marchetti, Phys. Rev. E **81**, 061916 (2010).

[29] F. Peruani, T. Klauss, A. Deutsch, and A. Voss-Boehme, Phys. Rev. Lett. **106**, 128101 (2011).

[30] A. Peshkov, I. S. Aranson, E. Bertin, H. Chate, and F. Ginelli, Phys. Rev. Lett. **109**, 268701 (2012).

[31] Y. Fily and C. Marchetti, Phys. Rev. Lett. **108**, 235702 (2012); Y. Fily, S. Henkes, and C. Marchetti, Soft Matter **10**, 2132 (2014).

[32] F. D. C. Farrell, M. C. Marchetti, D. Marenduzzo, and J. Tailleur, Phys. Rev. Lett. **108**, 248101 (2012); H. H. Wensink, V. Kantsler, R. E. Goldstein, and J. Dunkel Phys. Rev. E **89**, 010302 (2014).

[33] J. Bialke, T. Speck, and H. Lowen, Phys. Rev. Lett. **108**, 168301 (2012).

[34] G. S. Redner, M. F. Hagan, and A. Baskaran, Phys. Rev. Lett. **110**, 055701 (2013).

[35] J. Bialke, H. Lowen, and T. Speck, EPL **103**, 30008 (2013).

[36] J. D. Weeks, D. Chandlar, and H. C. Andersen, J. Chem. Phys. **54**, 5237 (1971).

[37] S. Ngo, A. Peshkov, I. S. Aranson, E. Bertin, F. Ginelli, and H. Chate, Phys. Rev. Lett. **113**, 038302 (2014).

[38] M. C. Marchetti, J. F. Joanny, S. Ramaswamy, T. B. Liverpool, J. Prost, M. Rao, and R. A. Simha, Rev. Mod. Phys. **85**, 1143 (2013)

[39] M. Cates, Rep. Prog. Phys. **75**, 042601 (2012).

[40] A. P. Solon, M. E. Cates, and J. Tailleur, Eur. Phys. J. **224**, 1231 (2015).

[41] A. Y. Grosberg and J.-F. Joanny, *arXiv:1502.08034*.

[42] J. Tailleur and M. Cates, Phys. Rev. Lett. **100**, 218103 (2008).

[43] M. E. Cates and J. Tailleur, EPL **101**, 20010 (2013).

[44] J. Stenhammar, A. Tiribocchi, R. J. Allen, D. Marenduzzo, and M. E. Cates, Phys. Rev. Lett. **111**, 145702 (2013).

[45] R. Wittkowski, A. Tiribocchi, J. Stenhammar, R. J. Allen, D. Marenduzzo, and M. E. Cates, Nat. Comm. **5**, 4351 (2014).

[46] J. Stenhammar, D. Marenduzzo, R. J. Allen, and M. E. Cates, Soft Matter **10**, 1489 (2014).

[47] M. E. Cates, D. Marenduzzo, I. Pagonabarraga, and J. Tailleur, PNAS **107**, 11715 (2010).

[48] T. Speck, J. Bialke, A. M. Menzel, and H. Lowen, Phys. Rev. Lett. **112**, 218304 (2014).

[49] J. Barre, R. Chetrite, M. Muratori, and F. Peruani, J. Stat. Phys. **158**, 589 (2015).

[50] S. C. Takatori, W. Yan, and J. F. Brady, Phys. Rev. Lett. **113**, 028103 (2014). S. C. Takatori and J. F. Brady, Phys. Rev. E **91**, 032117 (2015).

[51] S. A. Mallory, A. Saric, C. Valeriani, and A. Cacciuto, Phys. Rev. E **89**, 052303 (2014).

[52] A. P. Solon, J. Stenhammar, R. Wittkowski, M. Kardar, Y. Kafri, M. E. Cates, and J. Tailleur, Phys. Rev. Lett. **114**, 198301 (2015).

[53] A. P. Solon, Y. Fily, A. Baskaran, M. E. Cates, Y. Kafri, M. Kardar and J. Tailleur, Nat. Phys. (2015).

[54] X. Yang, M. L. Manning, and M. Marchetti, Soft Matter **10**, 6477 (2014).

[55] R. G. Winkler, A. Wysocki, and G. Gompper, *arXiv: 1506.03941.*

[56] D. Levis and L. Berthier, *arXiv: 1506.08553.*

[57] U. M. B. Marconi and C. Maggi, *arXiv: 1507.03443.*

[58] S. Ramaswamy, R. A. Simha, and J. Toner, Europhys. Lett. **62**, 196 (2003).

[59] J. Toner, Y. Tu, and S. Ramaswamy, Ann. Phys. (Berlin) **318**, 170 (2005).

[60] S. Mishra and S. Ramaswamy, Phys. Rev. Lett. **97**, 090602 (2006).

[61] S. Ramaswamy, Annu. Rev. Condens. Matter Phys. **1**, 323 (2010).

[62] P. G. de Gennes and J. Prost, *The Physics of Liquid Crystals* (Clarendon, Oxford), 2nd ed. (1993).

[63] H. Chate, F. Ginelli, and R. Montagne, Phys. Rev. Lett. **96**, 180602 (2006).

[64] J. M. Kosterlitz and D. Thouless, J. Phys. C **6**, 1181 (1973).

[65] D. Das and M. Barma, Phys. Rev. Lett. **85**, 1602 (2000).

[66] H. Gruler, U. Dewald, and M. Eberhardt, Eur. Phys. J. B, **11**, 187 (1999); R. Kemkemer, D. Kling, D. Kaufmann, and H. Gruler, Eur. Phys. J. E, **1**, 215 (2000).

[67] V. Narayan, N. Menon, and S. Ramaswamy, Science, **317**, 105 (2007).

[68] V. Narayan, N. Menon, and S. Ramaswamy, J. Stat. Mech., **P01005** (2006).

[69] T. F. F. Farage, P. Krinninger, and J. M. Brader, Phys. Rev. E **91**, 042310 (2015).

[70] S. Dey, D. Das, and R. Rajesh, Phys. Rev. Lett. **108**, 238001 (2012).

[71] T. Vicsek, A. Cziro, E. Ben-Jacob, I. Cohen, and O. Shochet, Phys. Rev. Lett. **75**, 1226 (1995).

[72] J. Toner and Y. Tu, Phys. Rev. Lett. **75**, 4326 (1995).

[73] J. Toner and Y. Tu, Phys. Rev. E. **58**, 4828 (1998).

[74] S. Heidenreich, J. Dunkel, S. H. L. Klapp, and M. Bar, *arXiv: 1509.08661.*

[75] C. W. Gardiner, *Handbook of Stochastic Methods* (Springer-Verlag, Berlin, 2004), 3rd edition.

[76] N. Clisby and B. M. McCoy, J. Stat. Phys. **114**, 1343 (2004); N. Clisby and B. M. McCoy, J. Stat. Phys. **114**, 1361 (2004);

[77] R. Hoste and W. van Dael, J. Chem. Soc., Faraday Trans. (2) **80**, 477 (1984).

[78] M. G. Mazza, N. Giovambattista, H. E. Stanley, and F. W. Starr, Phys. Rev. E **76**, 031203 (2007); C. K. Mishra and R. Ganapathy, Phys. Rev. Lett. **114**, 198302 (2015); J. Kim and B. J. Sung, Phys. Rev. Lett. **115**, 158302 (2015).

[79] G. Gregoire and H. Chate, PRL. **92**, 025702 (2004).

[80] A. Einstein, Ann. Phys. **17**, 549 (1905); *Investigations on the Theory of Brownian Movement* (Dover, New York, 1956).

[81] M. S. Green, J. Chem. Phys. **22**, 398 (1954); R. Kubo, J. Phys. Soc. Jpn. **12**, 570 (1957); R. Kubo, Rep. Prog. Phys. **29**, 255 (1966).

[82] J. L. Lebowitz and H. Spohn, J. Stat. Phys. **95**, 333 (1999).

[83] I. K. Ono, C. S. O'Hern, D. J. Durian, S. A. Langer, A. J. Liu, and S. R. Nagel, Phys. Rev. Lett. **89**, 095703 (2002).

[84] K. Hayashi and S. Sasa, Phys. Rev. E **68**, 035104 (2003).

[85] V. Blickle, T. Speck, C. Lutz, U. Seifert, and C. Bechinger, Phys. Rev. Lett. **98**, 210601 (2007).

[86] K. Hayashi and S.-i. Sasa, Phys. Rev E **69**, 066119 (2004).

[87] K. Hayashi and S.-i. Sasa, Phys. Rev E **71**, 046143 (2005).

[88] A. Prados, A. Lasanta, and Pablo I. Hurtado, Phys. Rev. E **86**, 031134 (2012).

[89] S. N. Majumdar, S. Krishnamurthy, and M. Barma, Phys. Rev. Lett. **81**, 3691 (1998).

[90] In a private communication with Arghya Das.

[91] O. J. O'Loan and M. R. Evans, J. Phys. A: Math. Gen. **32**, L99 (1999).

[92] J. R. Raymond and M. R. Evans, Phys. Rev. E **73**, 036112 (2006).

[93] A. B. Slowman, M. R. Evans, and R. A. Blyth, Phys. Rev. Lett. **116**, 218101 (2016).

[94] A. B. Slowman, M. R. Evans, and R. A. Blyth, J. Phys. A: Math. Theor. **50**, 375601 (25pp) (2017).

[95] K. Malakar, V. Jemseena, A. Kundu, K. V. Kumar, S. Sabhapandit, S. N. Majumdar, S. Redner, and A. Dhar, J. Stat. Mech. **043215** (2018).